

DEVELOPMENT OF THE TIMING SYSTEM FOR THE BUNCH-TO-BUCKET TRANSFER BETWEEN THE FAIR ACCELERATORS

Vom Fachbereich
Institut für Angewandte Physik
der Goethe-Universität, Frankfurt am Main
zur Erlangung des akademischen Grades
eines Doktor der Naturwissenschaften
genehmigte Dissertation

Von
Jiaoni Bai
geboren am 9. November 1986 in Taiyuan, Shanxi Province, China

Referent: Prof. Dr. U. Ratzinger
Korreferent: Prof. Dr. O. Kester
Tag der Einreichung: Date. Month Year
Tag der mündlichen Prüfung: Date. Month Year

Darmstadt 2016

I would like to dedicate this dissertation to my dear parents,
loving husband and good friends ...

Acknowledgement

First and foremost, I would like to thank my professor Prof. Dr. Oliver Kester. I have been so lucky to be his Ph.D. student. He gave me the chance to study at Goethe Universität, Frankfurt am Main and work in GSI for this interesting Ph.D. topic. It has been an honor to be his Ph.D. student. I appreciate all his contributions of time, ideas and funding to make my Ph.D. experience productive and stimulating. I was deeply influenced by his enthusiasm for his research and his selfless support for his students. I was thankful for his support, that I participated many international conferences, schools and workshops. This experience enriched my life and broadened my horizons.

I wish to express my sincere gratitude to Dr. David Ondreka and Dr. Dietrich Beck for their supervision, valuable guidance and helpful suggestions throughout my Ph.D. study. I have been greatly lucky to have so good supervisors, who cared much about my work and who answered my doubts patiently. They were like a lighthouse in the ocean, which guides me in the right direction. They are not only my scientific supervisors, but also my mentors. They encouraged and motivated me during tough time of my Ph.D. Hence, I will keep a positive attitude and keep moving forward when I face with challenges, difficulties and temporary setbacks in the future.

I would like to acknowledge all colleagues in the timing group, CSCO department, GSI, Mathias Kreider, Stefan Rauch, Marcus Zweig, Alexander Hahn and former employee Dr. Wesley Terpstra, who provided me much technical support. I would like to extend my appreciation to department leader Dr. Ralph Bär, who gave much support for my Ph.D. topic. Thanks for their friendship and collaboration. I am especially grateful for the group member Cesar Prados, by whom I learned not only technical knowledge, but also how to work efficiently and how to become a good engineer. I would also like to thank Matthias Thieme, who provided me the devices for the test setup and Marko Stanislav Mandakovic for the discussion about the MPS.

I am also thankful for the good cooperation with Thibault Ferrand, who studies at Technische Universität Darmstadt and works in PBRF department, GSI. Thanks for his valuable contribution of the development of the LLRF system for the B2B transfer system for FAIR. I would like to extend my sincerest thanks and appreciation to PBRF department leader Prof. Dr. Ing. Harald Klingbeil for his support. In addition, a special thanks is also extended to Dr. Dieter Lens and Stefan Schäfer for their technical support. Thanks for Dr. Bernhard Zipfel to give me support about BuTiS.

I wish to express my sincere gratitude to SBES department leader Dr. Markus Steck for his technical support of ESR and CRYRING, Dr. Blell Udo in PBHV department for the technical support of kicker and Dr. Michael Block in SHE-P department for the supply of two SRS function generators.

I must express my gratitude to GSI, who provides the Facility for Antiproton and Ion Research project for my experiment. And also HGS-HiRe, who provided the scholarship which allowed me to undertake this research.

Lastly, I would like to thank my family for all their love and encouragement. My parents always support me to pursuing my dreams. Most of all, my loving husband Zigao Li is so appreciated, who always encourages me to realize my dreams. Thank you.

Jiaoni Bai
Darmstadt, September 2016

Abstract

This dissertation contributes to the conceptual development, systematic investigation and timing system realization of the Bunch-to-Bucket (B2B) transfer system for FAIR, Facility for Antiproton and Ion Research at GSI Helmholtzzentrum für Schwerionenforschung GmbH.

The B2B transfer system for FAIR plays an important role for the FAIR project, which will achieve various complex bunch to bucket transfer for FAIR accelerators in the future. It focuses first of all on the transfer from SIS18 to SIS100, but it will be firstly tested for the transfer from SIS18 to ESR and further to CRYRING. The system is developed based on the FAIR existing infrastructures, LLRF and FAIR control systems. It coordinates with the Machine Protection System (MPS), which protects SIS100/SIS300 from unacceptable failure or situation and indicates beam for Beam Instrumentation (BI).

The B2B transfer system obtains the radio frequency (rf)-phase difference between two synchrotrons by means of a campus wide distributed reference signal with picosecond precision, which is provided by the Bunchphase Timing System (BuTiS). The source synchrotron works as a “B2B transfer master“ for the rf phase collection, data (e.g. synchronization window indicating the coarse time frame for the transfer, phase shift for the phase match between two rf systems, phase correction for the bucket label and so on) calculation, synchronization window redistribution and B2B transfer status check (see Chap.). The synchronization window is a coarse time frame for the transfer and the bucket label signal is used to indicate the fine transfer. This system is applied to all FAIR B2B transfer cases and all transfers achieve the bunch-to-bucket injection center mismatch smaller than the tolerance.

Because the system focuses first of all on the transfer from SIS18 to SIS100, the beam dynamic of the B2B transfer from SIS18 to SIS100 is simulated for two synchronization methods, the phase shift and the frequency beating method. In addition, the SIS18 extraction and SIS100 injection kickers are analyzed for different triggering strategies. This dissertation also explains the timing constraints of the system, the calculation of the synchronization window and presents the usage of the WR network for the B2B transfer system.

A test setup of the timing system of the B2B transfer system for FAIR is also presented in this dissertation.

Kurzfassung

Contents

Abstract	v
Glossary	xiii
List of Abbreviations	xvi
List of Symbols	xix
1 Introduction	2
1.1 First overview of the FAIR bunch-to-bucket transfer system	5
1.2 Objectives, Contribution and Structure of the Dissertation	5
2 Theoretical background	8
2.1 Energy match, Phase match and voltage match	8
2.2 Loop freeze	9
2.3 Phase difference between two RF systems	9
2.4 RF synchronization	9
2.4.1 Phase shift method	11
2.4.2 Frequency beating method	15
2.5 Bucket label	17
2.6 Synchronization of the extraction and injection kicker	17
2.7 Beam indication for the beam instrumentation	18
3 Technical basis for the B2B transfer system	19
3.1 FAIR control system	19
3.1.1 BuTiS	19
3.1.2 GMT	20
3.1.3 FESA	20
3.1.4 Settings Management	21
3.2 LLRF system	21
3.3 MPS system	23
3.4 Comparison	24
4 Concept of the FAIR B2B transfer system [1]	25
4.1 Basic idea of the FAIR B2B transfer system	25
4.1.1 Phase alignment	25
4.1.2 Calculation of the trigger time for the extraction and injection kickers	26
4.2 Basic procedure of the FAIR B2B transfer system	28

CONTENTS

4.3	Realization of the FAIR B2B transfer system	29
4.3.1	Phase measurement and corresponding timestamp of one rf system	29
4.3.1.1	Measurement of actual phase values in one rf system	30
4.3.1.2	Phase extrapolation in one rf system	30
4.3.1.3	Timestamp the extrapolated phase	31
4.3.2	Exchange of the measured data	32
4.3.3	RF synchronization	33
4.3.4	Coarse synchronization	35
4.3.5	Bucket label	36
4.3.6	Fine synchronization of the extraction and injection kicker . .	39
4.3.7	B2B transfer status check	40
4.4	Data flow of the FAIR B2B transfer system	40
5	Application of the FAIR B2B transfer system for FAIR accelerators	43
5.1	Circumference ratio is an ideal integer	44
5.1.1	Harmonic ratio equals to the circumference ratio	46
5.1.1.1	use case of the U^{28+} B2B transfer from SIS18 to SIS100	46
5.1.2	Harmonic ratio does not equal to the circumference ratio . .	46
5.1.2.1	Use case of the H^+ B2B transfer from SIS18 to SIS100	47
5.1.2.2	use case of the B2B transfer from ESR to CRYRING	48
5.2	Circumference ratio is not an ideal integer	49
5.2.1	Circumference ratio is close to an ideal integer	50
5.2.1.1	use case of h=4 B2B transfer from SIS18 to ESR . .	51
5.2.1.2	use case of h=1 B2B transfer from SIS18 to ESR . .	52
5.2.2	Circumference ratio is far away from an ideal integer . .	52
5.2.2.1	use case of H^+ B2B transfer from SIS100 to CR . .	54
5.2.2.2	use case of RIB B2B transfer from SIS100 to CR . .	54
5.2.2.3	use case of B2B transfer from CR to HESR	55
5.2.2.4	use case of B2B transfer from SIS18 to ESR via FRS	56
5.3	Summary of the synchronization for different scenarios	57
6	Realization and systematic investigation of the FAIR B2B transfer system	59
6.1	Investigation of two synchronization methods for U^{28+} B2B transfer from SIS18 to SIS100 from the beam dynamics viewpoint	59
6.1.1	Phase shift method	59
6.1.1.1	Longitudinal dynamic analysis for the simulation . .	61
6.1.1.2	Transverse dynamics analysis for the simulation . .	65
6.1.2	Frequency beating method	66
6.1.2.1	Longitudinal dynamics analysis of the frequency beating for SIS18	66
6.2	GMT systematic investigation for the B2B transfer system	67
6.2.1	Calculation of the synchronization window	67
6.2.1.1	The best estimate of alignment and the probable range of alignment for the phase shift method	70
6.2.1.2	The best estimate of alignment and the probable range of alignment for the frequency beating method	72

CONTENTS

6.2.1.3	Calculation the synchronization window and its accuracy	73
6.2.2	Characterization of the WR network for the B2B transfer	75
6.2.2.1	WR network test setup	77
6.2.2.2	Frame loss rate test result for B2B frames	77
6.2.2.3	Latency and jitter test result for B2B frames	79
6.2.2.4	Result and conclusion	81
6.3	Kicker systematic investigation for the B2B transfer system	82
6.3.1	SIS18 extraction kicker units	83
6.3.2	SIS100 injection kicker units	84
6.4	Test setup for the data collection, merging and redistribution of the B2B transfer system	85
6.4.1	Test functional requirement	85
6.4.2	Test setup	86
6.4.3	The firmware of the B2B transfer system	88
6.4.4	The time constraints of the B2B transfer system	91
6.4.5	Test result	93
7	Conclusion and outlook	95
A	B2B timing frames	97
B	Timing frames transfer for the B2B transfer	99
C	Parameters of B2B transfer for FAIR accelerator pairs	101
C.1	Parameters for the B2B transfer from SIS18 to SIS100	101
C.2	Parameters for the B2B transfer from SIS18 to ESR	103
C.3	Parameters for the B2B transfer from SIS18 to ESR via FRS	105
C.4	Parameters for the B2B transfer from ESR to CRYRING	107
C.5	Parameters for the B2B transfer from CR to HESR	108
C.6	Parameters for the B2B transfer from SIS100 to CR	109
	Bibliography	109
	Publications	114

List of Figures

1.1	Bunch-to-bucket transfer described in the picture of James Bond jumping from a truck to a helicopter	2
1.2	Structure of the dissertation.	6
2.1	The illustration of the phase shift method.	11
2.2	The illustration of the frequency beating method.	16
3.1	Reference RF Signal distribution system	22
3.2	Local Cavity Synchronization	23
4.1	The illustration of B2B transfer from SIS18 to SIS100.	26
4.2	The procedure for the B2B transfer within one acceleration cycle. . . .	28
4.3	The realization of the phase advance measurement at one synchrotron	30
4.4	The realization of the phase advance extrapolation at one synchrotron	31
4.5	Implementation of the Phase Advance Prediction Module in the B2B source SCU	32
4.6	The synchronization of the extrapolated phase to the timestamp in one synchrotron	32
4.7	One example of the transfer path of the B2B timing frame in the WR network	33
4.8	The normalized frequency and phase modulation profile and the actual profiles	34
4.9	Implementation of the Phase Shift Module in the B2B source SCU .	35
4.10	Implementation of the Phase Correction Module in the Trigger SCU .	37
4.11	The realization of the bucket label for the normal extraction and injection.	37
4.12	The realization of the bunch gap for the emergency extraction.	38
4.13	Implementation of the Trigger Decision module in the Trigger SCU .	39
4.14	The data flow of the B2B transfer system	42
6.1	Examples of RF frequency modulation.	60
6.2	Time derivation of four modulations	61
6.3	The phase shift modulation of four cases	61
6.4	Average radial excursions of four cases.	62
6.5	Relative momentum shift of four cases.	63
6.6	Changes in synchronous phase of four cases	64
6.7	Ratio of bucket areas of a running bucket to the stationary bucket of four cases	64
6.8	Adiabaticity parameter estimation of case (3) and (4)	65

LIST OF FIGURES

6.9	RF frequency derivation of the U^{28+} rf ramp	67
6.10	The illustration of the best estimate of alignment, the probable range of alignment and the synchronization window	68
6.11	The illustration of symbols for the calculation	68
6.12	Scenarios for the phase shift method	70
6.13	Two scenarios for the frequency beating method	72
6.14	The illustration of the synchronization window and its accuracy . . .	74
6.15	The WR network test setup	77
6.16	The frame loss rate for B2B Broadcast and B2B Unicast frames . . .	78
6.17	The average latency and jitter for B2B Broadcast frames	79
6.18	The maximum latency and jitter for B2B Broadcast frames	80
6.19	The average latency and jitter for B2B Unicast frames	80
6.20	The maximum latency and jitter for B2B Unicast frames	81
6.21	Three scenarios for the delay of SIS18 extraction kicker	83
6.22	SIS100 injection kicker	85
6.23	Schematic of the test setup	86
6.24	The front and back view of the test setup	87
6.25	Flow chart of the firmware for B2B source SCU.	88
6.26	Flow chart of the firmware for B2B target SCU.	90
6.27	The time constraints of the B2B transfer system.	92
B.1	Timing frames transfer for the B2B transfer	100

List of Tables

5.1	FAIR use cases of the B2B transfer	44
5.2	Synchronization when the circumference ratio is an ideal integer	45
5.3	Synchronization when the revolution frequency ratio is an ideal integer .	45
5.4	Synchronization of U^{28+} B2B transfer from SIS18 to SIS100	47
5.5	Synchronization of H^+ B2B transfer from SIS18 to SIS100	48
5.6	Synchronization of B2B transfer from ESR to CRYRING	49
5.7	Synchronization when circumference ratio is close to an ideal integer .	50
5.8	Synchronization of $h=4$ B2B transfer from SIS18 to ESR	51
5.9	Synchronization of $h=1$ B2B transfer from SIS18 to ESR	52
5.10	Synchronization when circumference ratio is far away from an ideal integer	53
5.11	Synchronization of H^+ B2B transfer from SIS100 to CR	54
5.12	Synchronization of RIB B2B transfer from SIS100 to CR	55
5.13	Synchronization of B2B transfer from CR to HESR	56
5.14	Synchronization of B2B transfer from SIS18 to ESR via FRS	57
5.15	Summary of the synchronization	58
6.1	The maximum average radial excursion of four cases	62
6.2	The maximum relative momentum shift of four cases	63
6.3	The minimum bucket area factor of four cases	65
6.4	The B2B transfer requirements for the WR network	76
6.5	The connection between the traffic generator and WR switches	78
6.6	The average latency and jitter of the B2B Broadcast frames	79
6.7	The maximum latency and jitter of the B2B Broadcast frames	80
6.8	The result of the WR network test for the B2B transfer	81
6.9	The delay for firing two crates of SIS18 extraction kicker	84
6.10	The delay for firing SIS00 injection kicker	85
A.1	B2B timing frames	98
C.1	Parameters for the B2B transfer from SIS18 to SIS100	102
C.2	Parameters for the B2B transfer from SIS18 to ESR	104
C.3	Parameters for the B2B transfer from SIS18 to ESR via FRS	106
C.4	Parameters for the B2B transfer from ESR to CRYRING	107
C.5	Parameters for the B2B transfer from CR to HESR	108
C.6	Parameters for the B2B transfer from from SIS100 to CR	109

Glossary

accuracy	Closeness of agreement between the observed start and the best estimate of the start of the synchronization window, which is the sum of the precision and trueness
B2B target SCU	Collects the predicted phase of the target synchrotron and transfers it to the source synchrotron
B2B source SCU	B2B master: data collection, calculation and distribution for the B2B transfer system
batch	SIS100 batch: Train of $4 \times 2 U^{28+}$ bunches injected into SIS100 in one SIS18 to SIS100 super cycle. Or train of $4 \times 1 H^+$ bunches injected into SIS100 in one SIS18 to SIS100 super cycle
best estimate of alignment	Fine time for the alignment of two RF Reference Signals
bucket	The RF system provides longitudinal focusing which constrains the particle motion in the longitudinal phase space to a confined region called the RF bucket
bucket pattern	Rules for the buckets to be filled
bunch	Collection of particles captured within one RF bucket
bunch gap	Area without any bunches in the bunch train that fits the time required for building up the nominal field of the kicker

Glossary

Cavity DDS	Cavity DDS provides RF signal for cavities
circumference ratio	Ratio of the circumference of the injection/extraction orbit of the large synchrotron to that of the small synchrotron
error propagation	Uncertainties in the original measurements “propagate“ through calculations to cause uncertainties in the calculated final answers
frame loss rate	The ratio of the number of the lost Ethernet frames to the number of the theoretic received frames of a tested port
Group DDS	DDS module that generates an Reference RF Signal for a group of cavities
jitter	The absolute value of the difference between the latency of two consecutive received frames belonging to the same stream from one Xena port to another Xena port
latency	The time interval between the time of Xena port receiving frame and the time of another Xena port sending frame
machine cycle	One complete operation cycle of a machine, i.e. injection, ramp up, flattop, ejection and ramp down
precision	Closeness of agreement between the actual start of the synchronization window of different SCUs
probable range of alignment	Range within which the fine alignment lies because of the propagation of the uncertainty
Reference RF Signal	Signal generated by the Group DDS and delivered to an individual RF cavity as a reference for the gap signal
revolution frequency ratio	Ratio of the revolution frequency of the small to that of the large synchrotrons

Glossary

Synchronization Reference Signal	Shared reference signal whose frequency is a multiple of the BuTiS T0 100 kHz and whose zero-crossing is aligned with T0 edges
timing frame	A specified ethernet frame with 110 byte frame length, which contains one or more timing message
Trigger SCU	Production of the trigger signal for kicker electronics
trueness	Closeness of agreement between the average actual start of the synchronization window of different SCUs and the best estimation start of the synchronization window
tune	Number of particle trajectory oscillations during one revolution in the ring (transverse and longitudinal)
uncertainty	A non-negative parameter characterizing the dispersion of the values attributed to a measured quantity
virtual RF cavity	A virtual position around the ring, to which the Reference RF Signal corresponds

List of Abbreviations

API	Application Programming Interface
B2B	Bunch to Bucket
BI	Beam Instrumentation
CCS	Central Control System
CERN	European Organization for Nuclear Research
CM	Clock Master
CPU	Central Processing Unit
CR	Collector Ring
CSCO	Common Systems Control Systems
DDS	Direct Digital Synthesizer
DM	Data Master
DSP	Digital Signal Processor
ESR	Experimental Storage Ring
FAIR	Facility for Antiproton and Ion Research
FESA	Front-End software Architecture
FPGA	Field Programmable Gate Array
FRS	Fragment Separator
GCD	Greatest Common Divisor
GMT	General Machine Timing
GUI	Graphical User Interface

List of Abbreviations

LLRF	Low-level RF
LSA	LHC Software Architecture
MM	Management Master
MPS	Machine Protection System
NESR	New Experimental Storage Ring
PAM	Phase Advance Measurement
PAP	Phase Advance Prediction
PBHV	Primary Beam High Voltage
PBRF	Primary Beam Radio Frequency
PC	Personal Computer
PCM	Phase Correction Module
PSM	Phase Shift Module
RESR	Recycled Experimental Storage Ring
RF	Radio Frequency
SBES	Experimentierspeicherring ESR
SCU	Scalable Control Unit
SHE-P	SHE-Physik
SM	Settings Management
SR	Signal Reproduction
TD	Trigger Decision
TM	Timing Master
TOF	Time Of Flight
TTL	Transistor–Transistor Logic
UNILAC	Universal Linear Accelerator

List of Abbreviations

WR White Rabbit

List of Symbols

e	Charge of the particle
ρ_0	Bending radius of a particle immersed in a magnetic field B
β	Relative speed to the speed of light
$R(t)$	Orbit radius. R_0 the nominal value
$B(t)$	Magnetic field
α_p	Momentum compaction factor
$p(t)$	Particle momentum
$f(t)$	Revolution frequency
$v(t)$	Velocity of particle
$\gamma(t)$	Relativistic factor, which measures the total particle energy, $E(t)$, in units of the particle rest energy, E_0
$E(t)$	Total particle energy
E_0	Particle rest energy
γ_t	Transition energy
$\eta(t)$	Phase-slip factor
$F(t)$	Force
$V(t)$	RF accelerating voltage
$\omega_s(t)$	Small-amplitude synchrotron frequency
ε	Adiabaticity parameter

List of Symbols

t_{bucket}	Time delay for a specified bucket pattern
t_{TOF}	Time-of-Flight between two synchrotrons
t_{v_ext}	Time corresponds to the distance between the virtual RF cavity driving signals and the extraction position of the source synchrotron
t_{v_inj}	Time corresponds to the distance between the virtual RF cavity driving signals and the injection position of the target synchrotron
t_{ext}	Extraction kicker delay
t_{inj}	Injection kicker delay
t_{diff_sync}	Time difference between rf systems of two synchrotrons after the synchronization
$\Delta\varphi 1$	Phase difference between the Reference RF Signal and the Synchronization Reference Signal of the source synchrotron, measured by PAM module
$\Delta\varphi 2$	Phase difference between the Reference RF Signal and the Synchronization Reference Signal of the target synchrotron, measured by PAM module
$\psi 1$	Phase difference between the Reference RF Signal and the Synchronization Reference Signal of the source synchrotron at BuTiS T0 edges, predicted by PAP module
$\psi 2$	Phase difference between the Reference RF Signal and the Synchronization Reference Signal of the target synchrotron at BuTiS T0 edges, predicted by PAP module
$f_{normalized}$	Normalized rf frequency modulation profile, preloaded from SM
f_{actual}	Actual rf frequency modulation profile, calculated by PSM
T_{sync_win}	Length of the synchronization window

List of Symbols

$\Delta\theta$	Mismatch between the bunch and bucket center
Δf	Beating frequency
t_{v_emg}	Time corresponds to the distance between the virtual RF cavity and the emergency extraction position of SIS100
t_{emg}	Extraction kicker delay of SIS100
h^X	X=l, Cavity harmonic of large synchrotron; X=s, Cavity harmonic of small synchrotron
$\alpha_b(\phi_s)$	Bucket area factor
ϕ_s	Synchronous phase
Q_x	Horizontal chromaticity
Q_y	Vertical chromaticity
ΔQ_x	Horizontal chromatic tune shift due to the rf frequency modulation
ΔQ_y	Vertical chromatic tune shift due to the rf frequency modulation
t_{best}	Best estimate of alignment of zero crossing points of Reference RF Signals of source and target synchrotrons
δt_{best}	Uncertainty of the best estimate of alignment of zero crossing points of Reference RF Signals of source and target synchrotrons
$\psi_{h=1}^{SIS100}$	Predicted SIS100 h=1 rf phase at t_ψ
h	Harmonic number of the rf signal
$\psi_{h=1/5}^{SIS18}$	Predicted SIS18 h=1/5 rf phase at t_ψ
t_ψ	Time of the predicted phase
$\phi_{h=2}^{SIS18}$	RF phase at the cavity frequency h=2 of SIS18 at t_ψ

List of Symbols

$\phi_{h=10}^{SIS100}$	RF phase at the cavity frequency h=10 of SIS100 at t_ψ
δt_ψ	Uncertainty of the predicted phase advance at time domain
$\delta\psi_{h=1}^{SIS100}$	Uncertainty of the predicted SIS100 rf phase at h=1
$\delta\psi_{h=1/5}^{SIS18}$	Uncertainty of the predicted SIS18 rf phase at h=1/5
$\delta\phi_{h=10}^{SIS100}$	Uncertainty of RF phase at the cavity frequency h=10 of SIS100
$\delta\phi_{h=2}^{SIS18}$	Uncertainty of RF phase at the cavity frequency h=2 of SIS18
$T_{phase_shift}^{upper_bound}$	Upper bound time of the phase shift process
$\delta T_{phase_shift}^{upper_bound}$	Uncertainty of the upper bound time of the phase shift process
$\Delta\phi_{adjustment}$	Phase adjustment of the frequency beating method, calculated by B2B source SCU
$\psi_{s_alignment}$	RF phase of the cavity driving frequency at the start of the probable rang of alignment
$\Delta t_{win_correct}$	Time correction for the start of the probable range of alignment $[t_{best}-\delta t_{best}, t_{best}+\delta t_{best}]$ to the best estimate of the start of the synchronization window
G	Bunch gap
L	Distance from the leftmost to the rightmost SIS18 extraction/SIS100 injection kicker unit
D	Sum distance of d and the 2nd crate
d	Distance between two extraction kicker crates of SIS18
c	Speed of the light
t_{B2B}	Start time of the B2B transfer

List of Symbols

Δt	Beating time for the synchronization
$\Delta\phi_s(t)$	Change of the synchronous phase
$\Delta\phi_{shift}$	Phase shift to be achieved by the phase shift method
$\Delta f_{rf}(t)$	Rf frequency modulation for the phase shift method
T_{rev}^X	Period of the revolution period of machine X
T_{rf}^X	Period of the cavity frequency of machine X
C^X	X=l, Circumference of the injection/extraction orbit of large synchrotron; X=s, Circumference of the injection/extraction orbit of small synchrotron
f_{rev}^X	oder $f_{h=1}^X$. X=l, Revolution frequency of large synchrotron; X=s, Revolution frequency of small synchrotron
f_{rf}^X	oder $f_{h=cavity_harmonic}^X$. X=l, Cavity frequency of large synchrotron; X=s, Cavity frequency of small synchrotron
κ	Integer, m and n are also integer
λ	Decimal
Y	Greatest common divisor
T	Period of rf frequency modulation for the phase shift method
t_0	Start time of the rf frequency modulation for the phase shift method

Chapter 1

Introduction

The rf system provides longitudinal focusing which constrains the particle motion in the longitudinal phase space to a confined region. The confined region is called the “rf bucket” [2]. The “bunch” is the collection of particles captured within one rf bucket [2]. The bunch-to-bucket (B2B) transfer is transferring bunches from a source ring accelerator into the center of specified buckets of a target ring accelerator.

The bunch-to-bucket transfer is best described in the picture of James Bond jumping from a truck to catch the fast rope of a helicopter, see Fig. 1.1. The bucket of the source ring accelerator is regarded as the truck and James Bond as a bunch within this bucket. The helicopter is seen as a bucket of the target ring accelerator. The truck and the helicopter must move at constant speed (the bunch-to-bucket transfer only when the rf frequencies of two rf systems of the source and target ring accelerators are constant). They should have the same speed. If the truck moves with 600 km/h and the helicopter with 600 km/h, then James Bond won’t survive (the bunches and the buckets are with same speed, namely two rf systems have correct frequencies). They must be of the right relative position, so that James Bond will catch the fast rope, when he jumps (the phase difference between two rf systems must be correct). Of course the time of James Bond’s jump is of extreme importance (the bunches must be injected into the correct buckets).



Figure 1.1: Bunch-to-bucket transfer described in the picture of James Bond jumping from a truck to a helicopter

CHAPTER 1. INTRODUCTION

FAIR¹, Facility for Antiproton and Ion Research, is a new international accelerator facility under construction at GSI Helmholtz center for Heavy Ion Research GmbH (short: GSI)² [3, 4]. It is aiming at providing high-energy beams of ions from antiprotons to uranium with high intensities. The new FAIR accelerator complex with storage rings consists of SIS100, SIS300, Collector Ring CR, accumulator/decelerator ring RESR, New Experimental Storage Ring NESR and High Energy Storage Ring HESR [5, 6]. FAIR has so many rings, so the bunch-to-bucket transfer among FAIR ring accelerators is of great importance to accelerate beam to higher energy and achieve beam for various experiments. Based on the existing GSI UNILAC and SIS18 serving as injectors, high intensity ion beams over the whole range of stable isotopes will be accelerated in the new heavy ion machine SIS100/SIS300 to higher energies. The beam from SIS100 will be transferred to CR via Pbar or Super-Fragment Separator³. CR has the purpose of stochastic precooling of both secondary rare isotope and antiproton beams and of measuring nuclear masses in an isochronous mode [7, 8]. The CR transfers the beam to HESR and further to RESR for the accumulation. HESR serves experiments with high energy antiprotons and rare isotope beams [9]. The proton and heavy ion beam is transported from SIS18 to the existing GSI Experimental Storage Ring (ESR) and further to the first FAIR-storage ring CRYRING@ESR for the atomic and nuclear physics experiment [10, 11]. The proton and heavy ion could also be transferred from SIS18 to ESR via the Fragment Separator (FRS)⁴. The FAIR B2B transfer system in this dissertation focuses first of all on the transfer from SIS18 to SIS100, but it will be firstly tested for the transfer from SIS18 to ESR and further to CRYRING@ESR.

Nowadays, there are several accelerator institutes in the world, who operate the bunch-to-bucket transfer for specific purposes.

CERN, the European Organization for Nuclear Research, is one of the world's largest and most respected centres for scientific research. At CERN, the world's largest and most complex scientific instruments are used to study the laws of nature.

The LHC proton beam injection chain achieves the proton beam with the energy of 7 TeV. From a source, protons are injected into a linear accelerator, LINAC-2. Protons are accelerated to an kinetic energy of 50 MeV. Pre-accelerated proton bunches are then injected into the first synchrotron of the chain, namely Proton Synchrotron Booster (PSB). The PSB is composed of four identical rings stacked on the top of one another. This acceleration stage carries the proton bunches up to 1.4 GeV. The protons with an energy of 1.4 GeV are injected into the Proton Synchrotron (PS), which accelerates the protons to the energy of 25 GeV. The proton beams are further transferred to the Super Proton Synchrotron (SPS), which served as the final injector for high-intensity proton beams for the Large Hadron Collider (LHC) [12].

The LHC heavy ion beam injection chain achieves the heavy ion with the energy of 2.76 TeV/u. Heavy ions like lead and argon ions are produced by an ECR ion source⁵ and sent to LINAC-3 to reach the energy of 4.2 MeV/u, which is required

¹https://en.wikipedia.org/wiki/Facility_for_Antiproton_and_Ion_Research

²Planckstrasse 1, 64291 Darmstadt, www.gsi.de

³<http://www.fair-center.eu/public/experiment-program/nustar-physics/superfrs.html>

⁴An ion-optical device used to focus and separate products from the collision of relativistic ion beams with thin targets.

⁵https://en.wikipedia.org/wiki/Electron_cyclotron_resonance

CHAPTER 1. INTRODUCTION

for injection into the Low Energy Ion Ring (LEIR). The LEIR injects ion beam in the PS at the energy of 72.2 MeV/u. The beam is accelerated to the energy of 5.9 GeV/u and than transferred to SPS. SPS accelerated the beam to 177 GeV/u and SPS transfers the beam further to LHC [12].

J-PARC, Japan Proton Accelerator Complex, is a high-intensity proton accelerator to provide various secondary particles for a variety of experiments. The J-PARC accelerator consists of the Linac, the Rapid Cycle Synchrotron (RCS) and the Main Ring (MR). The Linac accelerates negative hydrogen ions up to 181 MeV to inject to the RCS. The negative ions are converted to protons at the injection point of the RCS by a charge-stripping foil. The RCS accelerates protons up to 3 GeV, then extract them to the Material and Life science Facility (MLF) and the MR. The MR accelerates the protons up to 30 GeV, then extract in one turn to a target [13].

BNL, Brookhaven National Laboratory, specializes in high energy physics, energy technologies, environmental science, and nanotechnology. High energy physics of BNL studies the nature of the particles that constitute matter and radiation . The BNL accelerator complex contains Linac, Booster, Alternating Gradient Synchrotron (AGS) and Relativistic Heavy Ion Collider (RHIC). The Booster accepts ions from Electron Beam Ion Source (EBIS) and protons from the LINAC, and accelerates the beam to the minimum AGS energy before injecting it into the AGS for further acceleration and delivery to RHIC ring [14].

Fermi National Accelerator Laboratory's accelerator complex comprises seven particle accelerators and storage rings. It produces powerful, high-energy neutrino beam and provides proton beams for a broad range of new and existing experiments. Proton beams enter the Fermilab Booster from the Linac, accelerating to an energy of 8 GeV. The Recycler is a kind of staging area for proton beams after they exit the Booster. Once beam enters the Recycler, protons form a more intense beam with the energy of 8 GeV. Then the proton beam enters the Main Injector, which situated directly beneath the Recycler. The beam is accelerated to the energy of 120 GeV. Some of the proton beam from the Booster will be used to produce pions in a specially designed target system. These pions will then decay into particles called muons. These muons will be injected into Muon Delivery Ring. The Muon Delivery Ring delivers these muons into a muon storage ring for further study [15].

IMP, Institute of Modern Physics of the Chinese Academy of Sciences, operates the Heavy Ion Research Facility (HIRFL) in Lanzhou. HIRFL is used to conduct fundamental research in nuclear and atomic physics, which consists of the Sector Focusing Cyclotron (SFC), the Separated Sector Cyclotron (SSC), the Cooler Storage Ring (CSR) and a number of experimental terminals. CSR includes a main ring (CSRm), an experimental ring (CSRe) and radioactive beam line to connect the two rings. The two existing cyclotrons SFC and SSC will be used as its injector system for CSRm, which is able to accumulate, cool and accelerate beam to higher energy. Then the beam is extracted to produce radioactive ion beams or highly-charged heavy ions. The radioactive ion beams or highly-charged heavy ions can be transferred to CSRe for many experiments [16, 17].

1.1 First overview of the FAIR bunch-to-bucket transfer system

From the example of James Bond, we know several precondition for the B2B transfer. The first precondition is that the bunch of the source ring and the bucket of the target ring have a constant speed, namely the rf frequency of two rf systems of the source and target ring accelerators must be constant. The second one is that the bunch and bucket are with same speed, which requires that two rf systems must have correct frequencies.

In order to transfer bunches to buckets, two rf systems must have correct phase difference. The process of achieving the correct phase difference is named as “synchronization”. There are two methods for the synchronization. The synchronization is achieved by an azimuthal positioning of the bunch in the source synchrotron or the bucket in the target synchrotron. This is so-called ”phase shift method”. When two rf frequencies are slightly different, they are beating, perceived as periodic variations in phase difference, whose rate is the difference between the two frequencies. The synchronization is automatically achieved. This is so-called ”frequency beating method”. The phase shift method provides a theoretically infinite time frame for the B2B transfer and the frequency beating method provides a finite time frame, within which bunches could be transferred into buckets with the bunch-to-bucket center mismatch smaller than the upper bound $\pm 1^\circ$. The time frame is called “synchronization window”, which achieves the “coarse synchronization”.

The bunch are switched from one path to another path by dipole magnets, which are called “kicker magnet” or “kicker”. The extraction kicker kicks the bunch out of the source ring and the injection kicker kicks the bunch in the target ring. After the synchronization between two rf systems, the extraction kicker must kick the bunch in the source ring at the exact time-of-flight between two rings before the center of a specific bucket passes the injection kicker. With the synchronization window, the extraction and injection kickers must be fired at the correct time in order to transfer bunches into correct buckets. The process of the kicker firing at the correct time is called “fine synchronization”.

1.2 Objectives, Contribution and Structure of the Dissertation

This dissertation contributes to the development of the FAIR B2B transfer system from the timing perspective. It concentrates on the introduction of the concept of the system and its application for FAIR accelerators. In addition, it explains the systematic investigation of the FAIR B2B transfer system in details.

The dissertation is structured as follows and as depicted in Fig. 1.2.

1.2. Objectives, Contribution and Structure of the Dissertation

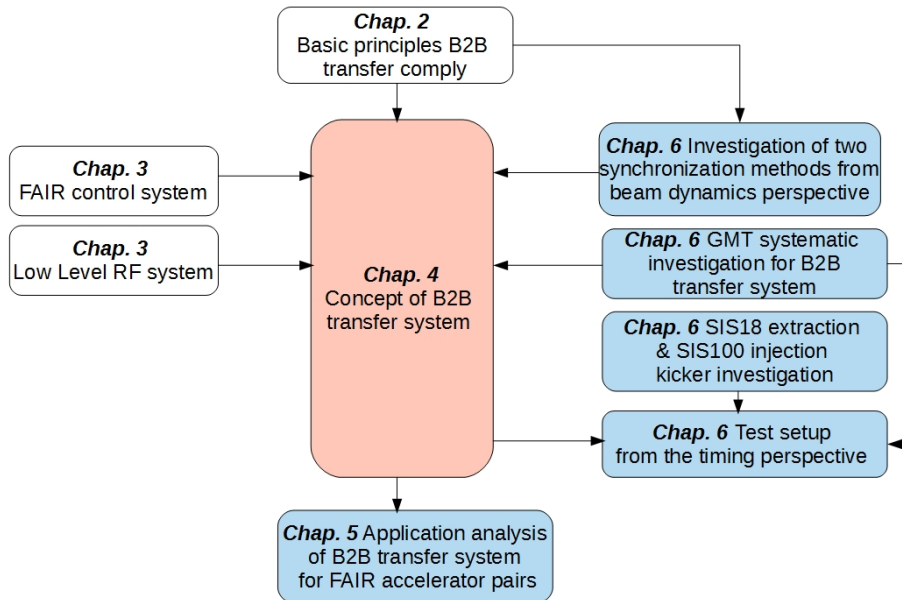


Figure 1.2: Structure of the dissertation.

Contributions are marked blue and red is team work; existing system or theory are not colored.

In Chap.2 the basic principles for the B2B transfer are reviewed. First of all, the energy match between the source and target synchrotrons is introduced. Secondly, two rf synchronization methods are discussed from the perspective of beam dynamics in order for the phase match. Once more, the bucket label and the extraction/injection kicker synchronization are discussed. At the end of this chapter, the beam indication for the beam instrumentation is mentioned.

Chap.3 is concerned with the existing FAIR technical basis for the development of the B2B transfer system and the uniqueness of the system. The B2B transfer system is realized based on the FAIR control system and Low-Level rf system, so these two systems are introduced. In addition, the uniqueness of the B2B transfer system for FAIR is discussed before the chapter ends.

In Chap.4, a brief overview on the basic idea of the B2B transfer system is presented. After that the basic procedure of the B2B transfer is introduced and the realization of each step of the procedure. In addition, the B2B transfer system is explained from the data/signal flow perspective.

The application of the B2B transfer system for FAIR accelerators are outlined in Chap.5. The applications are classified into two categories according to the feature of the circumference ratio. The ratio of the circumference between many pair of machines in FAIR is not a perfect integer, e.g. SIS18 and ESR (injection orbit), SIS100 and CR, CR and HESR. So the frequencies of two synchrotrons begin beating automatically. For the pairs with the perfect integer ratio of the circumference, e.g. SIS18 and SIS100, the rf frequency of one synchrotron is detuned to get the frequency beating. For each category, the corresponding FAIR applications are presented.

Chap.6 presents the systematic investigation for the B2B transfer system, mainly focusing on the timing aspect. The calculation of the synchronization window is explained and the transfer of the B2B messages via the WR network is tested. In addition, for the B2B transfer from SIS18 to SIS100, two synchronization methods are analyzed from the perspective of beam dynamics. The SIS18 extraction and

1.2. Objectives, Contribution and Structure of the Dissertation

SIS100 injection kicker are systematically investigated. Finally, the test setup is presented and the result is analyzed.

Chapter 2

Theoretical background

Transferring bunches of particles from a synchrotron into specified buckets of another synchrotron has several underlying basic principles. The energy of the beam is same before and after the B2B transfer, so the energy of the source synchrotron must first of all match that of the target synchrotron. Principally speaking, every synchrotron has its independent RF system. Then the phase advance between the bunch and the bucket must be precisely controlled before the bunch is ejected. The process of achieving the detailed phase adjustment between two RF systems is termed "RF synchronization". For the correct bucket injection, the filled buckets and the bucket to be filled must be marked. The bunch fast extraction must happen exactly one "time of flight" before the required bucket of the target synchrotron passes the injection region. The injection kicker must kick when the bucket passes the injection region. In this chapter, all of the B2B basic principles will be explained.

2.1 Energy match, Phase match and voltage match

The bunch coordinates in the longitudinal phase plane of the source synchrotron, just before transfer, must be accurately controlled, according to the bucket to be filled [18]. The energy of a beam is determined by the 'magnetic rigidity', which is defined as the following:

$$B(t)\rho_0 = \frac{p(t)}{e} \quad (2.1)$$

where $p(t)$ is the magnitude of the particle momentum, e is the charge of the particle, $B(t)$ is magnetic field, and ρ_0 is the bending radius of a particle immersed in a magnetic field $B(t)$. The ratio of $p(t)$ to e describes the 'stiffness' of a beam, it can be considered as a measure of how much angular deflection results when a particle travels through a given magnetic field [19].

The bunch is transferred from the source to the target synchrotron with the same energy. So the beam has the same momentum and velocity for both synchrotrons. According to eq. 2.1, the magnetic rigidity of two synchrotrons must be matched:

$$B^{src}(t)\rho_0^{src} = \frac{p}{e} = B^{trg}(t)\rho_0^{trg} \quad (2.2)$$

Where the superscript of the symbol denotes the synchrotron, "src" represents the source synchrotron and "trg" the target synchrotron.

2.4. RF synchronization

Besides, the rf frequency of two synchrotrons must meet the following relation [18].

$$C^{src} \frac{f_{rf}^{src}(t)}{h^{src}} = \beta c = C^{trg} \frac{f_{rf}^{trg}(t)}{h^{trg}} \quad (2.3)$$

where C is the circumference of the synchrotron, h the harmonic number of the rf signal and f_{rf} denotes the cavity rf frequency, β the fraction of the particle velocity to the lightspeed.

2.2 Loop freeze

During the B2B transfer process, feedback loops for the deviations correction of the particles from reference states (e.g. position and velocity) must switch off or freeze. E.g. Beam phase feedback loop [20] and bunch-by-bunch longitudinal rf feedback loop [21].

2.3 Phase difference between two RF systems

For the RF synchronization between two synchrotrons, the prerequisite is to know the phase difference between two independent RF systems.

2.4 RF synchronization

There are usually two methods available for the synchronization process. The synchronization is achieved by an azimuthal positioning of the bunch in the source synchrotron or the bucket in the target synchrotron. This is so-called "phase shift method". When two rf frequencies are slightly different, they are beating, perceived as periodic variations in phase difference, whose rate is the difference between the two frequencies. The synchronization is automatically achieved. This is so-called "frequency beating method". Both methods provide a time frame for the B2B transfer, within which a bunch could be transferred into a bucket with the bunch-to-bucket center mismatch smaller than the upper bound. The time frame is called "synchronization window".

For both methods, the accompanying beam dynamics must be taken into consideration. The momentum of particle is given by

$$p(t) = e\rho_0 \left[\frac{R(t)}{R_0} \right]^{1/\alpha_p} B(t) \quad (2.4)$$

where R_0 is its nominal value, $R(t)$ the orbit radius, $B(t)$ the magnetic field and α_p , the momentum compaction factor. From eq. 2.4, the first-order total differential of $p(t)$ is given as

$$dp(t) = \frac{e\rho_0}{\alpha_p(R_0)^{1/\alpha_p}} B(t) R(t)^{1/\alpha_p - 1} dR(t) + e\rho_0 \left[\frac{R(t)}{R_0} \right]^{1/\alpha_p} B(t) dB(t) \quad (2.5)$$

2.4. RF synchronization

Dividing both sides of eq. 2.5 by $p(t)$, we obtain

$$\frac{dp(t)}{p(t)} = \gamma_t^2 \frac{dR(t)}{R(t)} + \frac{dB(t)}{B(t)} \quad (2.6)$$

Now, for circular accelerators, the following general relation holds

$$f(t) = \frac{v(t)}{2\pi R(t)} \quad (2.7)$$

where $f(t)$ is the revolution frequency and $v(t)$ the velocity. The total differential of $f(t)$ is given by

$$df(t) = \frac{1}{2\pi} \left[\frac{dv(t)}{R(t)} - \frac{v(t)}{R^2(t)} dR(t) \right] \quad (2.8)$$

Dividing both sides of eq. 2.8 by $f(t)$ yields

$$\frac{df(t)}{f(t)} = \frac{dv(t)}{v(t)} - \frac{dR(t)}{R(t)} \quad (2.9)$$

The fractional change in $v(t)$ is related to the fractional change in $p(t)$:

$$\frac{dp(t)}{p(t)} = \gamma^2(t) \frac{dv(t)}{v(t)} \quad (2.10)$$

where $\gamma(t)$ is the relativistic factor, which measures the total particle energy, $E(t)$, in units of the particle rest energy, E_0 . Solving $dv(t)/v(t)$ from eq. 2.10 and substituting it into eq. 2.9 yields

$$\frac{df(t)}{f(t)} = \gamma^2(t) \frac{dp(t)}{p(t)} - \frac{dR(t)}{R(t)} \quad (2.11)$$

Replacing $dp(t)/p(t)$ in eq. 2.11 with eq. 2.6, we have

$$\frac{df(t)}{f(t)} = \gamma^2(t) \frac{dB(t)}{B(t)} + \left[\frac{\gamma_t^2}{\gamma^2(t)} - 1 \right] \frac{dR(t)}{R(t)} \quad (2.12)$$

where γ_t is the transition gamma, which is related to α_p as $\gamma_t = 1/\sqrt{\alpha_p}$. In the same way, solving $dR(t)/R(t)$ from eq. 2.6 and substituting it into eq. 2.11, we obtain

$$\frac{df(t)}{f(t)} = \left(\frac{1}{\gamma^2(t)} - \frac{1}{\gamma_t^2} \right) \frac{dp(t)}{p(t)} + \frac{1}{\gamma_t^2} \frac{dB(t)}{B(t)} \quad (2.13)$$

where $\eta(t)$ is the phase-slip factor defined as

$$\eta(t) = \frac{1}{\gamma^2(t)} - \frac{1}{\gamma_t^2} = \alpha_p - \frac{1}{\gamma_t^2} \quad (2.14)$$

Of the four variables, $f(t)$, $B(t)$, $p(t)$ and $R(t)$, only two are independent. This leads to four very useful differential relations, eq. 2.6, eq. 2.11, eq. 2.12 and eq. 2.13 [22, 23].

2.4. RF synchronization

2.4.1 Phase shift method

The rf system of the source or target or both synchrotrons are modulated away from their nominal value for a period of time and then modulated back so that the phase shift created by the frequency modulation could compensate for the expected phase difference.

Eq. 2.15 gives the relation between the required phase shift $\Delta\phi_{shift}$ and the frequency modulation.

$$\Delta\phi_{shift} = 2\pi \int_{t_0}^{t_0+T} \Delta f_{rf}(t) dt \quad (2.15)$$

The required phase shift is determined by the frequency offset $\Delta f_{rf}(t)$ and the duration of the frequency modulation T . For the RF synchronization, the maximum phase shift required of one synchrotron is one bucket length of the other synchrotron, 360° . Because the phase can be shifted backward or forward, a phase shift of up to $\pm 180^\circ$ can be implemented.

After the phase shift, the bunches of the source synchrotron are synchronized with random buckets of the target synchrotron. Theoretically the synchronization window is infinitely long by the phase shift method. The beam feedback loop on the rf system is frozen or switched off during the B2B transfer, the beam is stable for short time, e.g. 10 ms. So the bunch must be transferred as early as possible. Besides, the length of the synchronization window equals to a sequence of all buckets, which guarantees the possibility to transfer bunch into all buckets. The phase shift process must be performed adiabatically for the longitudinal emittance to be preserved.

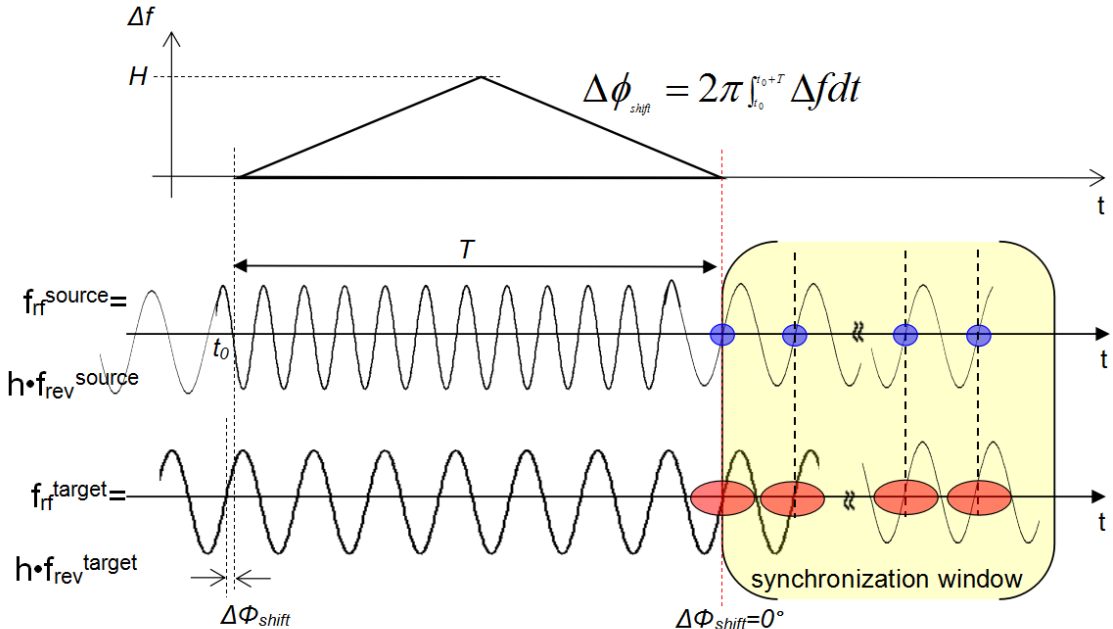


Figure 2.1: The illustration of the phase shift method.

Fig. 6.12 illustrates the phase shift method. The first and second sinusoidal signals are RF signals respectively from the source and target synchrotrons. For

2.4. RF synchronization

the phase shift method two RF signals are of the same frequency. The blue dots show the position of the bunches of the source synchrotron, the red dots correspond to the bucket positions of the target synchrotron. The time-of-flight between the bunch and bucket is compensated here. The red dashed line shows the end of the phase shift process ($\Delta\phi_{shift} = 0^\circ$) and the beginning of the synchronization window, drawn in yellow. After the phase shift, bunches match with the random buckets. The triangle frequency modulation is used as an example for the phase shift. Based on eq. 2.15, the area of the triangle equals to $\Delta\phi_{shift}/2\pi$, see eq. 2.16. The base of the triangle is T , the height of the triangle is determined by eq. 2.17.

$$\frac{\Delta\phi_{shift}}{2\pi} = \frac{1}{2}TH \quad (2.16)$$

$$H = \frac{\Delta\phi_{shift}}{\pi T} \quad (2.17)$$

A particular case of the B2B synchronization occurs, when the target synchrotron is empty, i.e. it did not capture any bunch yet, the phase shift can be done for the target synchrotron without adiabatical consideration (e.g. Phase jump is possible).

Now we analyze the rf frequency modulation of the phase shift from the beam dynamics viewpoint.

- Radial excursion and momentum shift due to rf frequency modulation

$$f(t) = \frac{\beta c}{2\pi R(t)} \quad (2.18)$$

The differential of eq. 2.18 is

$$\frac{df(t)}{f(t)} = \frac{d\beta(t)}{\beta(t)} - \frac{dR(t)}{R(t)} \quad (2.19)$$

The beam momentum and its differential are related to β and $d\beta$ as follows:

$$p = \gamma\beta m_0 c \quad (2.20)$$

$$\left(\frac{p}{m_0 c}\right)^2 = \frac{\beta^2}{1 - \beta^2} \quad (2.21)$$

$$\left(\frac{dp(t)}{p(t)}\right)^2 = \gamma^2 \frac{d\beta(t)}{\beta(t)} \quad (2.22)$$

Substituting $d\beta(t)/\beta(t)$ into eq. 2.19, we get

$$\frac{df(t)}{f(t)} = \frac{1}{\gamma^2} \frac{dp(t)}{p(t)} - \frac{dR(t)}{R(t)} \quad (2.23)$$

For the constant magnetic field, a particle will have a different orbit, if it is slightly shifted in momentum. The “momentum compaction factor” is defined as:

$$\alpha_p = \frac{dR(t)/R(t)}{dp(t)/p(t)} \quad (2.24)$$

2.4. RF synchronization

The transition gamma γ_t is related to α_p as $\gamma_t = 1/\sqrt{\alpha_p}$.

Substituting eq. 2.24 into eq. 2.23, we get respectively the accompanying radial excursion and momentum shift by the frequency modulation.

$$\frac{\Delta f(t)}{f(t)} = \left(\frac{\gamma_t^2}{\gamma^2} - 1\right) \frac{\Delta R(t)}{R(t)} \quad (2.25)$$

and

$$\frac{\Delta f(t)}{f(t)} = \left(\frac{1}{\gamma^2} - \frac{1}{\gamma_t^2}\right) \frac{\Delta p(t)}{p(t)} \quad (2.26)$$

- Transverse dynamics analysis

The momentum spread $\Delta p/p \neq 0$ during the phase shift process causes chromaticity drift ΔQ . Q is the chromaticity of the machine [24].

$$\Delta Q = Q \cdot \frac{\Delta p}{p} \quad (2.27)$$

- Shift of synchronous phase

The synchronous phase deviates from 0° during the frequency modulation. From the expression of the particle momentum, $p(t)$, given in eq. 2.4, the time derivative of $p(t)$ can be written as

$$\frac{dp(t)}{dt} = \frac{e\rho_0 B(t)}{\alpha_p R_0^{1/\alpha_p}} R(t)^{1/\alpha_p - 1} \frac{dR(t)}{dt} + e\rho_0 \left(\frac{R(t)}{R_0}\right)^{1/\alpha_p} \frac{dB(t)}{dt} \quad (2.28)$$

Now, the relationship between the rate of change in momentum of a particle, $dp(t)/dt$, and the force applied on it, $F(t)$, is governed by Newton's second law:

$$\frac{dp(t)}{dt} = F(t) \quad (2.29)$$

$F(t)$ is given by the product of the accelerating electric field, $E(t)$, and the charge of particle, e . Substituting $dp(t)/dt$ given in eq. 2.28 and $F(t) = eE(t)$ into eq. 2.29, we have

$$\frac{e\rho_0 B(t)}{\alpha_p R_0^{1/\alpha_p}} R(t)^{1/\alpha_p - 1} \frac{dR(t)}{dt} + e\rho_0 \left(\frac{R(t)}{R_0}\right)^{1/\alpha_p} \frac{dB(t)}{dt} = eE(t) \quad (2.30)$$

From this equation, we obtain the expression of energy gain in one turn,

$$2\pi R_0 \left[\frac{e\rho_0 B(t)}{\alpha_p R_0^{1/\alpha_p}} R(t)^{1/\alpha_p - 1} \frac{dR(t)}{dt} + e\rho_0 \left(\frac{R(t)}{R_0}\right)^{1/\alpha_p} \frac{dB(t)}{dt} \right] = eV(t) \sin[\phi_{s0}(t) + \Delta\phi_s(t)] \quad (2.31)$$

where $V(t)$ is the RF accelerating voltage per turn; ϕ_{s0} , the synchronous phase in the operation with no frequency modulation; and $\Delta\phi_s(t)$, the change in the synchronous phase originating from the rf frequency modulation.

The magnetic field is not affected by the frequency change, we can assume $dB(t)/dt = 0$. Before the synchronization, it is a stationary bucket with the synchronous phase 0° . Then, eq. 2.31 reduce to

$$2\pi R_0 \left[\frac{e\rho_0 B(t)}{\alpha_p R_0^{1/\alpha_p}} R(t)^{1/\alpha_p - 1} \frac{dR(t)}{dt} \right] = eV(t) \sin[\Delta\phi_s(t)] \quad (2.32)$$

2.4. RF synchronization

Solving $\Delta\phi_s(t)$ from eq. 2.32, we have

$$\Delta\phi_s(t) = \sin^{-1} \left[\frac{2\pi\rho_0 B}{\alpha_p V} \left(\frac{R(t)}{R_0} \right)^{1/\alpha_p - 1} \frac{dR(t)}{dt} \right] \quad (2.33)$$

From eq. 2.33, we know that $\Delta\phi_s(t)$ is only determined by $dR(t)/dt$ during the frequency modulation.

- Bucket area factor

At the flattop, the bucket is a stationary bucket with $\phi_{s0}(t) = 0$. During the frequency modulation process, the bucket becomes a running bucket with $\Delta\phi_s(t) \neq 0$. The ratio of bucket areas of a running bucket to a stationary bucket is bucket area factor $\alpha(\Delta\phi_s)$. The bucket area factor could be estimated by [25].

$$\alpha_b(\Delta\phi_s) \approx (1 - \sin(\Delta\phi_s))(1 + \sin(\Delta\phi_s)) \quad (2.34)$$

- Adiabaticity analysis

$\omega_s(t)$ is the small-amplitude synchrotron frequency given by

$$\omega_s(t) = \left[-\frac{\eta(t) h \omega_{rev}^2(t) e V(t) \cos\phi_s(t)}{2\pi\beta^2(t) E(t)} \right]^{1/2} \quad (2.35)$$

A process is called “adiabatic” when the RF parameters are changed slowly enough for the longitudinal emittance to be preserved. The condition that the parameters are slowly varying can be expressed by

$$\varepsilon = \frac{1}{\omega_s^2(t)} \left| \frac{d\omega_s(t)}{dt} \right| \ll 1 \quad (2.36)$$

Compared with $\phi_s(t)$, all of the other variables change very slowly. $\phi_s(t) = \phi_{s0}(t) + \Delta\phi_s(t)$. From eq. (2.36) and eq. (2.35), we can write the adiabaticity parameter ε , as follows [22]:

$$\varepsilon \approx \frac{1}{2\omega_{s0}(t)} \left| \tan\phi_s(t) \frac{d\phi_s(t)}{dt} \right| \quad (2.37)$$

- Constraints on the RF frequency modulation

From eq. 2.37, we can clearly see that $\phi_s(t)$ and $d\phi_s(t)/dt$ play deterministic roles for the adiabaticity when the frequency is modulated. Now let us deduce how the rf frequency modulation affects $\phi_s(t)$ and $d\phi_s(t)/dt$. From eq. (2.25), we could get the following equation.

$$\frac{dR(t)}{dt} \left(\frac{\gamma_t^2}{\gamma^2} - 1 \right) f_0 = \frac{df(t)}{dt} R_0 \quad (2.38)$$

Substituting eq. 2.38 into eq. 2.32, we get

$$V \sin\phi_s = \frac{2\pi R_0 \rho B}{f_0 \left(\frac{1}{\gamma}^2 - \frac{1}{\gamma_t}^2 \right)} \left[\frac{R(t)}{R_0} \right]^{\left(\frac{1}{\alpha_p} - 1 \right)} \frac{df(t)}{dt} \quad (2.39)$$

2.4. RF synchronization

Because $(R(t) - R_0)/R_0$ is about 10^{-4} , $[1 + \frac{\Delta R}{R_0}]^{(\frac{1}{\alpha_p} - 1)} \approx 1$. We can get the relation between $df(t)/dt$ and ϕ_s from eq. 2.39.

$$V \sin \phi_s = \frac{2\pi R_0 \rho B}{f_0 (\frac{1}{\gamma}^2 - \frac{1}{\gamma_t}^2)} \frac{df(t)}{dt} \quad (2.40)$$

From eq. 2.34, we know that the bucket area factor is determined by the synchronous phase change $\Delta\phi_s$. Based on eq. 2.40, we know the synchronous phase $\Delta\phi_s$ is determined by $df(t)/dt$, so $df(t)/dt$ is important for the bucket size.

In order to get the relation between $d\phi_s(t)/dt$ and the frequency modulation, we get the time derivative of eq. 2.40

$$V \cos \phi_s \frac{d\phi_s}{dt} = \frac{2\pi R_0 \rho B}{f_0 (\frac{1}{\gamma}^2 - \frac{1}{\gamma_t}^2)} \frac{df(t)/dt}{dt} \quad (2.41)$$

Based on the adiabaticity eq. (2.37), $d\phi_s(t)/dt$ must be existing and small enough. So $\frac{df(t)/dt}{dt}$ must be existing and small enough. It means that $df(t)/dt$ and $\phi_s(t)$ must be continuous. In a word, there are three constraints for the rf frequency modulation.

- The $df(t)/dt$ of the rf frequency modulation must be small enough to guarantee the bucket size.
- The $df(t)/dt$ of the rf frequency modulation must be continuous to guarantee the continuous synchronous phase.
- The $df(t)/dt/dt$ of the rf frequency modulation must be small enough to guarantee the change of the synchronous phase slow enough for the beam to follow.

2.4.2 Frequency beating method

The frequency beating method uses the effect of two RF signals of slightly different frequencies, perceived as periodic variations in phase difference whose rate is the difference between the two frequencies. The RF frequency of the source or the target or both synchrotrons is detuned long before the ejection, then the difference between the phase of the bunch and bucket is measured. Based on the measured phase, the synchronization is realized when the phase difference of the two RF frequencies corresponds to the ideal phase difference ($\Delta\theta = 0^\circ$). The $\Delta\theta$ is the mismatch between the bunch center and the corresponding bucket center. Because of the slightly different RF frequencies, a mismatch between the bunch and bucket centers exists. In principle, the B2B transfer requirement for FAIR allows a bunch to bucket center mismatch of $\pm 1^\circ$, which brings a symmetric time frame with respect to the time of the ideal phase difference. This is called the maximum synchronization window, drawn in yellow, see Fig. 2.2. The red dashed line shows the time for the expected phase difference.

- For one bunch to one bucket injection per B2B transfer, the bunch is “perfectly” injected into the center of the bucket. The “perfect” injection does

2.4. RF synchronization

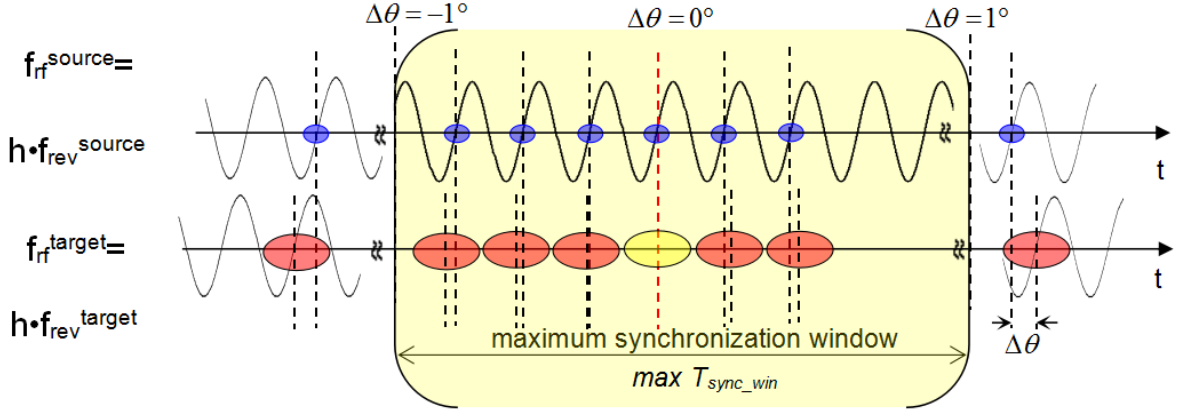


Figure 2.2: The illustration of the frequency beating method.

not mean that the bunch-to-bucket center mismatch $\Delta\theta$ is 0° . It means the smallest mismatch with regard to other injection. The “perfect” injection is determined by the beating speed and the initial phase difference between these two signals. The maximum initial phase difference $\Delta\varphi$ is calculated by eq. 2.42.

$$\frac{|1/(f_1 - f_2)|}{360^\circ} = \frac{1/f_1}{\Delta\varphi} \quad (2.42)$$

Where f_1 and f_2 are two slightly different RF frequencies, the beating frequency is expressed as $f_1 - f_2$.

When the initial phase difference is 0° , the “perfect” injection is with the mismatch $\Delta\theta = 0^\circ$.

When the initial phase difference is slightly less than $\Delta\varphi$, the “perfect” injection is with the mismatch $\Delta\theta$ slightly less than $\Delta\varphi$.

- For multi bunch to multi bucket injection per B2B transfer, only one bunch is “perfectly” injected into the corresponding bucket, which is represented by the yellow dot in Fig. 2.2. Other bunches on both side of this bunch (red dots) are injected into their corresponding buckets with the mismatch due to two slightly different frequencies. The maximum synchronization window is determined by the maximum tolerable bunch-to-bucket center mismatch $\pm 1^\circ$, see eq. 2.43.

$$\frac{|1/(f_1 - f_2)|}{360^\circ} = \frac{T_{sync_win}}{1^\circ - (-1^\circ)} \quad (2.43)$$

The RF frequency is detuned at the end of the ramp. During the RF frequency detune process, the magnetic field and radius excursion react to the frequency detune in order to guarantee the energy match.

- Longitudinal dynamics analysis

Because the momentum should not be affected by the frequency change, namely $\Delta p(t)=0$, we can get the general relation between the radial excursion and RF frequency change by substituting $\Delta p(t)=0$ into eq. 2.23.

$$\frac{\Delta f}{f} = -\frac{\Delta R}{R} \quad (2.44)$$

2.6. Synchronization of the extraction and injection kicker

Taking differentials of both sides of eq. 2.1 gives

$$\frac{\Delta\rho}{\rho} = \frac{\Delta p(t)}{p(t)} - \frac{\Delta B(t)}{B(t)} \quad (2.45)$$

The relation between $\Delta\rho/\rho$ and $\Delta R(t)/R(t)$ is

$$\frac{\Delta\rho}{\rho} = \gamma_t^2 \frac{\Delta R(t)}{R(t)} \quad (2.46)$$

Substituting eq. 2.46 into eq. 2.45, we could get

$$\gamma_t^2 \frac{\Delta R(t)}{R(t)} = \frac{\Delta p(t)}{p(t)} - \frac{\Delta B(t)}{B(t)} \quad (2.47)$$

Substituting $\Delta p = 0$ into eq. 2.47, we get

$$\gamma_t^2 \frac{\Delta R(t)}{R(t)} = \frac{\Delta B(t)}{B(t)} \quad (2.48)$$

Substituting eq. 2.48 into eq. 2.49, we get the general relation between the magnetic field change and RF frequency change.

$$\frac{\Delta f}{f} = \frac{1}{\gamma_t^2} \times \frac{\Delta B}{B} \quad (2.49)$$

2.5 Bucket label

After the synchronization, all bunches are synchronized to all RF buckets. For the proper injection, we must know which buckets are already filled and which buckets should be filled by next injection cycle. The fast extraction can only proceed when the required bucket comes.

2.6 Synchronization of the extraction and injection kicker

Kicker magnets (or kickers) are dipole magnets, which are used to rapidly switch a particle beam between two paths¹. After switching on, a kicker needs a certain period of time to reach a stable magnetic field. This period is called “rise time”. It must maintain a stable magnetic field for some minimum time, which is called “flat-top”. When the kicker is switched off, it needs also a certain period of time to reduce to zero magnetic field. This period is called “fall time”. The kicker time consists of the rise time, flat-top and fall time [26]. For the proper B2B transfer, the extraction and injection kickers must be synchronized with the beam.

¹https://en.wikipedia.org/wiki/Injection_kicker_magnets

2.7. Beam indication for the beam instrumentation

- Extraction kicker

An extraction kicker diverts a circulating beam to leave a synchrotron. Most commonly, an extraction kick is used to eject all bunches. If there is no empty RF bucket of the synchrotron, the rise time of the extraction kicker must be shorter than the area, which are without any bunches in a bunch train. It is called “bunch gap”. If there is at least one empty RF bucket, the rise of the magnetic field could be achieved within the gap of the empty RF buckets. The flattop has at least the length of all bunches to be extracted and the fall time is not constrained.

- Injection kicker

An injection kicker merges one beam into a circulating beam in a synchrotron. As soon as the tail of the circulating bunch has passed the kicker, the magenetic field is switched on. The magnet must then be switched off in time in order not to affect the head of the next coming bunch in the synchrotron.

For multi-batch injection, the rise time of the injection kicker must be shorter than the bunch gap. The flat-top is determined by the length of the bunches to be injected. If all buckets must be filled, the fall time must be shorter than the remaining time until the next circulating bunch passes the kicker. If the synchrotron needs only one time injection, the rise time is not constrained. The flat-top determined by the length of the bunches to be injected. The fall time must not exceed the bunch gap or the gap of the empty RF buckets.

2.7 Beam indication for the beam instrumentation

In order to observe the beams and measure related parameters for accelerators and transfer lines [27], the beam instrumentation (BI) equipments must be synchronized and triggered within the beam schedule. For the B2B transfer, the data acquisition for the beam instrumentation equipments should be triggered before the bunch is extracted. They should not be triggered too early because of the limitation of sampling time. So a pre-trigger is necessary, which indicates that the bunch will be extracted/injected soon.

Chapter 3

Technical basis for the B2B transfer system

For the FAIR accelerator complex, synchronization of the B2B transfer will be realized by the FAIR control system and the Low-Level RF (LLRF) system. For the synchronization of LLRF system, the General Machine Timing (GMT) system is complemented and linked to the Bunchphase Timing System (BuTiS). Machine Protection System (MPS) protects SIS100 and subsequent accelerators or experiments from damage. Hence, the B2B transfer system for FAIR coordinates with the MPS system.

3.1 FAIR control system

The FAIR control system takes advantage of collaborations with CERN in using framework solutions like Front-End System Architecture (FESA) [28], LHC Software Architecture (LSA), White Rabbit (WR) [29]. It consists of the equipment layer, middle layer and application layer. The equipment layer consists of equipment interfaces, GMT and software representations of the equipment FESA. The middle layer provides service functionality both to the equipment layer and the application layer through the IP control system network. LSA is used for the Settings Management (SM). The application layer combines the applications for operators as GUI applications or command line tools. The application layer and the middle layer only request what the FAIR accelerator complex should do and transmit set values to the equipment layer. The SM supplies the schedule for the GMT by LSA [29, 30].

3.1.1 BuTiS

Bunch Phase Timing System (BuTiS) serves as a campus-wide clocks distribution system with sub nanosecond resolution and stability over distances of several hundred meters while maintaining 100 ps per km timing stability [31]. Two BuTiS reference clocks 100 kHz P0 pulse and 10 MHz S1 phase reference signal are generated centrally in the BuTiS center. A star-shaped optical fiber BuTiS distribution system transfers these two reference clocks to the BuTiS local reference synthesizer all over the FAIR campus. The optical signal transmission delay between the BuTiS center and the different BuTiS local reference synthesizer is measured by a measurement setup in the BuTiS center. This measurement information is used to correct

3.1. FAIR control system

the phases of the signals generated in each BuTiS local reference synthesizer for the delay compensation. So at each BuTiS reference synthesizer, two delay compensated clock signals, 200 MHz C2 sine and 100 kHz T0 ident clocks, are generated from 100 kHz P0 and 10 MHz S1 reference clocks [31, 32]. The main task of BuTiS is the supply of the reference clock signals for Reference RF Signal RF systems, see Sec. 3.2 .

3.1.2 GMT

The GMT system is contained in the equipment layer. It does not only synchronize all timing nodes with nanosecond accuracy over the whole FAIR campus, but also distributes timing messages to all timing nodes and controls all timing nodes to execute real-time actions at a designated time [30]. The GMT system is a time based system. The GMT consists of the Timing Master (TM), the White Rabbit (WR) timing network and timing nodes. The timing master is a logical device, containing the data master (DM), the clock master (CM) and the management master (MM). The data master receives a schedule for the operation of the FAIR accelerator complex from the Settings Management and provides the real-time schedule by broadcasting timing messages to the WR timing network, which will be received and executed by the corresponding timing node at the designated time. The clock master is a dedicated WR switch. It is the topmost switch layer of the WR timing network and provides the grandmaster clock and timestamps which are distributed to all other timing nodes in the timing network. The clock master derives its clock from BuTiS 200 MHz C2 and 100 kHz T0 clocks and timestamps distributed are phase locked to BuTiS clocks. The GMT system could generate BuTiS T0 and C2 with any timing nodes and timing nodes are capable to timestamp clock edges. All active components including timing nodes and WR switches are registered to the MM. The MM monitors and manages the active components of the GMT system [33, 34].

A timing message is sent across the WR network, so it must be contained in the Ethernet frame. An Ethernet frame including one timing message has a length of 110 byte, which is called “timing frame” in this dissertation. A Virtual LAN (VLAN)¹ is a group of FECs in the WR network that is logically segmented by function or application, without regard to the physical locations of the FECs. All FECs in the WR network are assigned to the DM VLAN, within which the DM forwards broadcast timing telegrams downwards to all FECs.

3.1.3 FESA

The FESA² is a framework used to fully integrate the large amount of front-end equipments into the accelerator control system. FESA was developed by CERN and has already been implemented into the CERN control system. Now it is developed further in collaboration with GSI for the FAIR project. FESA develops FESA classes, the equipment-type specific front-end software [28]. For a specific type of equipments, a FESA class implementation accesses to the control interface of the equipments. The FESA class models the equipment as device, so the FESA output

¹https://en.wikipedia.org/wiki/Virtual_LAN

²<https://www-acc.gsi.de/wiki/FESA/WhatIsFESA>

3.2. LLRF system

is called device class. One device class can instantiate several devices and thus generally handles several independent pieces of equipments. FESA provides JAVA based graphical user interfaces (GUI) to design, deploy, instantiate and test the device classes. For the FAIR project the necessary interaction with the timing nodes is realized in a lab-specific timing library of the FESA framework. The FEC use FESA to implement generic and equipment specific functions in form of the device classes. Interaction with the equipment is synchronized with the GMT system.

For time multiplexed operation of the accelerators, the FESA framework supports defining multiplexed properties. Before an accelerator schedule is started, the setting properties of FESA classes are pre-supplied by LSA from SM for all scheduled beams with specific settings accordingly. At runtime, FESA's real time software actions are triggered by timing message, the actual beam specific data is then selected based on information carried by the timing message and send to the equipment.

3.1.4 Settings Management

The Settings Management (SM) is based on a physics model for accelerator optics, parameter space and overall relations between parameters and between accelerators, which is contained in the middle layer of the FAIR control system. It supports off-line generation of synchrotron settings, sending these settings to all involved devices, and programming the schedule for the GMT system [29]. The SM uses the LSA framework. A standardized LSA-API allows accessing data in a common way as basis for generic client applications for all accelerators. Using the LSA-API, applications can coherently modify synchrotron settings [29]. E.g. the application generates timing constraints (e.g. ramp curve) as well as the equipment's data settings (e.g. field) for all devices derived from physics parameters (e.g. beam energy). For FAIR, LSA is extended to model the overall schedule of all accelerators. Beams are described as “Beam Production Chains“ to allow a description from beam source to beam target for settings organization and data correlation.

3.2 LLRF system

The FAIR low-level rf (LLRF) system will be used in the existing synchrotrons SIS18 and ESR, as well as in the FAIR synchrotrons SIS100 and SIS300 and in CR, NESR, and accumulator ring (RESR). It supports fast ramp rates and large frequency span for the acceleration of a variety of ion species, It supports different RF manipulations, including operation at different harmonic numbers, barrier bucket generation, bunch compression and longitudinal feedback. [35].

Each RF supply room has a Reference RF Signal distribution system shown in Fig. 3.1. The Reference RF Signals in different supply rooms are synchronized by BuTiS. BuTiS 200MHz C2 and 100kHz T0 clock signals are generated by BuTiS receivers in different supply rooms in phase. In Fig. 3.1, a number of Group DDS units are located in each supply room, which are synchronized by BuTiS local reference. The Group DDS signals can be routed to the different cavity systems by a Switch Matrix. All cavities in a synchrotron could be providing with the same Group DDS signal. The cavities at different harmonic numbers could be realized by using Group DDS signals with different harmonic numbers and by adjusting the

3.2. LLRF system

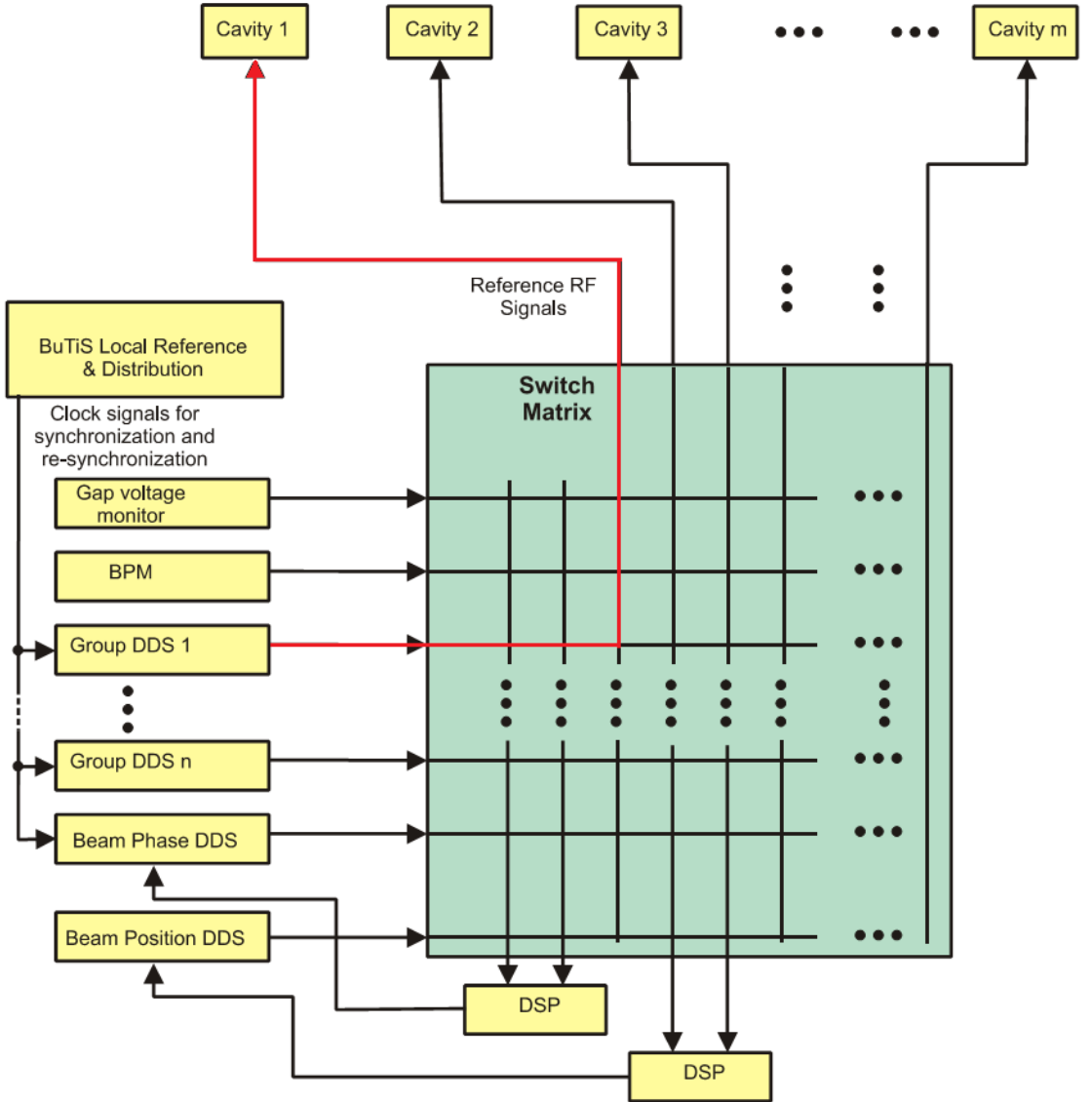


Figure 3.1: Reference RF Signal distribution system
[35]

harmonic number at the Cavity DDS accordingly. The Group DDS concept allows to synchronize a variety of cavities in a very flexible way [35].

All the cavities of SIS18 are driven from one supply room. The SIS100 cavities will be gathered in five acceleration sections, each of them is driven by a dedicated supply room.

RF cavities are driven by one of Reference RF Signals, which are supplied in every supply room . Fig. 3.2 shows the local cavity synchronization system, which synchronizes the local Cavity Direct Digital Synthesizer (DDS) unit to the Reference RF Signal. The cavity gets the RF signal from a local Cavity DDS unit, which receives RF Frequency Ramps from the Central Control System (CCS). A Digital Signal Processor (DSP)-System measures the phase difference between the Reference RF Signal and the gap voltage of the cavity. In the DSP system, a closed-loop control algorithm is implemented, which generates frequency corrections for the local Cavity DDS unit. This process is called local synchronization loop, which ensures that the

3.3. MPS system

phase of the gap voltage follows the phase of the Reference RF signal [35]. The path from the Group DDS 1 to Cavity 1 marked with the red line in Fig. 3.1 is realized by the local cavity synchroniyation in Fig. 3.2. The virtual RF cavity is a virtual position around the ring, to which the Reference RF Signal corresponds.

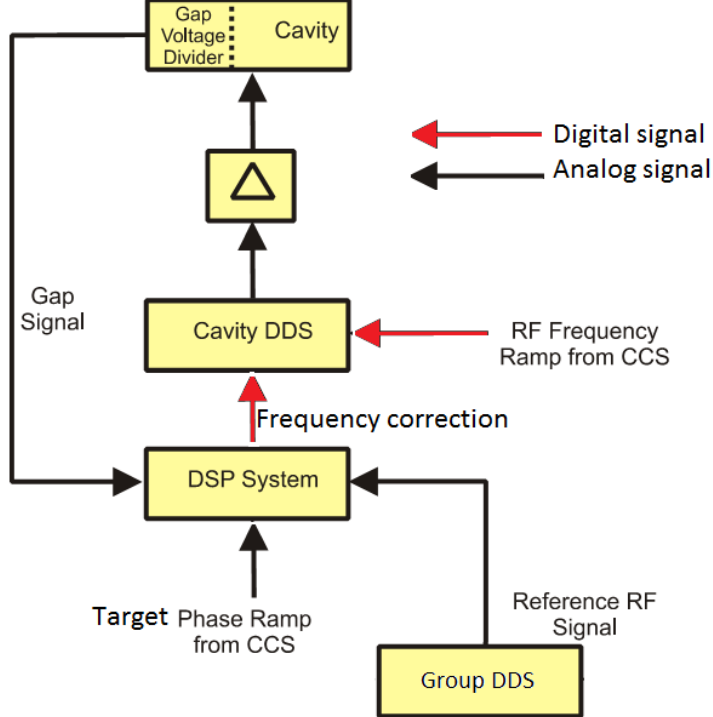


Figure 3.2: Local Cavity Synchronization
[35]

In order to damp coherent longitudinal rigid dipole oscillations, the beam phase control loop is used. The phase difference between the beam signal and the Reference RF Signal is fed back via an FIR filter. The beam signal is obtained by a fast current transformer or a beam position monitor. The filter output is converted in a phase-correction and forwarded to the Group DDS. The corrections are added to the phase of the frequency ramp in the Cavity DDS, which results in a change of the phase of the gap voltage and thus a feedback to the beam [36]. Unfortunately, the actual beam phase control loop in SIS18 is not able to damp incoherent longitudinal rigid dipole oscillations. For SIS100, a bunch-by-bunch longitudinal rf feedback loop will be developed. The bunch-by-bunch longitudinal rf feedback loop generates a correction voltage in dedicated feedback cavities for a specified bunch [21].

3.3 MPS system

A MPS protects current accelerator and subsequent accelerators or experiments from damage or unacceptable failure, e.g. beam position is out of tolerance, rf cavity failure and so on. Thereby, the individual equipment is assumed self-protecting, which

3.4. Comparison

could trigger accelerator safety critical actions, such as an emergency beam dump³, a shutdown of magnets or a beam injection inhibit. In case of relevant equipment failures or other inappropriate equipment states, a MPS signal is generated from this equipment [37]. The FAIR B2B transfer must coordinate with the SIS100 emergency dump signal and the beam injection inhibit signal from the MPS.

The SIS100 emergency dump signal indicates that the beam should be transferred to the emergency dump as soon as possible. If the beam injection inhibit signal is off, the B2B transfer extraction and injection kickers are allowed to be fired. If the beam injection inhibit signal is on, the injection and extraction kickers will be blocked for firing.

3.4 Comparison

Based on the FAIR existing infrastructures, the FAIR B2B transfer system is unique from existing GSI B2B transfer systems.

The existing GSI control system realizes the beam transfer from SIS18 to ESR and ESR back to SIS18. It is an event based system, that event execution will start at the corresponding immediately upon event receipt. Events are directly sent from a “Pulszentrale”, who makes the schedule. Each accelerator has its own Pulszentrale, e.g. ESR is equipped with ESR-Pulszentrale and SIS18 with SIS-Pulszentrale. All devices are connected to distributed Equipment Controllers (EC) via field bus. ES is responsible for the receipt of the event and produces the pulse for the devices. For the transfer between SIS18 and ESR, ESR-Pulszentrale and SIS-Pulszentrale are coupled, achieving two Pulszentrale to be started simultaneously, namely the synchronization between SIS18 and ESR [38, 39].

Compared with the transfer system of the existing GSI control system, the FAIR B2B transfer system is with smaller bunch-to-bucket injection center mismatch. The GMT system is a time based system and all timing nodes of the GMT system are time synchronized with nano second accuracy, while the existing GSI control system is without the propagation delay compensation.

Besides, the FAIR B2B transfer system for FAIR is more flexible. It supports several B2B transfers in parallel which are described by the Beam Production Chains, e.g. B2B transfer from SIS18 to SIS100 and B2B transfer from ESR to CRYRING at the same time. It is capable to transfer different species beam from one machine cycle to another. It is able to transfer the beam between two synchrotrons via Fragment Separator (FRS)⁴ or Super-Fragment Separator (Super FRS)..

The B2B transfer system coordinates with the MPS system, which protects SIS100/SIS300 from unacceptable failure or situation.

³A beam dump is a device designed to absorb the beam.

⁴An ion-optical device used to focus and separate products from the collision of relativistic ion beams with thin targets.

Chapter 4

Concept of the FAIR B2B transfer system [1]

In this Chapter, the basic idea of the FAIR B2B transfer system is presented in Sec. 4.1. The standard procedure of the system is defined and described in Sec. 4.2. Sec. 4.3 illustrates how the basic functionalities of the system are realized. In Sec. 4.4, the data flow of the system is described.

4.1 Basic idea of the FAIR B2B transfer system

The basic idea of the B2B transfer is simple. First of all, two rf systems of the source and target synchrotrons must be phase aligned. Secondly, the trigger for the extraction and injection kickers must be calculated. In the end, the actual beam injection must be indicated for the beam instrumentation and diagnostics, which shows the properties and the behavior of the beam.

4.1.1 Phase alignment

The phase alignment is one of the most important prerequisites for the B2B transfer. It makes sure that there must be buckets to be filled by the extracted bunch at the correct time. If the rf frequency of one rf system is integer times of the rf frequency of the other rf system, the phase difference between two rf systems is a constant. The phase difference must be adjusted by the phase shift method. Or the phase difference is adjusted automatically because of the beating frequency. The beating frequency must not be too small in order to satisfy the constraint of the maximum synchronization time, but also not too large to guarantee the precision of the phase alignment.

For the phase alignment, the following idea must be followed.

1. Measurement of the phase of the rf system and the corresponding timestamp in each synchrotron.
2. Exchange of the measured data.
3. Phase comparison between two rf systems.
4. Adjustment of the phase of one rf system.

4.1. Basic idea of the FAIR B2B transfer system

5. Calculation of the time for the phase alignment of two rf systems.

4.1.2 Calculation of the trigger time for the extraction and injection kickers

For the proper B2B transfer, the position of the bunch and bucket and the firing of the extraction and injection kicker must be precisely controlled. The extraction kicker must kick the bunch exactly the time-of-flight between two rings before the center of a certain bucket passes the injection kicker. For the calculation of the trigger time for the extraction and injection kickers, the following idea must be followed.

1. Kicker firing requires the B2B injection center phase mismatch less than $\pm 1^\circ$, which defines “coarse synchronization“.
2. Bucket counting requires the kicker firing based on $h=1$. With the help of the bucket counting, bunches are injected into correct buckets. This process is called “fine synchronization“.

Before the detailed idea of the calculation are explained, some basic concepts and their symbols are introduced, see Fig. 4.1.

- Bucket pattern t_{bucket} .
- Time-Of-Flight (TOF) between two synchrotrons t_{TOF} .
- Time-Of-Flight between the virtual RF cavity and the extraction/injection kicker, t_{v_ext} and t_{v_inj} .
- Extraction and injection kicker rise time, t_{ext} and t_{inj} .

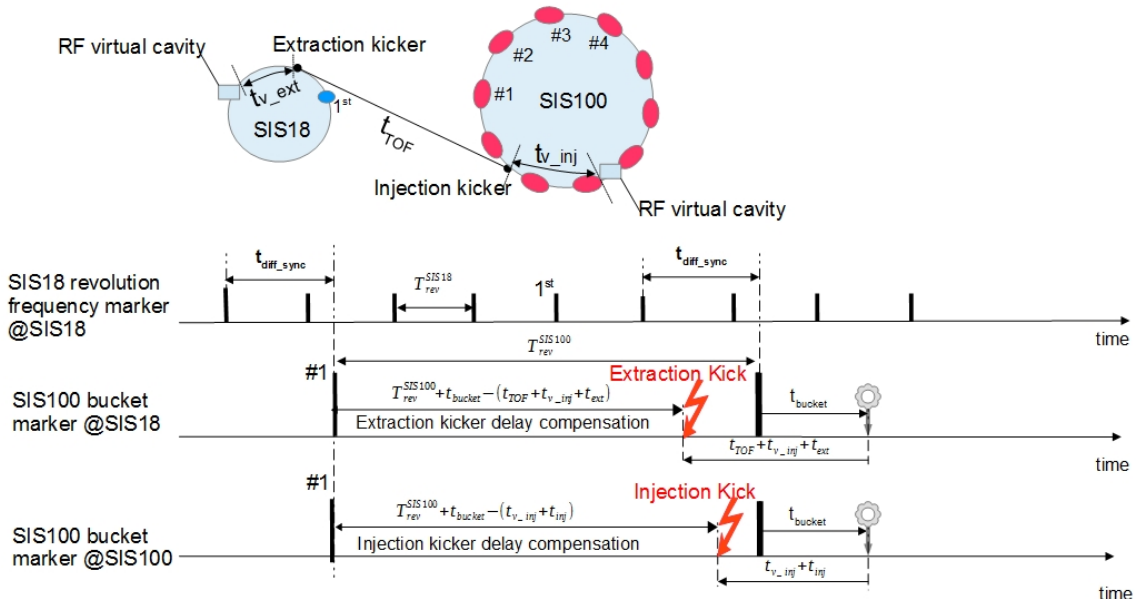


Figure 4.1: The illustration of B2B transfer from SIS18 to SIS100.

4.1. Basic idea of the FAIR B2B transfer system

Fig. 4.1 illustrates the B2B transfer from SIS18 to SIS100. The SIS18 U^{28+} super cycle consists of four SIS18 cycles. Each cycle produces two U^{28+} bunches. From SIS18, four cycles, each of two bunches, are injected into eight out of ten buckets of SIS100. The SIS18 H^+ super cycle consists of four SIS18 cycles. Each cycle produces one H^+ bunch. From SIS18, four cycles, each of one bunch, are injected into four out of ten buckets of SIS100 [40, 41]. The SIS18 and SIS100 revolution frequency markers (black bars on the first time axis and bars on the second/third time axis in Fig. 4.1) indicate the time when the first bunch or the first bucket pass by the RF virtual cavity (black bars correspond to 1st and #1). The extraction and injection kicker firing (red lighting bolts) have a delay with respect to the first bars of the SIS100 revolution frequency marker at SIS18 and SIS100. This delay is called extraction/injection kicker delay compensation. The mentioned four instances of time are related to the second bars of the SIS100 revolution frequency marker. T_{rev}^X represents the revolution period of the synchrotron X, e.g. SIS18 revolution period T_{rev}^{SIS18} . T_{rf}^X represents the period of the cavity frequency of synchrotron X, e.g. SIS18 rf period of the cavity frequency T_{rf}^{SIS18} . After the rf phase alignment, the time difference between the SIS18 and SIS100 revolution frequency markers is represented by t_{diff_sync} , e.g. $t_{diff_sync}=t_{v_ext} + t_{TOF} + t_{v_inj}$ for U^{28+} and H^+ odd bucket injection, $t_{diff_sync}=t_{v_ext} + t_{TOF} + t_{v_inj} - T_{rf}^{100}$ for H^+ even bucket injection, more details about the use case from SIS18 to SIS100, please see Sec. 5.1.1 and Sec. 5.1.2.

The kicker magnet must have zero magnetic field when the bunch passes by it and the kicker magnet only can be switched on during the bunch gap. The bunch gap depends on the cavity frequency, the filling pattern and the bunch length.

- Extraction kick

In order to inject into specific buckets, the extraction kicker delay compensation for the first bar of the SIS100 revolution frequency marker is $T_{rev}^{SIS100} + t_{bucket}$, see gray gear at the SIS100 revolution frequency marker at SIS18. For example, when two U^{28+} bunches of SIS18 are to be injected into the bucket #3 and #4 of SIS100, $t_{bucket} = 1 \times T_{rev}^{SIS18}$. The extraction kicker must be fired $t_{v_inj} + t_{TOF} + t_{ext}$ earlier as the bucket passes the virtual RF cavity, so the extraction kicker delay compensation is $T_{rev}^{SIS100} + t_{bucket} - (t_{TOF} + t_{v_inj} + t_{ext})$, see red lighting bolt at the SIS100 revolution frequency marker at SIS18.

- Injection kick

With the consideration of the bucket pattern, the injection kicker delay compensation for the first bar of the SIS100 revolution frequency marker is $T_{rev}^{SIS100} + t_{bucket}$, see gray gear at the SIS100 revolution frequency marker at SIS100. The injection kicker must be fired $t_{v_inj} + t_{inj}$ time earlier as the bucket passes the virtual RF cavity, so the injection kicker delay compensation is $T_{rev}^{SIS100} + t_{bucket} - (t_{v_inj} + t_{inj})$, see red lighting bolt at the SIS100 revolution frequency marker at SIS100.

4.2 Basic procedure of the FAIR B2B transfer system

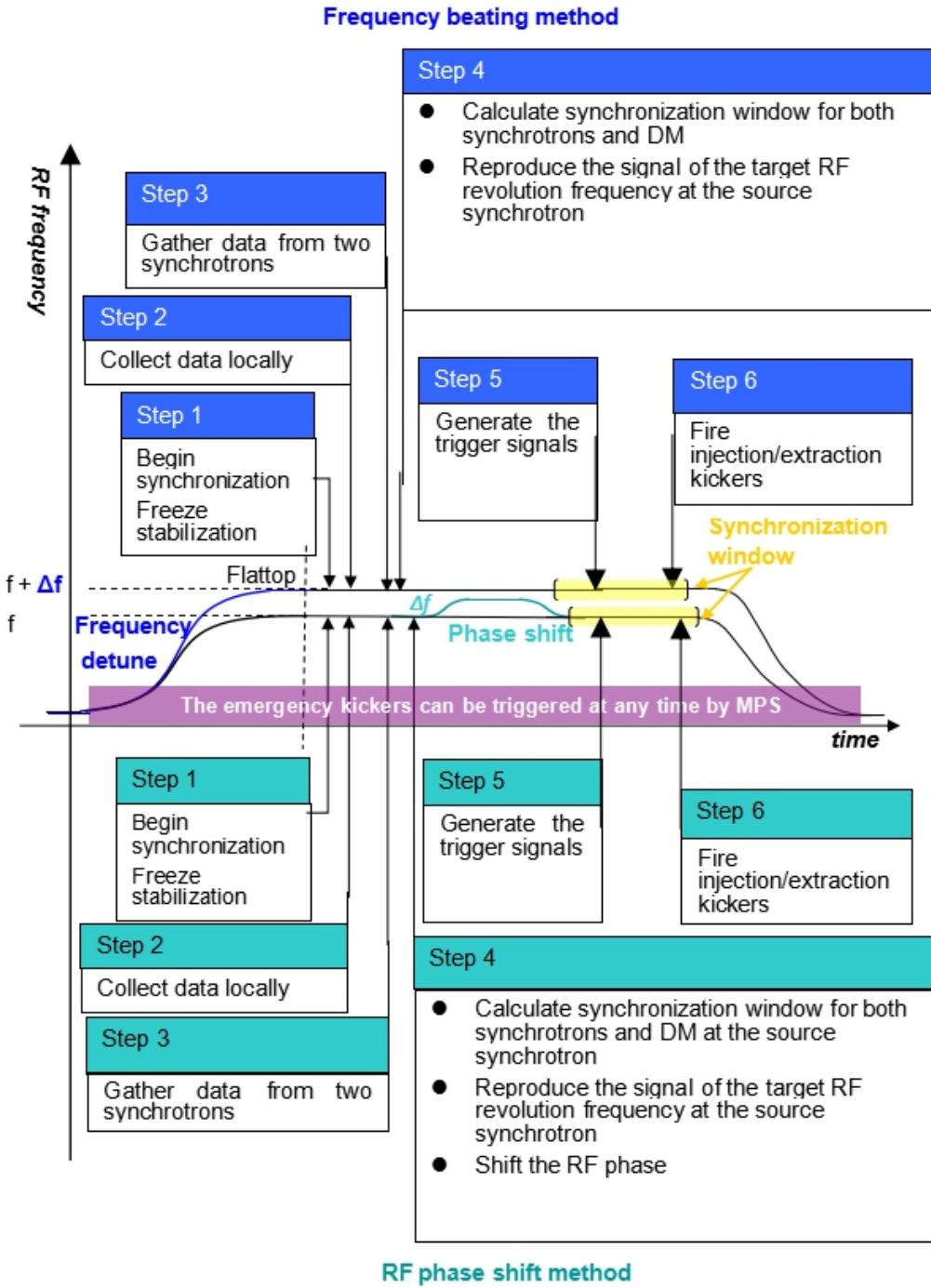


Figure 4.2: The procedure for the B2B transfer within one acceleration cycle. Shown are the frequency beating method (blue, top) and the phase shift method (green, bottom).

Fig. 4.2 illustrates the basic procedure of the B2B transfer with two different synchronization scenarios. The top part shows the chronological steps with the frequency

4.3. Realization of the FAIR B2B transfer system

beating method, while the bottom part shows the steps with the phase shift method. The emergency kickers can be triggered at any time during the acceleration cycle by the MPS. The purple region shows the valid time for the emergency kicker. The yellow region shows the synchronization window.

The B2B transfer process basically needs to follow six steps [42]:

1. The DM announces the B2B transfer and requests the freez of the feedback loop (e.g. beam phase feedback loop), when required.
2. The two synchrotrons measure the rf phase locally.
3. The source synchrotron receives the measured rf phase from the target synchrotron.
4. The source synchrotron calculates the synchronization window with the kicker delay and sends it to both synchrotrons and to the DM. Besides, it reproduces the revolution frequency marker of the target synchrotron at the source synchrotron.

For the phase shift method, the source synchrotron generally achieves the phase shift. But when the target synchrotron is empty, the phase shift is achieved by the method of the phase jump at the target synchrotron for simplicity's sake. Although the synchronization window is infinite theoretically, the B2B should be transferred as soon as the phase shift is done, in order to guarantee the stability of the beam. The duration of the synchronization window is defined as two revolution periods of the large synchrotron.

5. The trigger signal is generated for the kickers with the delay compensation.
6. The kicker electronics fire the kickers. The actual beam injection time and the B2B transfer status are send from the source synchrotron to the DM and the DM sends them further to the beam instrumentation.

4.3 Realization of the FAIR B2B transfer system

In this section, how the FAIR B2B transfer system is realized based on the FAIR control system and LLRF system is introduced.

4.3.1 Phase measurement and corresponding timestamp of one rf system

Two rf systems are assumed to be stable during the B2B transfer process. The phase measurement of one rf system follows the following principles.

1. Measurement of the actual phase values.
2. Extrapolation of the phase value in the future based on the measured phase values.
3. Timestamp the extrapolated phase values.

4.3. Realization of the FAIR B2B transfer system

4.3.1.1 Measurement of actual phase values in one rf system

The phase measurement of one rf system is achieved by measuring the phase advance between the rf system and a reference sine signal. The phase advance is a linear relationship, with the range from -180° to $+180^\circ$.

In order to get the phase difference between two rf systems of the source and target synchrotrons, a shared reference signal at both source and target synchrotrons is used, which is called “Synchronization Reference Signal”. It is with the fixed frequency and always in the same phase at two synchrotrons. It is a sine wave, whose frequency is a multiple of 100 kHz and whose zero-crossing is aligned with the first zero-crossing of C2 clocks after T0 edges in order to ensure the synchronization of the Synchronization Reference Signal in different synchrotrons [43, 44].

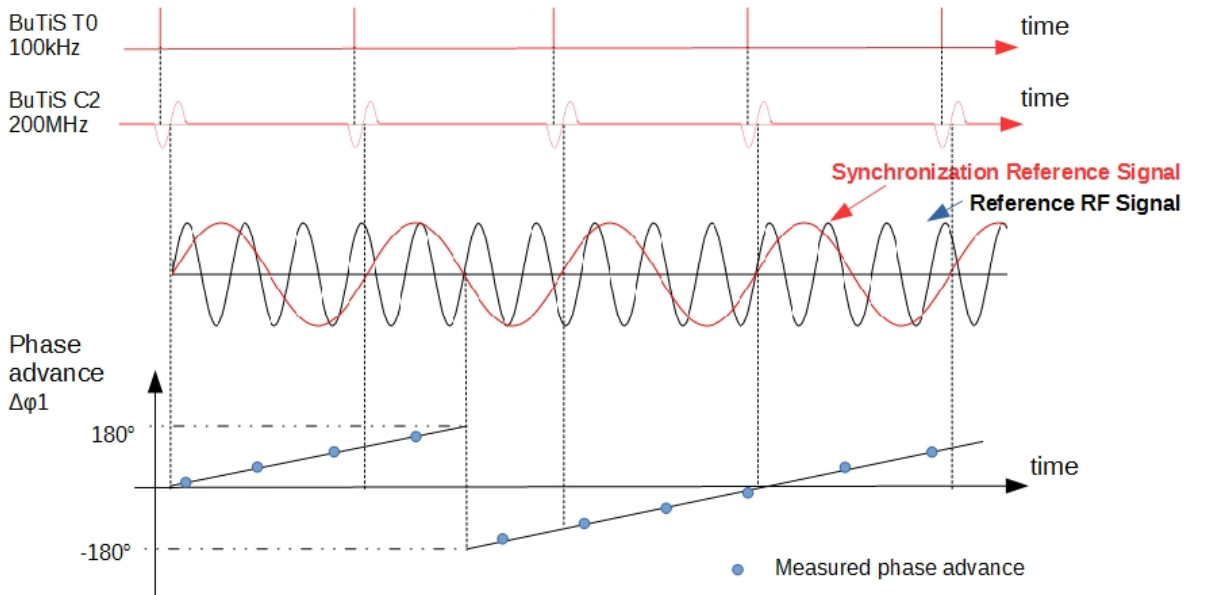


Figure 4.3: The realization of the phase advance measurement at one synchrotron

Fig. 4.3 shows the phase measurement of a rf system at a synchrotron. The red sine wave represents the Synchronization Reference Signals (e.g 100 kHz) in two synchrotrons and the black wave the Reference RF Signals (e.g. 1000/3 kHz) from the Group DDS. The phase advance $\Delta\varphi_1$ between the Reference RF Signal and the Synchronization Reference Signal is measured by the Phase Advance Measurement (PAM) Module at the source synchrotrons and $\Delta\varphi_2$ at the target synchrotron. The phase advance measurement is performed synchronously to an internal clock, which is represented by the blue dots. For more details about the implementation and realization of the PAM module, please see “Development of the LLRF system for a deterministic Bunch-to-Bucket transfer for FAIR” [45].

4.3.1.2 Phase extrapolation in one rf system

The phase advance can be extrapolated due to the linear relationship between time and the phase advance. Based on a series of the phase advance measurements, the phase advance at first zero-crossing of C2 clocks after T0 edges ψ_1 and ψ_2 could be

4.3. Realization of the FAIR B2B transfer system

extrapolated at the source and target synchrotrons by the Phase Advance Prediction (PAP) Module. The extrapolated phase advance is represented by the red diamonds in Fig. 4.4. Because the phase advance extrapolation is synchronized with the first zero-crossing of C2 clocks after T0 edges and the Synchronization Reference Signal is zero phase aligned with the first zero-crossing of C2 clocks after T0 edges, ψ_1 and ψ_2 are the phase of the Reference RF Signals (represented as the black dot in Fig. 4.4). For more details about the implementation and realization of the PAP module, please see “Development of the LLRF system for a deterministic Bunch-to-Bucket transfer for FAIR” [45].

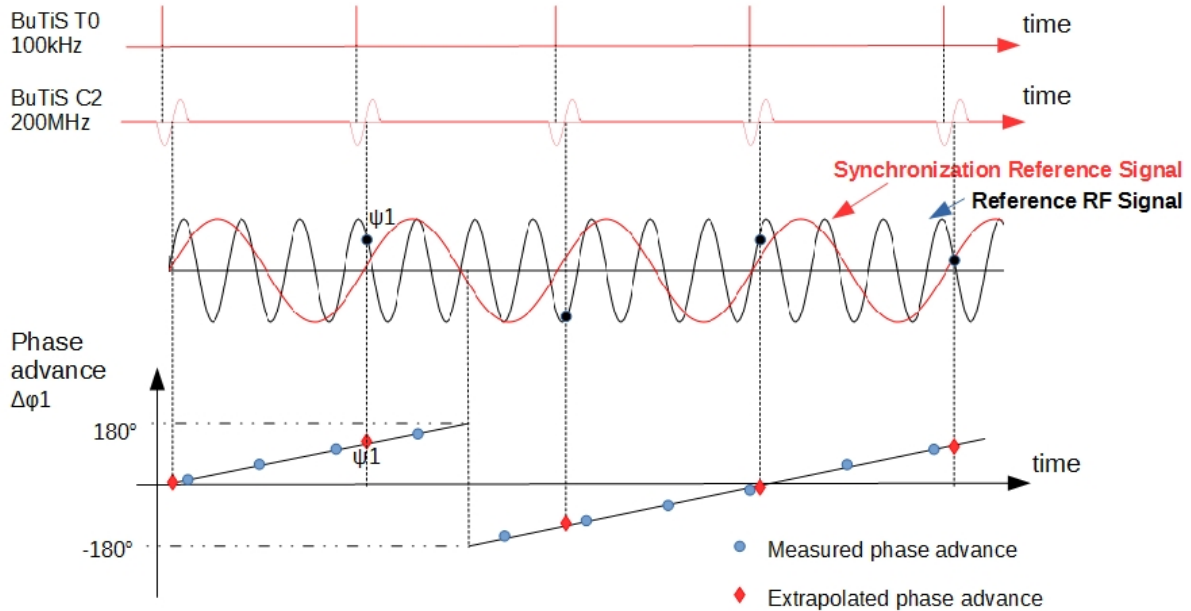


Figure 4.4: The realization of the phase advance extrapolation at one synchrotron

4.3.1.3 Timestamp the extrapolated phase

The timestamp of the first zero-crossing of C2 clocks after T0 edges corresponds to the extrapolated phase.

The timing nodes, the B2B source and target SCUs [30, 46], are equipped in the source and target synchrotrons. The PAP module is as a slave¹ in the B2B source and target SCU, see Fig. 4.5. Both B2B source and target SCUs could get the timestamp of zero-crossing of BuTiS C2 clocks.

Fig. 4.6 illustrates the synchronization of the extrapolated phase to the timestamp. DM broadcasts the timing frame of CMD_START_B2B to the WR network. This timing frame will be received by the B2B source SCU and B2B target SCU. The B2B source and target SCUs start the B2B process at the designated time, the first zero-crossing of C2 clock after a specified T0 edge (represented as the pink dot in Fig. 4.6). They need maximum 1 µs to inform the PAP modules to start the phase advance extrapolation respectively. The PAP modules use e.g. 500 µs for the phase extrapolation and updates the extrapolated phase value every first zero-crossing of C2 clocks after T0 edges. After 500 µs, the B2B source and target SCUs

¹[https://en.wikipedia.org/wiki/Master/slave_\(technology\)](https://en.wikipedia.org/wiki/Master/slave_(technology))

4.3. Realization of the FAIR B2B transfer system

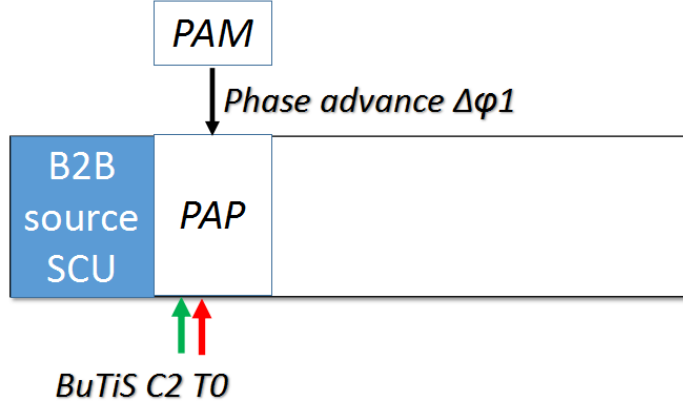


Figure 4.5: Implementation of the Phase Advance Prediction Module in the B2B source SCU

need another maximum 1 μ s to get the extrapolated phase ψ_1 (represented as the red diamond in Fig. 4.6) from the PAP modules and they also get the timestamp of the first zero-crossing of C2 clock after T0 edge t_{ψ_1} which corresponds to the extrapolated phase, as well as the slope of the phase advance k .

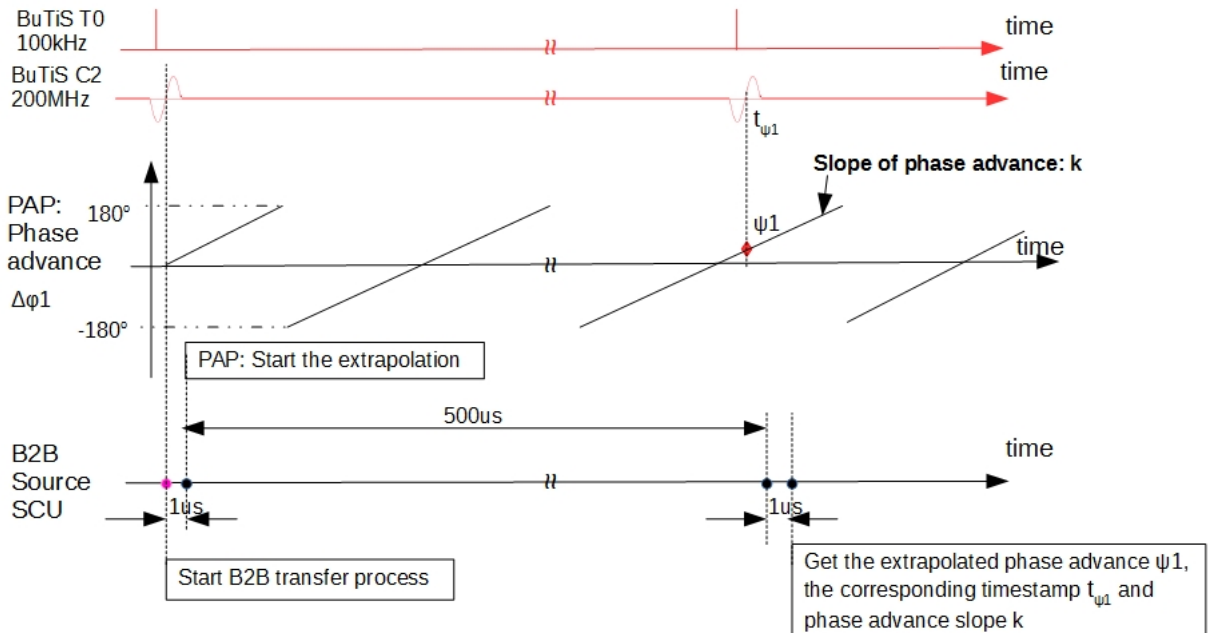


Figure 4.6: The synchronization of the extrapolated phase to the timestamp in one synchrotron

4.3.2 Exchange of the measured data

For the B2B transfer, there is a “B2B transfer master“, which is responsible for the data collection of two synchrotrons, data calculation, data redistribution and B2B transfer status check. The data of the source and target synchrotron must be transferred to the “B2B transfer master“ via the deterministic WR network in the format of the timing frame.

4.3. Realization of the FAIR B2B transfer system

For the simplicity, the B2B source SCU works as “B2B transfer master”, so the extrapolated phase ψ_1 , the corresponding timestamp t_{ψ_1} and the phase advance slope k are transferred by the B2B target SCU to the B2B source SCU via the WR network. The transfer of the data is achieved by the timing frame TGM_PHASE_TIME. The B2B transfer involves a certain amount of timing frames. More details about the B2B timing frames, please see Appendix A. The timing frames are not sent via DM in order to reduce the traffic of the WR network and reduce the timing frame transfer delay on the WR network [1], so a specified VLAN, B2B VLAN, is defined. All SCUs for the B2B transfer are assigned to the B2B VLAN. Fig. 4.7 illustrates an example of the transfer path of the B2B timing frame in the WR network. The frame is transferred along the path with orange color instead of the path with blue color.

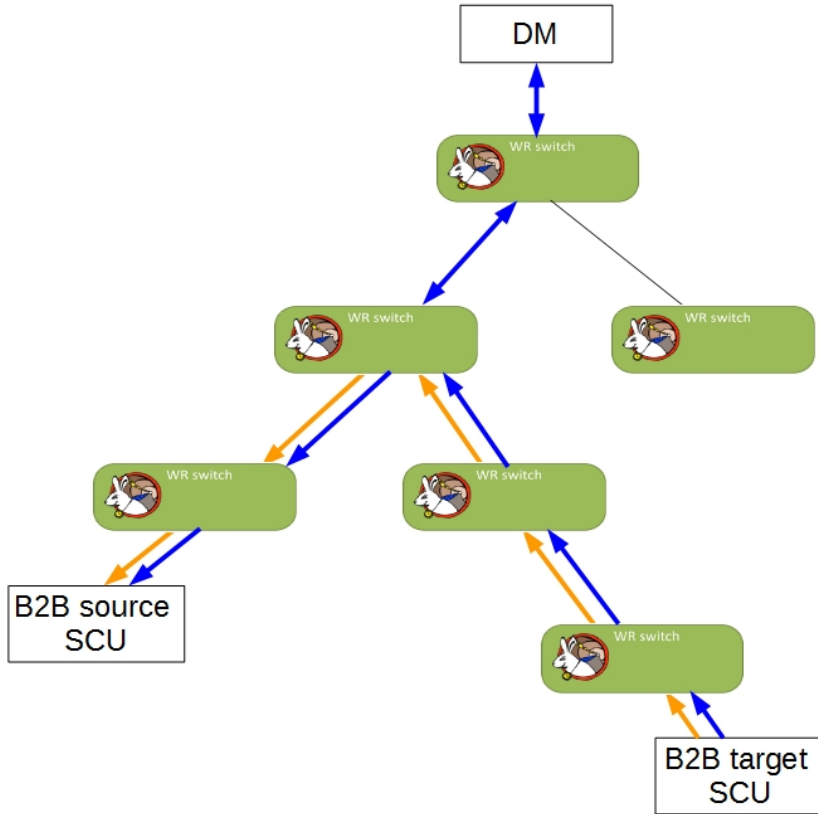


Figure 4.7: One example of the transfer path of the B2B timing frame in the WR network

4.3.3 RF synchronization

The FAIR B2B transfer system is available for both the phase shift and frequency beating methods, see Sec. 2.4. The phase difference between two rf systems allows for the realization of the RF synchronization. With the phase shift method, a frequency modulation with a fixed duration is applied to one rf system. With the frequency beating method, the phase difference varies at the rate of the frequency difference between two rf systems.

4.3. Realization of the FAIR B2B transfer system

- RF synchronization with the phase shift method

Eq. 4.1 gives the relation between the required phase shift $\Delta\phi_{shift}$ and the frequency modulation.

$$\Delta\phi_{shift} = 2\pi \int_{t_0}^{t_0+T} \Delta f_{rf}(t) dt \quad (4.1)$$

The required phase shift is determined by the frequency offset $\Delta f_{rf}(t)$ and the duration of the frequency modulation T . The phase shift must be executed adiabatically in order to guarantee the bucket size and continuous synchronous phase, see Sec. 2.4 at page 15. For the RF synchronization, the maximum phase shift required of one synchrotron is one bucket length of the other synchrotron, namely 360° . Because the phase can be shifted backward or forward, a phase shift of up to $\pm 180^\circ$ can be implemented for the simplicity of the rf frequency modulation. A normalized frequency modulation profile $f_{normalized}$ for 180° can be precalculated, which guarantees the adiabaticity. The actual frequency modulation profile f_{actual} is decided by the normalized frequency modulation profile and the required phase shift, see eq. 4.2. The required phase shift, $\Delta\phi_{shift}$, is calculated by the B2B source SCU.

$$\frac{\Delta\phi_{shift}}{180^\circ} = \frac{f_{actual}}{f_{normalized}} \quad (4.2)$$

Fig. 4.8 shows an example of a normalized and several actual frequency modulation profiles and the corresponding phase shift profiles. The magenta profile is the normalized profile $f_{normalized}$ with the phase shift of 180° . The blue one is $1/2f_{normalized}$ with the phase shift of 90° and the green one is $1/3f_{normalized}$ with 60° .

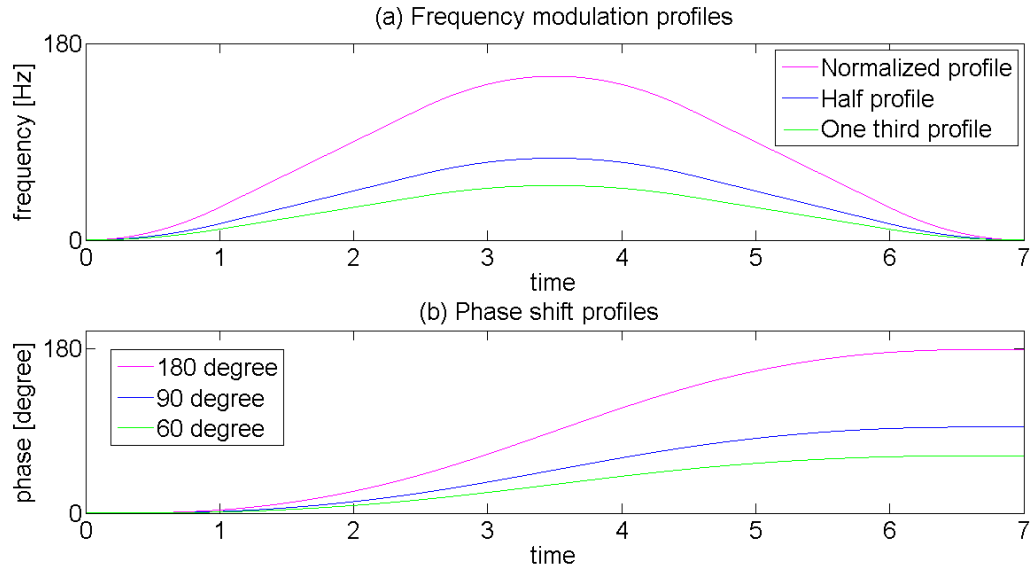


Figure 4.8: The normalized frequency and phase modulation profile and the actual profiles

Fig. 4.9 shows the implementation of the PSM in the B2B source SCU. The B2B source SCU sends the required phase shift to the Phase Shift Module

4.3. Realization of the FAIR B2B transfer system

(PSM), which controls the phase shift of the Reference RF Signal of Group DDS by means of either frequency (Fig. 4.8 (a)) or phase (Fig. 4.8 (b)) modulation. The Reference RF Signal is routed to the different cavity systems by a Switch Matrix to realize the phase shift of all cavities on the synchrotron. For more details about the implementation and realization of the PSM modules, please see “Development of the LLRF system for a deterministic Bunch-to-Bucket transfer for FAIR“.

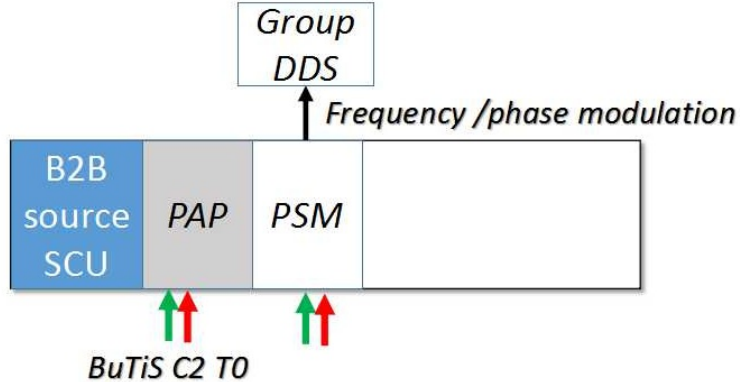


Figure 4.9: Implementation of the Phase Shift Module in the B2B source SCU

A particular case of the B2B synchronization occurs, when the target synchrotron is empty, i.e. it does not capture any bunch yet, the phase shift can be done for the target synchrotron without adiabatical consideration (e.g. Phase jump is possible). In this case, the B2B source SCU sends the timing frame TGM_PHASE_JUMP to the B2B target SCU, which contains the required phase jump. After the B2B target SCU receives the timing frame, it sends the value to the PSM for the phase jump of the Group DDS of the target synchrotron. For more details about the implementation and realization of the PSM module, please see “Development of the LLRF system for a deterministic Bunch-to-Bucket transfer for FAIR“ [45].

- RF synchronization with the frequency beating method The frequency is detuned at one rf system at the acceleration ramp. The ratio of the circumference between many pair of machines in FAIR is not a perfect integer, the frequencies of two synchrotrons begin beating automatically. For the pairs with the perfect integer ratio of the circumference, the rf frequency of the source synchrotron is detuned by modifying the magnetic field and radial excursion during the acceleration ramp. The Group DDS produces the detuned Reference RF Signal.

4.3.4 Coarse synchronization

The coarse synchronization is achieved by the synchronization window with a certain length. Within this window, the bunch is transferred into the bucket with the center mismatch smaller than the upper bound². The length of the synchro-

²B2B transfer from SIS18 to SIS100: upper bound of the bunch-to-bucket center mismatch is $\pm 1^\circ$

4.3. Realization of the FAIR B2B transfer system

nization window T_{sync_win} is two times the period of the reproduced signal for the bucket label, see Sec. 4.3.5. For the phase shift method, the bunch-to-bucket injection center mismatch within the synchronization window is almost 0° . For the frequency beating method, the maximum bunch-to-bucket center mismatch $\Delta\theta$ with the synchronization window is calculated by

$$\frac{T_{sync_win}}{1/\Delta f} = \frac{\Delta\theta}{360^\circ} \quad (4.3)$$

where Δf is the beating frequency.

The B2B source SCU is capable of receiving the values (kicker delay for extraction kicker of the source synchrotron, kicker delay for injection kicker of the target synchrotron, t_{TOF} , rf frequencies of the source and target synchrotrons, the upper bound time for the phase shift of the source synchrotron) from the SM by FESA classes via the accelerator network. The B2B source SCU calculates the synchronization window, taking kicker delays into consideration and transfers the timestamp of the start of the synchronization window, TGM_SYNCH_WIN, to the DM and the source and target Trigger SCUs via the WR network. The Trigger SCUs are used to produce the kicker trigger signal. The TGM_SYNCH_WIN could also be used for the triggering of the bunch rotation of both machines (e.g. SIS100 and CR) with a specified advance.

4.3.5 Bucket label

The bucket label is realized by a delay based on an indication signal. The indication signal is used to indicate the first bucket and the delay is used to indicate a specific bucket. The indication signal is with the revolution frequency of the target synchrotron. Because the evolution of the phase advance of the RF system of the target synchrotron ψ can be calculated according to the slope of the phase advance k , see eq. 4.4, the indication signal can be corrected exactly in phase with the revolution frequency of the target synchrotron. The indication signal is exactly a copy of the revolution frequency of the target synchrotron, so it is called "reproduced signal". The reproduced signal could be reproduced campus-wide. A specific bucket is just a certain number of the RF periods delay based on the reproduced signal.

$$\psi = kt + b \quad (4.4)$$

Where ψ_2 and t_{ψ_2} coincidence with the linear relationship, so b can be calculated as $\psi_2 - kt_{\psi_2}$.

The FAIR B2B transfer system needs the bucket label not only at the rf flattop, but also during the whole acceleration cycle. The former is used for the normal extraction and injection and the latter could be used for the emergency dump. For the emergency kick, the reproduced signal has always the same frequency and is always in phase with the revolution signal, so it is called the "real-time reproduced signal". The delay based on the real-time reproduced signal always indicates the bunch gap.

The bucket label is realized by the Trigger SCU, the Signal Reproduction (SR) module and the PCM, see Fig. 4.10. The reproduced signal is produced by SR module. The Trigger SCU is responsible for the receipt of the phase correction value from the B2B source SCU and the transfer of this value to PCM. The PCM

4.3. Realization of the FAIR B2B transfer system

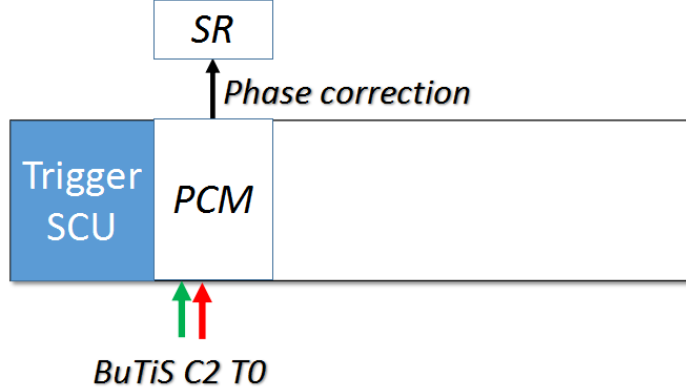


Figure 4.10: Implementation of the Phase Correction Module in the Trigger SCU

module is used to correct phase of the reproduced signal. The PCM module is as a slave in the Trigger SCU. For more details about the implementation and realization of the PCM and SR module, please see “Development of the LLRF system for a deterministic Bunch-to-Bucket transfer for FAIR“ [45].

- Bucket label for the normal extraction and injection

For the bucket label for the normal extraction and injection, three steps are necessary. Fig. 4.11 shows these three steps for the reproduction of the bucket label. Here we use B2B transfer from SIS18 to SIS100 as an example.

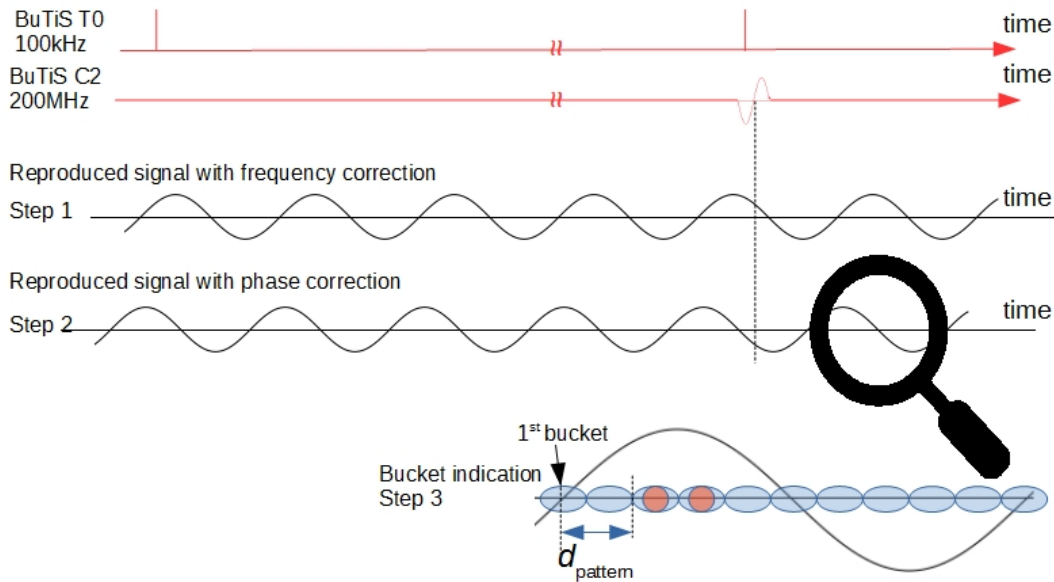


Figure 4.11: The realization of the bucket label for the normal extraction and injection.

- Step 1. Frequency correction

The Signal Reproduction (SR) module produces the ”reproduced signal” with the same frequency as the Reference RF Signal at the flattop of the target synchrotron (e.g. RF revolution frequency of SIS100). The

4.3. Realization of the FAIR B2B transfer system

zero-crossing of the reproduced signal always indicates the start of the 1st bucket.

- Step 2. Phase correction

The reproduced signal must do phase correction at a specified first zero-crossing of C2 clock after T0 edge. The phase correction value is calculated by the B2B source SCU and transferred by the timing frame TGM_PHASE_CORRECTION to the Trigger SCU. Then the Trigger SCU gives the phase correction value to the SR module.

- Step 3. Bucket indication

The SM considers the bucket pattern $d_{pattern}$ within the kicker delay compensation, see Sec. 4.1.2. In Fig. 4.11, the 3rd and 4th buckets will be filled with $d_{pattern} = 1 \times T_{rev}^{SIS18}$.

- Bunch gap label for the emergency extraction

Only for SIS100 emergency procedure, the bunch gap label is important during the whole acceleration cycle. There are two steps for the realization of the bunch gap label, see Fig. 4.12.

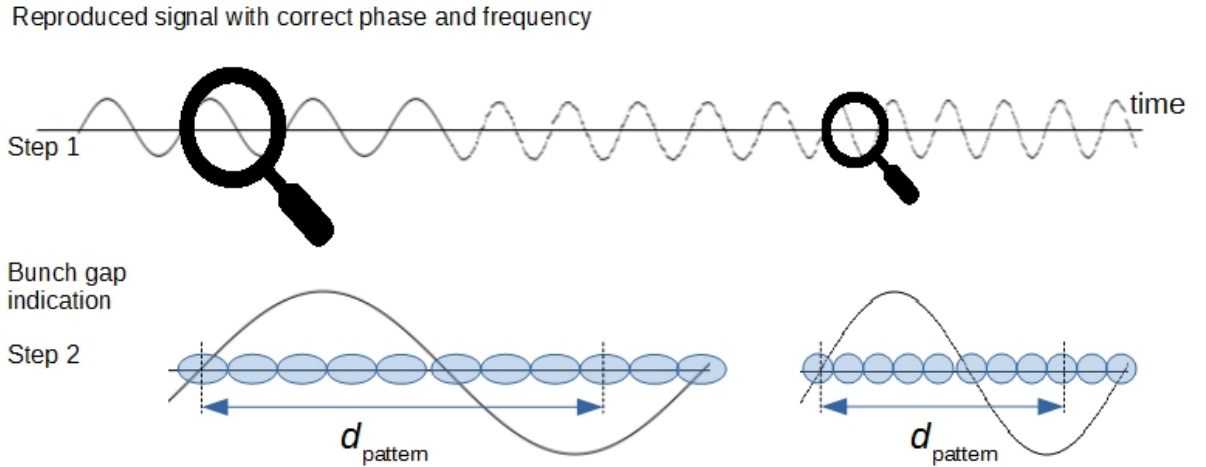


Figure 4.12: The realization of the bunch gap for the emergency extraction.

- Step 1. The real-time reproduced signal is directly distributed from the switch matrix, which synchronizes with the Reference RF Signal in frequency and phase.

- Step 2. Bunch gap indication

The SM considers the bunch gap $d_{pattern}$ within the kicker delay compensation. In Fig. 4.12, the 9th and 10th buckets are taken as an example as the bunch gap. The $d_{pattern} = 4 \times T_{rev}^{SIS18}$.

4.3.6 Fine synchronization of the extraction and injection kicker

After the synchronization between two RF systems, the exact time-of-flight between two synchrotrons before the center of a certain bucket passes the injection kicker, the extraction kicker must kick the bunch in the source synchrotron. When there are some emergency, the emergency kicker must kick the beam into the emergency dump as soon as possible.

The first pulse of the reproduced signal within the synchronization window is selected. The triggers for the extraction and injection kicker are produced after the selected reproduced signal with the delay of the extraction and injection kicker delay compensation. When some emergency happens, the coming bunch gap label outputs to trigger the emergency kicker. Fig. 4.13 shows the implementation of the

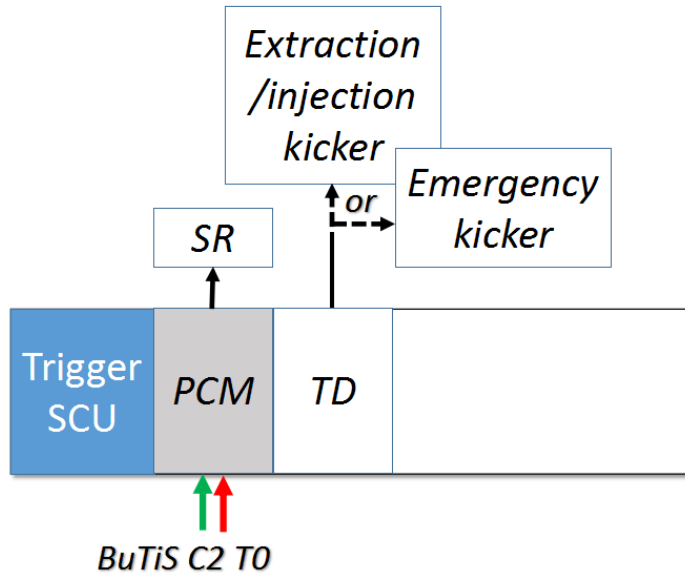


Figure 4.13: Implementation of the Trigger Decision module in the Trigger SCU

TD module in the Trigger SCU. The TD module is responsible for the production of trigger for the kicker.

For the normal B2B extraction/injection, the synchronization window is a gating signal, which is received by the source and target Trigger SCUs from the WR network by TGM_SYNCH_WIN. Within this window, the first reproduced signal from the SR module will be selected by the Trigger Decision (TD) module. The extraction and injection kicker are synchronized with the bunch and bucket by the extraction and injection kicker delay compensation. The extraction kicker will be triggered by the extraction kick delay compensation, $T_{rev}^{SIS100} + T_{rev}^{SIS18} - (t_{TOF} + t_{v,inj} + t_{ext})$ and the injection kicker will be triggered by the injection kick delay compensation, $T_{rev}^{SIS100} + T_{rev}^{SIS18} - (t_{v,inj} + t_{inj})$, see Fig. 4.1. Both extraction and injection kick delay compensation values are preloaded from the SM to the Trigger SCU and the Trigger SCU gives these values to the TD module. The kicker delay compensation is applied to the first selected reproduced signal by TD module.

For the SIS100 emergency kick, the extraction delay compensation is calculated by $T_{rev}^{SIS100} + t_{bucket} - (t_{v,emg} + t_{emg})$, where $t_{v,emg}$ is the time delay between the virtual RF cavity and the emergency extraction position and t_{emg} the emergency

4.4. Data flow of the FAIR B2B transfer system

kicker delay. The emergency extraction delay compensation values are preloaded from the SM to the Trigger SCU and the Trigger SCU gives these values to the TD module. The kicker delay compensation is applied to the real-time reproduced signal by TD module. Only when the emergency dump signal from MPS is valid, the emergency kicker will be triggered by the TD module.

4.3.7 B2B transfer status check

The B2B transfer status must be known by the DM. The B2B source SCU, the B2B transfer master, is responsible for the status check. The B2B source SCU receives the trigger time of the extraction kicker and actual beam extraction time, TGM_KICKER_TRIGGER_TIME_S, from the source Trigger SCU via the WR network and also the trigger time of the injection kicker and actual beam injection time, TGM_KICKER_TRIGGER_TIME_T, from the target Trigger SCU via the WR network. The Trigger SCU collects the kicker trigger time and the beam extraction/injection time. The B2B source SCU examines the status of the B2B transfer system and transfers the status and the actual beam injection time (TGM_B2B_STATUS) to the DM. If all components of the B2B transfer system work correctly and the B2B transfer process is successful. Otherwise it is defeat.

4.4 Data flow of the FAIR B2B transfer system

In this section, the procedure for the B2B transfer is explained from the perspective of the data flow, which follows the basic six steps in Fig. 4.2. Fig. 4.14 shows the data flow in the source and target synchrotrons and between two synchrotrons. The rectangle with the different color represents the basic six steps. The left part in each rectangle presents the data flow in the source synchrotron and the right part the data flow in the target synchrotron.

1. The DM sends the timing frame CMD_START_B2B to the B2B source and target SCUs for the start of the B2B transfer via the WR network. Besides, it requests the freez of the feedback loop, e.g. the beam phase control loop and the bunch-to-bunch longitudinal rf feedback loop, see Sec. 3.2.
2. After receiving CMD_START_B2B, the B2B source and target SCUs start the PAM module to measure the phase advance $\Delta\varphi$ with the help of the PAP module locally and the PAP module extrapolates the phase advance in the future. After a period of time, the B2B source and target SCU reads the extrapolated phase advance ψ and the slope of the phase advance k from the PAP module locally, timestamping the ψ .
3. The B2B target SCU sends the extrapolated phase ψ_2 , the corresponding timestamp t_{ψ_2} and the slope k in the format of the timing frame TGM_PHASE_TIME to the B2B source SCU via the WR network.
4. When the B2B source SCU receives the timing frame TGM_PHASE_TIME, it calculates the synchronization window and transfers the timestamp of the start of the window to the DM in the format of the timing frame TGM_SYNCH_WIN, as well as to the Trigger SCUs at the source and target synchrotrons. The

4.4. Data flow of the FAIR B2B transfer system

B2B source SCU calculates the phase correction value and transfers it to all Trigger SCUs via the WR network in the format of the timing frame TGM_PHASE_CORRECTION. Then the Trigger SCUs transfer the phase correction value to its PCM. The PCM starts the phase correction of the SR module.

Only for the phase shift method, the B2B source SCU calculates the required shifted phase $\Delta\phi_{shift}$ and transfers it to the PSM. Then the PSM transfers the phase or frequency modulation profile to the Group DDS.

5. When the source and target Trigger SCUs receive the timing frame TGM_SYNCH_WIN, they produce the synchronization window pulse for the TD module. With the help of the reproduced signal from the SR module, the kicker delay compensation from the Trigger SCU and the indication signals (the emergency dump signal and the beam injection inhibit signal) from the MPS, the TD module produces the normal extraction/injection trigger signals or the emergency kick trigger for the kicker.
6. The extraction and injection kickers or emergency kicker are fired. After that, the source Trigger SCU gets the actual beam extraction time and the timestamp of the extraction trigger signal from the TD module and transfers them to the source B2B SCU in the format of the timing frame TGM_KICKER_TRIGGER_TIME_S. The target Trigger SCU gets the timestamp of actual beam injection time and the timestamp of the injection trigger signal from the TD module and transfers them to the source B2B SCU in the format of the timing frame TGM_KICKER_TRIGGER_TIME_T. Then the B2B source SCU checks the B2B transfer status and transfers the status together with the beam injection time to the DM in the format of the timing frame TGM_B2B_STAUS (represented as the red line in the rectangle of step 6 in Fig. 4.14).

4.4. Data flow of the FAIR B2B transfer system

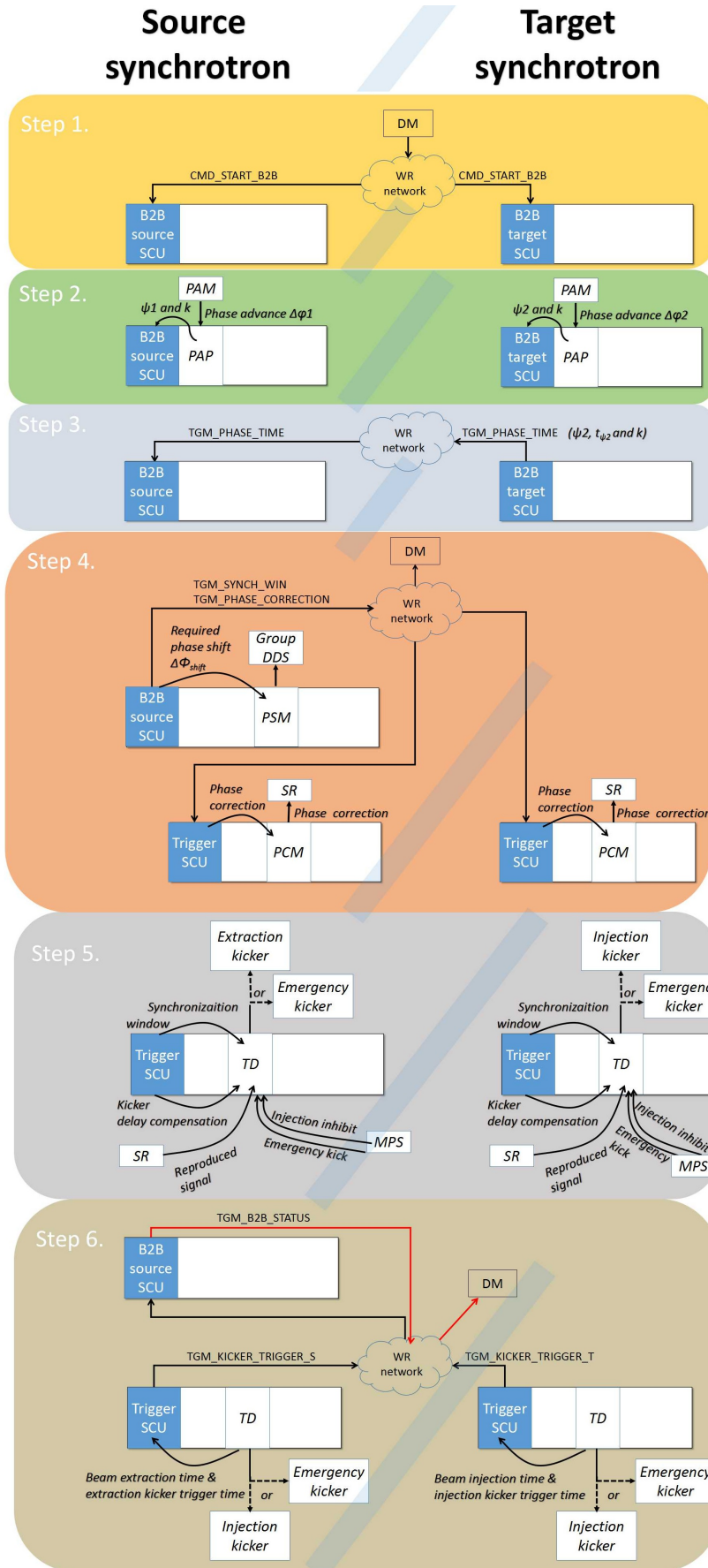


Figure 4.14: The data flow of the B2B transfer system

Chapter 5

Application of the FAIR B2B transfer system for FAIR accelerators

Due to the ratio of the circumference of the injection/extraction orbit, there are several use cases of the B2B transfer for FAIR.

- The circumference ratio between the large and small synchrotron is an ideal integer.
 - U^{28+} B2B transfer from SIS18 to SIS100
 - H^+ B2B transfer from SIS18 to SIS100
 - B2B transfer from ESR to CRYRING
- The circumference ratio between the large and small synchrotron is close to an ideal integer.
 - $h=4$ B2B transfer from SIS18 to ESR
 - $h=1$ B2B transfer from SIS18 to ESR
- The circumference ratio between the large and small synchrotron is far away from an ideal integer.
 - B2B transfer from CR to HESR

Besides, FAIR has many use cases of B2B transfers that the extraction and injection beam have different energy because of the targets installed between two synchrotrons (e.g. Pbar, FRS). In this situation, the beam revolution frequency ratio between the small and large synchrotrons is equivalent to the circumference ratio between the large and small synchrotrons .

- The revolution frequency ratio between the small and large synchrotron is far away from an ideal integer.
 - H^+ B2B transfer from SIS100 to CR via Pbar
 - RIB B2B transfer from SIS100 to CR via Super FRS
 - B2B transfer from SIS18 to ESR via FRS

5.1. Circumference ratio is an ideal integer

In this document, the circumference of the injection/extraction orbit of the synchrotron is denoted by C^X , the revolution frequency and rf cavity frequency by f_{rev}^X and f_{rf}^X , the beating frequency by Δf and the harmonic number by h^X . The superscript X could be either “l” or “s” denoting the large or small synchrotron. κ is used to represent integers and λ the decimal numbers.

Tab. 5.1 lists all FAIR use cases of the B2B transfer.

Table 5.1: FAIR use cases of the B2B transfer

Circumference ratio	C^l/C^s	$\frac{f_{rev}^s}{f_{rev}^l}$	use case of FAIR accelerators
$C^l/C^s = \kappa$ Integer	5		U^{28+} B2B transfer from SIS18 to SIS100
	5		H^+ B2B transfer from SIS18 to SIS100
	5		B2B transfer from ESR to CRYRING
$C^l/C^s = \iota + \lambda$ or $frev^s/frev^l = \iota + \lambda$ close to integer (ι is integer)	2-0.003		$h=4$ B2B transfer from SIS18 to ESR
	2-0.003		$h=1$ B2B transfer from SIS18 to ESR
$C^l/C^s = \iota + \lambda$ or $frev^s/frev^l = \iota + \lambda$ far away from integer (ι is expressed by $\frac{m}{n}$)		4.9-0.0004	H^+ B2B transfer from SIS100 to CR
		4.9-0.0004	RIB B2B transfer from SIS100 to CR
	2.6-0.003		B2B transfer from CR to HESR
		1.8+0.048	B2B transfer from SIS18 to ESR via FRS

5.1 Circumference ratio is an ideal integer

If the ratio of the circumference of the injection/extraction orbit of the large synchrotron to that of the small synchrotron is an ideal integer, we have the following relation.

$$\frac{C^l}{C^s} = \kappa \quad (5.1)$$

From the circumference ratio, the revolution frequency ratio of two synchrotrons can be calculated.

$$\frac{f_{rev}^l}{f_{rev}^s} = \frac{1}{\kappa} \quad (5.2)$$

Based on eq. 5.2 and harmonic number, the f_{rf}^X is calculated by eq. 5.3 and eq. 5.4

$$f_{rf}^s = h^s \times f_{rev}^s = h^s \times \kappa \times f_{rev}^l \quad (5.3)$$

5.1. Circumference ratio is an ideal integer

$$f_{rf}^l = h^l \times f_{rev}^l \quad (5.4)$$

Diving eq. 5.4 by eq. 5.3, we get

$$\frac{f_{rf}^l}{f_{rf}^s} = \frac{h^l}{h^s \times \kappa} \quad (5.5)$$

Y is defined as the GCD (Greatest Common Divisor) of h^l and $h^s \times \kappa$.

Tab. 5.2 shows the formulas for the frequency of the bucket label signal, two slightly different frequencies for beating, the length of the synchronization window and the bunch and bucket center mismatch in this scenario.

Table 5.2: Synchronization when the circumference ratio is an ideal integer
(the period of the beating frequency is longer than the revolution period)

	Large synchrotron is target synchrotron	Small synchrotron is target synchrotron
Bucket label	$\frac{f_{rf}^l}{h^l/Y}$	$\frac{f_{rf}^s}{(h^s \times \kappa)/Y}$
Different frequencies	$\frac{f_{rf}^l}{h^l/Y}$ and $\frac{f_{rf}^s}{(h^s \times \kappa)/Y} + \Delta f$ or $\frac{f_{rf}^l}{h^l/Y} + \Delta f$ and $\frac{f_{rf}^s}{(h^s \times \kappa)/Y}$	
Synchronization window	$2 \times (h^l/Y) \times T_{rf}^l$	$2 \times [(h^s \times \kappa)/Y] \times T_{rf}^s$
Center mismatch	$\pm \frac{1}{2} \times \frac{2 \times (h^l/Y) \times T_{rf}^l}{1/\Delta f} \times 360^\circ$	$\pm \frac{1}{2} \times \frac{2 \times [(h^s \times \kappa)/Y] \times T_{rf}^s}{1/\Delta f} \times 360^\circ$

The formulas in Tab. 5.2 is based on the assumption that $\frac{f_{rf}^l}{h^l/Y} < f_{rev}^l$, namely the frequency for beating is smaller than the revolution frequency, so the period of the frequency for beating is long enough to indicate all buckets in one revolution period. If $\frac{f_{rf}^l}{h^l/Y} \geq f_{rev}^l$, the period of the frequency for beating is shorter than the revolution period, which could not be used for the bucket indication. So does for the small synchrotron. In this case, we have the formulas in Tab. 5.3.

Table 5.3: Synchronization when the revolution frequency ratio is an ideal integer
(the period of the beating frequency is shorter than the revolution period)

	Large synchrotron is target synchrotron	Small synchrotron is target synchrotron
Bucket label	f_{rev}^l	f_{rev}^s
Different frequencies	$\frac{f_{rf}^l}{h^l/Y}$ and $\frac{f_{rf}^s}{(h^s \times \kappa)/Y} + \Delta f$ or $\frac{f_{rf}^l}{h^l/Y} + \Delta f$ and $\frac{f_{rf}^s}{(h^s \times \kappa)/Y}$	
Synchronization window	$2 \times T_{rev}^l$	$2 \times T_{rev}^s$
Center mismatch	$\pm \frac{1}{2} \times \frac{2 \times T_{rev}^l}{1/\Delta f} \times 360^\circ$	$\pm \frac{1}{2} \times \frac{2 \times T_{rev}^s}{1/\Delta f} \times 360^\circ$

5.1.1 Harmonic ratio equals to the circumference ratio

When the ratio of the harmonic number of the large synchrotron to that of the small synchrotron equals to the circumference ratio, we have the following relation.

$$\frac{h^l}{h^s} = \frac{C^l}{C^s} = \kappa \quad (5.6)$$

So the GCD of h^l and $h^s \times \kappa$ is $h^l = h^s \times \kappa$, namely $Y=h^l = h^s \times \kappa$.

Substituting eq. 5.6 into eq. 5.5, the following relation is deduced.

$$\frac{f_{rf}^l}{f_{rf}^s} = 1 \quad (5.7)$$

In this scenario, the rf cavity frequencies of two synchrotrons are same. For the RF synchronization, both phase shift and frequency beating methods are applicable for the small or large synchrotrons. There is no difference of the implementation of two methods either on the large or small synchrotron, because they implement their species dependent rf frequency modulation profiles for a same required phase shift and same frequency dutune for the frequency beating method. Only when the target synchrotron is empty, the phase will be shifted for the target synchrotron by the phase jump. With the phase shift method, the phase advance between two synchrotrons is a constant, so the synchronization window is ideally infinitely long, within which two synchrotrons remain perfect synchronized. Bunches can be transferred at any time within the window.

There exists $\frac{f_{rf}^l}{h^l/Y} >= f_{rev}^l = \frac{f_{rf}^l}{h^l}$, so the formulas in Tab. 5.3 is applicable.

5.1.1.1 use case of the U^{28+} B2B transfer from SIS18 to SIS100

The use case of the U^{28+} B2B transfer from SIS18 to SIS100 belongs to this scenario. Four batches of U^{28+} at 200 MeV/u are injected into continuous eight out of ten buckets of SIS100. Each batch consists of two bunches [40, 41]. The large synchroton is SIS100 and the small one SIS18. $\kappa = 5$, $h^{SIS100} = 10$ and $h^{SIS18} = 2$, so it complies with eq. 5.6. Substituting h^X , κ , f_{rf}^X , f_{rev}^X and Y into formulas in Tab. 5.3, the synchronization of U^{28+} B2B transfer from SIS18 to SIS100 is obtained, see Tab. 5.4. Here we assume that SIS18 is detuned with 200 Hz for the frequency beating method.

After the synchronization, the phase difference between the SIS18 and SIS100 revolution frequency markers equals to the sum of $t_{v.inj}$, $t_{v.ext}$ and t_{TOF} . The SIS100 revolution frequency marker works for the bucket label. When the 1st and 2nd buckets are to be filled, $t_{pattern}=0$. When the 3rd and 4th buckets, $t_{pattern}=T_{rev}^{SIS18}$. When the 5th and 6th buckets, $t_{pattern}=2 \times T_{rev}^{SIS18}$. When the 7th and 8th buckets, $t_{pattern}=3 \times T_{rev}^{SIS18}$. Detailed parameters of U^{28+} B2B transfer from SIS18 to SIS100, please see Appendix C.1.

5.1.2 Harmonic ratio does not equal to the circumference ratio

When the ratio of the harmonic number of the large synchrotron to that of the small synchrotron does not equal to the circumference ratio, we have the following

5.1. Circumference ratio is an ideal integer

Table 5.4: Synchronization of U^{28+} B2B transfer from SIS18 to SIS100

	Large synchrotron (SIS100) is target synchrotron
Bucket label	f_{rev}^{SIS100}
Different frequencies	$f_{rf}^{SIS18} + 200\text{Hz}$ and f_{rf}^{SIS100}
Synchronization window	$2 \times T_{rev}^{SIS100} = 12.718\text{ us}$
Center mismatch	$\pm \frac{1}{2} \times \frac{2 \times T_{rev}^{SIS100}}{1/200} \times 360^\circ = \pm 0.50^\circ$

relation.

$$\frac{h^l}{h^s} \neq \frac{C^l}{C^s} = \kappa \quad (5.8)$$

In this scenario, the rf cavity frequency of one synchrotron is integer times of that of the other synchrotron for FAIR accelerators. Both phase shift and frequency beating methods are applicable for the RF synchronization. There is no difference of the implementation of the phase shift method either on the large or small synchrotron, because they implement their species dependent rf frequency modulation profiles for a same required phase shift. Only when the target synchrotron is empty, the phase jump is applied to the target synchrotron. With the phase shift method, we have an infinite synchronization window.

For the frequency beating method, from eq. 5.5, we get

$$\frac{f_{rf}^l}{h^l} = \frac{f_{rf}^s}{h^s \times \kappa} \quad (5.9)$$

If we detune Δf for $\frac{f_{rf}^l}{h^l}$ of the large synchrotron, the rf cavity frequency f_{rf}^l must detune $\Delta f \times h^l$. If we detune Δf for $\frac{f_{rf}^s}{h^s \times \kappa}$ of the small synchrotron, the rf cavity frequency f_{rf}^s must detune $\Delta f \times (h^s \times \kappa)$. According to the relation between h^l and $h^s \times \kappa$, we have the following two cases.

- $h^l > h^s \times \kappa \rightarrow \Delta f \times h^l > \Delta f \times (h^s \times \kappa)$

The frequency detune for the rf cavity frequency of the small synchrotron is smaller than that of the large synchrotron, so the frequency detune is preferred for the small synchrotron.

- $h^l < h^s \times \kappa \rightarrow \Delta f \times h^l < \Delta f \times (h^s \times \kappa)$

The frequency detune for the rf cavity frequency of the large synchrotron is smaller than that of the small synchrotron, so the frequency detune is preferred for the large synchrotron.

5.1.2.1 Use case of the H^+ B2B transfer from SIS18 to SIS100

Four batches of H^+ at 4 GeV/u are injected into continuous four out of ten buckets of SIS100. Each batch consists of one bunch [40, 41]. The large synchrotron is

5.1. Circumference ratio is an ideal integer

SIS100 and the small one SIS18. $\kappa = 5$, $h^{SIS100} = 10$ and $h^{SIS18} = 1$. Substituting these values into eq. 5.5, we get

$$\frac{f_{rf}^{SIS100}}{f_{rf}^{SIS18}} = \frac{h^{SIS100}}{h^{SIS18} \times \kappa} = \frac{10}{1 \times 5} = \frac{2}{1} \quad (5.10)$$

For the frequency beating method, the frequency detune is preferred for SIS18 because of $h^{SIS100} > h^{SIS18} \times \kappa$. The GCD of $h^{SIS100} = 10$ and $h^{SIS18} \times \kappa = 1 \times 5$ is 5. There exists $\frac{f_{rf}^l}{h^l/Y} = \frac{f_{rf}^{SIS100}}{10/5} \geq f_{rev}^l = \frac{f_{rf}^{SIS100}}{10}$. Substituting h^X , κ , f_{rf}^X , f_{rev}^X and Y into formulas in Tab. 5.3, the synchronization of H^+ B2B transfer from SIS18 to SIS100 is obtained, see Tab. 5.5. Here we assume that SIS18 is detuned with 200 Hz for the frequency beating method.

Table 5.5: Synchronization of H^+ B2B transfer from SIS18 to SIS100

	Large synchrotron (SIS100) is target synchrotron
Bucket label	f_{rev}^{SIS100}
Different frequencies	$\frac{f_{rf}^{SIS100}}{2}$ and $f_{rf}^{SIS18} + \Delta f$
Synchronization window	$2 \times T_{rev}^{SIS100} = 7.356 \text{ us}$
Center mismatch	$\pm \frac{1}{2} \times \frac{2 \times T_{rev}^{SIS100}}{1/200} \times 360^\circ = \pm 0.31^\circ$

In order to inject into the odd and even number buckets, there are two scenarios of the phase difference between the SIS18 and SIS100 revolution frequency markers after the synchronization.

- Injection into the odd number buckets

The phase difference between the SIS18 and SIS100 revolution frequency markers equals to $t_{v_ext} + t_{v_inj} + t_{TOF}$. When the 1st bucket is to be filled, $t_{pattern}=0$. When the 3rd bucket is to be filled, $t_{pattern}=2 \times T_{rev}^{SIS18}$.

- Injection into the even number buckets

The phase difference between the SIS18 and SIS100 revolution frequency markers equals to $t_{v_ext} + t_{v_inj} + t_{TOF} - T_{rf}^{SIS100}$. When the 2nd bucket is to be filled, $t_{pattern}=1 \times T_{rev}^{SIS18}$. When the 4th bucket is to be filled, $t_{pattern}=3 \times T_{rev}^{SIS18}$.

The SIS100 revolution frequency marker works for the bucket label. Detailed parameters of the H^+ B2B transfer from SIS18 to SIS100, please see Appendix C.1.

5.1.2.2 use case of the B2B transfer from ESR to CRYRING

Only one bunch is injected into one bucket of CRYRING [10, 47]. The large synchrotron is SIS18 and the small one is CRYRING. $\kappa = 2$, $h^{ESR} = 1$ and $h^{CRYRING} = 1$, substituting into eq. 5.5.

$$\frac{f_{rf}^{ESR}}{f_{rf}^{CRYRING}} = \frac{h^{ESR}}{h^{CRYRING} \times \kappa} = \frac{1}{1 \times 2} = \frac{1}{2} \quad (5.11)$$

5.2. Circumference ratio is not an ideal integer

For the RF synchronization, the phase jump for CRYRING is preferred, because CRYRING is empty before the injection. The 1/2 CRYRING revolution frequency marker works for the bucket label. The phase difference between the ESR and 1/2 CRYRING revolution frequency markers equals to $t_{v,ext} + t_{v,inj} + t_{TOF}$ after the synchronization. For the frequency beating method, the frequency detune is preferred for ESR because of $h^{ESR} < h^{CRYRING} \times \kappa$. Here we assume 200 Hz frequency detune for 30 MeV/u proton of ESR. The GCD of $h^{ESR} = 1$ and $h^{CRYRING} \times \kappa = 1 \times 2$ is 1, namely Y=1.

There exists $\frac{f_{rf}^s}{(h^s \times \kappa)/Y} = \frac{f_{rf}^{CRYRING}}{(1 \times 2)/1} < f_{rev}^s = \frac{f_{rf}^{CRYRING}}{1}$, so Substituting h^X , κ , f_{rf}^X , f_{rev}^X and Y into formulas in Tab. 5.2, the synchronization of the B2B transfer from ESR to CRYRING is obtained, see Tab. C.4.

Table 5.6: Synchronization of B2B transfer from ESR to CRYRING

	Small synchrotron (CRYRING) is target synchrotron
Bucket label	$1/2 f_{rf}^{CRYRING}$
Different frequencies	$f_{rf}^{ESR} + 200\text{Hz}$ and $\frac{f_{rf}^{CRYRING}}{2}$
Synchronization window	$2 \times (2 \times T_{rf}^{CRYRING}) = 5.488\text{ us}$
Center mismatch	$\pm \frac{1}{2} \times \frac{2 \times 2 \times T_{rf}^{CRYRING}}{1/200} \times 360^\circ = \pm 0.20^\circ$

Detailed parameters of the B2B transfer from ESR to CRYRING, please see Appendix C.4.

5.2 Circumference ratio is not an ideal integer

If the ratio of the circumference of the injection/extraction orbit of the large synchrotron to that of the small synchrotron is not an ideal integer, κ could be expressed as $\iota + \lambda$ and we have the following relation.

$$\frac{C^l}{C^s} = \iota + \lambda \quad (5.12)$$

From the circumference ratio, the revolution frequency ratio of two synchrotrons can be calculated.

$$\frac{f_{rev}^l}{f_{rev}^s} = \frac{1}{\iota + \lambda} \quad (5.13)$$

Based on eq. 5.13 and harmonic number, the f_{rf}^X are calculated by eq. 5.14 and eq. 5.15

$$f_{rf}^s = h^s \times f_{rev}^s = h^s \times (\iota + \lambda) \times f_{rev}^l \quad (5.14)$$

$$f_{rf}^l = h^l \times f_{rev}^l \quad (5.15)$$

We could get the relation between f_{rf}^s and f_{rf}^l by dividing eq. 5.15 by eq. 5.14.

$$\frac{f_{rf}^l}{f_{rf}^s} = \frac{h^l}{h^s \times (\iota + \lambda)} = \frac{h^l}{h^s \times \iota + h^s \times \lambda} \quad (5.16)$$

5.2. Circumference ratio is not an ideal integer

In this scenario, two rf cavity frequencies begin beating automatically. So the frequency beating method is preferred. The synchronization window depends on the beating frequency. The beating frequency corresponding to this mismatch must not be too large in order to guarantee a long enough synchronization window, but also not too small to satisfy the constraint of the maximum synchronization time.

5.2.1 Circumference ratio is close to an ideal integer

When the circumference ratio of the large synchrotron to that of the small synchrotron is very close to an ideal integer, ι in eq. 5.12 is an integer and λ has the order of magnitude 10^{-2} .

In eq. 5.16, $h^s \times \lambda$ is much smaller than $h^s \times \iota$ and h^l , so the frequency beating method is preferred. Y is the GCD of h^l and $h^s \times \iota$.

Besides, it is also grouped to this scenario, that the revolution frequency ratio between the small and large synchrotrons is close to an ideal integer when the beam passes some target (e.g. FRS, Pbar) between two synchrotrons. The ratio between the revolution frequencies can be expressed as

$$\frac{f_{rev}^s}{f_{rev}^l} = \iota + \lambda \quad (5.17)$$

The realtion between two cavity rf frequencies is same as eq. 5.16.

Tab. 5.7 shows the formulas for the frequency of the bucket label signal, two slightly different frequencies for beating, the length of the synchronization window and the bunch and bucket center mismatch in this scenario.

Table 5.7: Synchronization when circumference ratio is close to an ideal integer

	Large synchrotron is target synchrotron	Small synchrotron is target synchrotron
Bucket label	$\frac{f_{rf}^l}{h^l/Y}$	$\frac{f_{rf}^s}{(h^s \times \iota)/Y}$
Different frequencies	$\frac{f_{rf}^l}{h^l/Y}$ and $\frac{f_{rf}^s}{(h^s \times \iota)/Y}$	
Beating frequencies	$\Delta f = \frac{f_{rf}^l}{h^l/Y} - \frac{f_{rf}^s}{(h^s \times \iota)/Y}$	
Synchronization window	$2 \times [h^l/Y] \times T_{rf}^l$	$2 \times [(h^s \times \iota)/Y] \times T_{rf}^s$
Center mismatch	$\pm \frac{1}{2} \times \frac{2 \times (h^l/Y) \times T_{rf}^l}{1/\Delta f} \times 360^\circ$	$\pm \frac{1}{2} \times \frac{2 \times [(h^s \times \iota)/Y] \times T_{rf}^s}{1/\Delta f} \times 360^\circ$

In fact, two slightly different frequencies could be fraction (between 1/Y and 1) times of the $\frac{f_{rf}^l}{h^l/Y}$ and $\frac{f_{rf}^s}{(h^s \times \iota)/Y}$. The bucket label frequency and the beating frequency are proportional to the slightly difference frequencies by the coefficient of the fraction and the length of the synchronization window is inversely proportional to the slightly difference frequencies by the coefficient of the reciprocal for the fraction. The bunch to bucket center mismatch is proportional to the synchronization window and the beating frequency, whose coefficient product is 1, so the mismatch is determined by $\frac{f_{rf}^l}{h^l/Y}$ and $\frac{f_{rf}^s}{(h^s \times \iota)/Y}$.

5.2. Circumference ratio is not an ideal integer

5.2.1.1 use case of h=4 B2B transfer from SIS18 to ESR

Continuous two of four bunches are injected into one bucket of the injection orbit of ESR [48]. The beam is accumulated in ESR. The large synchrotron is SIS18 and the small one is ESR. $h^{SIS18} = 4$ and $h^{ESR} = 1$. Substituting the circumference of SIS18 and ESR into eq. 5.12, we get

$$\frac{C^l}{C^s} = \iota + \lambda = 2 - 0.003 \quad (5.18)$$

Substituting h^{SIS18} , h^{ESR} , ι and λ into eq. 5.16, we get

$$\frac{f_{rf}^{SIS18}}{f_{rf}^{ESR}} = \frac{h^{SIS18}}{h^{ESR} \times (\iota + \lambda)} = \frac{4}{1 \times (2 - 0.003)} \quad (5.19)$$

The GCD of $h^{SIS18} = 4$ and $h^{ESR} \times \iota = 1 \times 2 = 2$ is 2, namely Y=2. Substituting h^X , ι , λ , f_{rf}^X and Y into formulas in Tab. 5.7, the synchronization of h=4 B2B transfer from SIS18 to ESR is obtained, see Tab. 5.8. Here we use 30 MeV/u heavy ion as an example.

Table 5.8: Synchronization of h=4 B2B transfer from SIS18 to ESR

	Small synchrotron (ESR) is target synchrotron
Bucket label	$\frac{1}{2/2} f_{rf}^{ESR}$
Different frequencies	$\frac{f_{rf}^{SIS18}}{4/2} = 686.600 \text{ kHz}$ and $\frac{f_{rf}^{ESR}}{2/2} = 685.652 \text{ kHz}$
Beating frequencies	948 Hz
Synchronization window	$2 \times (2/2) \times T_{rf}^{ESR} = 2.917 \text{ us}$
Center mismatch	$\pm \frac{1}{2} \times \frac{2 \times (2/2) \times T_{rf}^{ESR}}{1/948} \times 360^\circ = \pm 0.51^\circ$

Detailed parameters of the $h = 4$ B2B transfer from SIS18 to ESR, please see Appendix C.2.

In the real operation, ESR uses different methods, e.g. barrier bucket or unstable fixed point, to accumulate beam instead of normal bucket [48]. Presently two general schemes of the particle accumulation are possible: moving or fixed barrier RF bucket [49]. In the scheme with moving barrier RF bucket, the bunch is injected in the longitudinal gap prepared by two barrier pulses. The injected beam becomes coasting after switching off the barrier voltages and merges with the previously stacked beam. The barrier voltages are switched on and moved away from each other to prepare the empty space for the next beam injection. In the fixed barrier bucket scheme, one prepares a stationary voltage distribution consisting of two barrier pulses of opposite sign. The resulting stretched rf potential separates the longitudinal phase space into a stable and an unstable region. After injection onto the unstable region (potential maximum), the particles circulate along all phases and cooling application leads to their capture in the stable region of the phase space

5.2. Circumference ratio is not an ideal integer

(potential well). After some time of the beam cooling the unstable region is free for a next injection without losing of the stored beam. With the barrier bucket, the bunch should be injected into the longitudinal gap or the unstable region of the barrier bucket.

After the synchronization, the phase difference between the 1/2 SIS18 and ESR cavity rf frequency markers depends on the accumulation method.

5.2.1.2 use case of h=1 B2B transfer from SIS18 to ESR

One bunch is injected into one bucket of the injection orbit of ESR. The beam is accumulated in ESR. The large synchrotron is SIS18 and the small one is ESR. $h^{SIS18} = 1$ and $h^{ESR} = 1$. Substituting the circumference of SIS18 and ESR into eq. 5.12, we get

$$\frac{C^l}{C^s} = \iota + \lambda = 2 - 0.003 \quad (5.20)$$

Substituting h^{SIS18} , h^{ESR} , ι and λ into eq. 5.16, we get

$$\frac{f_{rf}^{SIS18}}{f_{rf}^{ESR}} = \frac{h^l}{h^s \times (\iota + \lambda)} = \frac{1}{1 \times (2 - 0.003)} \quad (5.21)$$

The GCD of $h^{SIS18} = 1$ and $h^{ESR} \times \iota = 1 \times 2 = 2$ is 1, namely Y=1. Substituting h^X , ι , λ , f_{rf}^X and Y into formulas in Tab. 5.7, the synchronization of h=1 B2B transfer from SIS18 to ESR is obtained, see Tab. 5.9. Here we use 400 MeV/u proton as an example.

Table 5.9: Synchronization of h=1 B2B transfer from SIS18 to ESR

	Small synchrotron (ESR) is target synchrotron
Bucket label	$1/2 f_{rf}^{ESR}$
Different frequencies	$\frac{f_{rf}^{SIS18}}{1} = 989.756 \text{ kHz}$ and $\frac{f_{rf}^{ESR}}{2} = 988.388 \text{ kHz}$
Beating frequencies	1368 Hz
Synchronization window	$2 \times 2 \times T_{rf}^{ESR} = 2.034 \text{ us}$
Center mismatch	$\pm \frac{1}{2} \times \frac{2 \times 2 \times T_{rf}^{ESR}}{1/1368} \times 360^\circ = \pm 0.50^\circ$

Detailed parameters of the $h = 1$ B2B transfer from SIS18 to ESR, please see Appendix C.2. After the synchronization, the phase difference between the SIS18 and 1/2 ESR cavity rf frequency markers depends on the accumulation method.

5.2.2 Circumference ratio is far away from an ideal integer

When the circumference ratio of the large synchrotron to that of the small synchrotron is far away from an ideal integer, ι in eq. 5.12 could be denoted by $\frac{m}{n}$ (m and n are integers) and eq. 5.12 could be expressed as

5.2. Circumference ratio is not an ideal integer

$$\frac{C^l}{C^s} = \frac{m}{n} + \lambda \quad (5.22)$$

Substituting λ by $\frac{m}{n}$ into eq. 5.16, we could get the relation between f_{rf}^s and f_{rf}^l .

$$\frac{f_{rf}^l}{f_{rf}^s} = \frac{h^l \times n}{h^s \times m + h^s \times \lambda \times n} \quad (5.23)$$

Y is the GCD of $h^l \times n$ and $h^s \times m$.

Besides, it is also grouped to this scenario, that the revolution frequency ratio between the small and large synchrotrons is far away from an ideal integer when the beam passes some target (e.g. FRS, Pbar) between two synchrotrons. The revolution frequency ratio can be expressed as

$$\frac{f_{rev}^s}{f_{rev}^l} = \frac{m}{n} + \lambda \quad (5.24)$$

The relation between two rf cavity frequencies is same as eq. 5.23.

Tab. 5.10 shows the formulas for the frequency of the bucket label signal, two slightly different frequencies for beating, the length of the synchronization window and the bunch and bucket center mismatch in this scenario.

Table 5.10: Synchronization when circumference ratio is far away from an ideal integer

	Large synchrotron is target synchrotron	Small synchrotron is target synchrotron
Bucket label	$\frac{f_{rf}^l}{(h^l \times n)/Y}$	$\frac{f_{rf}^s}{(h^s \times m)/Y}$
Different frequencies	$\frac{f_{rf}^l}{(h^l \times n)/Y}$ and $\frac{f_{rf}^s}{(h^s \times m)/Y}$	
Beating frequencies	$\Delta f = \frac{f_{rf}^l}{(h^l \times n)/Y} - \frac{f_{rf}^s}{(h^s \times m)/Y}$	
Synchronization window	$2 \times [(h^l \times n)/Y] \times T_{rf}^l$	$2 \times [(h^s \times m)/Y] \times T_{rf}^s$
Center mismatch	$\pm \frac{1}{2} \times \frac{2 \times [(h^l \times n)/Y] \times T_{rf}^l}{1/\Delta f} \times 360^\circ$	$\pm \frac{1}{2} \times \frac{2 \times [(h^s \times m)/Y] \times T_{rf}^s}{1/\Delta f} \times 360^\circ$

There are various combination of $\frac{m}{n}$ and λ , λ determines the beating speed. The smaller, the more precise bunch to bucket injection. $(h^l \times n)/Y$ and $(h^s \times m)/Y$ determines the two slightly different frequencies. The bigger $(h^l \times n)/Y$ and $(h^s \times m)/Y$, the smaller two slightly different frequencies, which has higher requirement for LLRF system. So we have to find a balance between the bunch to bucket center mismatch and the low frequencies for beating.

Two slightly different frequencies could be fraction (between $1/Y$ and 1) times of the $\frac{f_{rf}^l}{(h^l \times n)/Y}$ and $\frac{f_{rf}^s}{(h^s \times m)/Y}$. The bucket label frequency and the beating frequency are proportional to the slightly difference frequencies by the coefficient of the fraction and the length of the synchronization window is inversely proportional to the slightly

5.2. Circumference ratio is not an ideal integer

difference frequencies by the coefficient of the reciprocal for the fraction. The bunch to bucket center mismatch is proportional to the synchronization window and the beating frequency, whose coefficient product is 1, so the mismatch is determined by $\frac{f_{rf}^l}{(h^l \times n)/Y}$ and $\frac{f_{rf}^s}{(h^s \times m)/Y}$.

5.2.2.1 use case of H^+ B2B transfer from SIS100 to CR

Only one out of five bunches of proton is extracted from SIS100 and goes to Pbar, then antiproton is produced and injected into one bucket of CR [48]. The large synchrotron is SIS100 and the small one is CR, $h^{SIS100} = 5$ and $h^{CR} = 1$. Here we take an example, that the proton energy before the Pbar is 28.8 GeV/u and the antiproton energy after the Pbar is 3 GeV/u. Substituting the extraction and injection revolution frequencies into eq. 5.24, we get

$$\frac{f_{rev}^{CR}}{f_{rev}^{SIS100}} = 4.9 - 0.0004 = \frac{m}{n} + \lambda = \frac{49}{10} - 0.0004 \quad (5.25)$$

Substituting h^{SIS100} , h^{CR} , m, n and λ into eq. 5.23, we get

$$\frac{f_{rf}^{SIS100}}{f_{rf}^{CR}} = \frac{h^{SIS100} \times n}{h^{CR} \times m + h^{CR} \times \lambda \times n} = \frac{5 \times 10}{1 \times 49 - 1 \times 0.0004 \times 10} \quad (5.26)$$

The GCD of $h^{SIS100} \times n = 5 \times 10 = 50$ and $h^{CR} \times m = 1 \times 49 = 49$ is 1, namely Y=1. Substituting h^X , m, n, λ , f_{rf}^X and Y into formulas in Tab. 5.10, the synchronization of proton B2B transfer from SIS100 to CR is obtained, see Tab. 5.11.

Table 5.11: Synchronization of H^+ B2B transfer from SIS100 to CR

	Small synchrotron (CR) is target synchrotron
Bucket label	$1/49 f_{rf}^{CR}$
Different frequencies	$\frac{f_{rf}^{SIS100}}{50} = 26.658 \text{ kHz}$ and $\frac{f_{rf}^{CR}}{49} = 26.873 \text{ kHz}$
Beating frequencies	215 Hz
Synchronization window	$2 \times 49 \times T_{rf}^{CR} = 74.382 \text{ us}$
Center mismatch	$\pm \frac{1}{2} \times \frac{2 \times 49 \times T_{rf}^{CR}}{1/215} \times 360^\circ = \pm 2.88^\circ$

The CR is empty before the injection, so the phase jump is preferred for CR. Detailed parameters of the H^+ B2B transfer from SIS100 to CR, please see Appendix C.6.

5.2.2.2 use case of RIB B2B transfer from SIS100 to CR

Only one out of two bunches is extracted from SIS100 and goes to Super FRS, then RIB is produced and injected into one bucket of CR. The large synchrotron is SIS100 and the small one is CR. $h^{SIS100} = 2$ and $h^{CR} = 1$. Here we take an example, that

5.2. Circumference ratio is not an ideal integer

the energy of the heavy ion beam before the Super FRS is 1.5 GeV/u and the RIB energy after the Super FRS is 740 MeV/u. Substituting the extraction and injection revolution frequencies into eq. 5.24, we get

$$\frac{f_{rev}^{CR}}{f_{rev}^{SIS100}} = 4.4 - 0.005 = \frac{m}{n} + \lambda = \frac{22}{5} - 0.01 \quad (5.27)$$

Substituting h^{SIS100} , h^{CR} , m, n and λ into eq. 5.23, we get

$$\frac{f_{rf}^{SIS100}}{f_{rf}^{CR}} = \frac{h^{SIS100} \times n}{h^{CR} \times m + h^{CR} \times \lambda \times n} = \frac{2 \times 5}{1 \times 22 - 1 \times 0.01 \times 5} \quad (5.28)$$

The GCD of $h^{SIS100} \times n = 2 \times 5 = 10$ and $h^{CR} \times m = 1 \times 22 = 22$ is 2, namely Y=2. Substituting h^l , h^s , m, n, λ , f_{rf}^X and Y into formulas in Tab. 5.10, the synchronization of RIB B2B transfer from SIS100 to CR is obtained, see Tab. 5.12.

Table 5.12: Synchronization of RIB B2B transfer from SIS100 to CR

	Small synchrotron (CR) is target synchrotron
Bucket label	$\frac{1}{22/2} f_{rf}^{CR}$
Different frequencies	$\frac{f_{rf}^{SIS100}}{10/2} = 102.326 \text{ kHz}$ and $\frac{f_{rf}^{CR}}{22/2} = 102.218 \text{ kHz}$
Beating frequencies	108 Hz
Synchronization window	$2 \times (22/2) \times T_{rf}^{CR} = 19.558 \text{ us}$
Center mismatch	$\pm \frac{1}{2} \times \frac{2 \times 22 \times T_{rev}^{CR}}{1/54} \times 360^\circ = \pm 0.39^\circ$

The CR is empty before the injection, so the phase jump is preferred for CR. Detailed parameters of RIB B2B transfer from SIS100 to CR, please see Appendix C.6.

5.2.2.3 use case of B2B transfer from CR to HESR

One bunch of CR is injected into one bucket of HESR. The beam is accumulated in HESR [9]. The large synchrotron is HESR and the small one is CR. $h^{HESR} = 1$ and $h^{CR} = 1$. Substituting the circumference of HESR and CR to eq. 5.22, we have

$$\frac{C^{HESR}}{C^{CR}} = 2.6 - 0.003 = \frac{m}{n} + \lambda = \frac{13}{5} - 0.003 \quad (5.29)$$

Substituting h^{HESR} , h^{CR} , m, n and λ into eq. 5.23, we get Eq. 5.23 is expressed as

$$\frac{f_{rf}^{HESR}}{f_{rf}^{CR}} = \frac{h^{HESR} \times n}{h^{CR} \times m + h^{ESR} \times \lambda \times n} = \frac{1 \times 5}{1 \times 13 - 1 \times 0.003 \times 5} \quad (5.30)$$

The GCD of $h^{HESR} \times n = 1 \times 5 = 5$ and $h^{CR} \times m = 1 \times 13 = 13$ is 1, namely Y=1. Substituting h^X , m, n, λ , f_{rf}^X and Y into formulas in Tab. 5.10, the synchronization

5.2. Circumference ratio is not an ideal integer

of B2B transfer from CR to HESR is obtained. Tab. 5.13 shows two operations for antiproton and RIB.

Table 5.13: Synchronization of B2B transfer from CR to HESR

	Larger synchrotron (HESR) is target synchrotron
Bucket label	$1/5f_{rf}^{HESR}$
	3 GeV/u antiproton
Different frequencies	$\frac{f_{rf}^{CR}}{13} = 101.290 \text{ kHz}$ and $\frac{f_{rf}^{HESR}}{5} = 101.426 \text{ kHz}$
Beating frequencies	136 Hz
Synchronization window	$2 \times 5 \times T_{rf}^{HESR} = 19.719 \text{ us}$
Center mismatch	$\pm \frac{1}{2} \times \frac{2 \times 5 \times T_{rev}^{CR}}{1/136} \times 360^\circ = \pm 0.48^\circ$
	740 MeV/u RIB
Different frequencies	$\frac{f_{rf}^{CR}}{13} = 86.493 \text{ kHz}$ and $\frac{f_{rf}^{HESR}}{5} = 86.608 \text{ kHz}$
Beating frequencies	113 Hz
Synchronization window	$2 \times 5 \times T_{rf}^{HESR} = 23.090 \text{ us}$
Center mismatch	$\pm \frac{1}{2} \times \frac{2 \times 5 \times T_{rev}^{CR}}{1/113} \times 360^\circ = \pm 0.47^\circ$

After the synchronization, the phase difference between the 1/13 CR and 1/5 HESR revolution frequency markers depends on the accumulation method. Detailed parameter about the B2B transfer from CR to HESR, please see Appendix C.5.

5.2.2.4 use case of B2B transfer from SIS18 to ESR via FRS

Only one bunch is extracted from SIS18 and goes to FRS, then RIB is produced and injected into one bucket of ESR. The large synchrotron is SIS18 and the small one is ESR. $h^{SIS18} = 1$ and $h^{ESR} = 1$. Here we take an applied case as an example, that the energy of the heavy ion beam before the FRS is 550 MeV/u and the RIB energy after the FRS is 400 MeV/u. Substituting the extraction and injection revolution frequencies into eq. 5.24, we get

$$\frac{f_{rev}^{ESR}}{f_{rev}^{SIS18}} = 1.8 + 0.048 = \frac{m}{n} + \lambda = \frac{9}{5} + 0.048 \quad (5.31)$$

Substituting h^{SIS18} , h^{ESR} , m, n and λ into eq. 5.23, we get

$$\frac{f_{rf}^{SIS18}}{f_{rf}^{ESR}} = \frac{h^{SIS18} \times n}{h^s \times m + h^{ESR} \times \lambda \times n} = \frac{1 \times 5}{1 \times 9 + 1 \times 0.048 \times 5} \quad (5.32)$$

5.3. Summary of the synchronization for different scenarios

The GCD of $h^{SIS18} \times n = 1 \times 5 = 5$ and $h^s \times m = 1 \times 9 = 9$ is 1, namely Y=1. Substituting h^X , m, n, λ , f_{rf}^X and Y into formulas in Tab. 5.10, the synchronization of B2B transfer from SIS18 to ESR via FRS is obtained, see Tab. 5.14.

Table 5.14: Synchronization of B2B transfer from SIS18 to ESR via FRS

	Small synchrotron (ESR) is target synchrotron
Bucket label	$1/9f_{rf}^{ESR}$
Different frequencies	$\frac{f_{rf}^{SIS18}}{5/1} = 215.393 \text{ kHz}$ and $\frac{f_{rf}^{ESR}}{9/1} = 219.642 \text{ kHz}$
Beating frequencies	4.249 kHz
Synchronization window	$2 \times 9 \times T_{rf}^{ESR} = 9.106 \text{ us}$
Center mismatch	$\pm \frac{1}{2} \times \frac{2 \times 9 \times T_{rev}^{ESR}}{1/4249} \times 360^\circ = \pm 6.92^\circ$

More parameters about the B2B transfer from SIS18 to ESR via FRS, please see Appendix C.3. For the detailed realization and implementation of two slightly different frequencies, please see “Development of the LLRF system for a deterministic Bunch-to-Bucket transfer for FAIR“.

5.3 Summary of the synchronization for different scenarios

In this section, all the synchronization methods are summarized in Tab. 5.15.

5.3. Summary of the synchronization for different scenarios

Table 5.15: Summary of the synchronization

Circumference ratio	RF cavity frequency ratio f_{rf}^l/f_{rf}^s	Bucket label ¹ (large or small is target synchrotron)	Frequency beating Two slightly different frequencies	Frequency beating Bunch-Bucket center mismatch (large or small is target synchrotron)
$C^l/C^s = \kappa$ Integer	$\frac{h^l}{h^{s \times \kappa}}$	$\frac{f_{rf}^l}{h^l/Y} \text{ and } \frac{f_{rf}^s}{(h^{s \times \kappa})/Y}$ or $\frac{f_{rf}^l}{h^l/Y} + \Delta f \text{ and } \frac{f_{rf}^s}{(h^{s \times \kappa})/Y}$	$\frac{f_{rf}^s}{h^l/Y} \text{ and } \frac{f_{rf}^l}{(h^{s \times \kappa})/Y} + \Delta f$ or $\frac{f_{rf}^l}{h^l/Y} + \Delta f \text{ and } \frac{f_{rf}^s}{(h^{s \times \kappa})/Y}$	$\pm \frac{1}{2} \times \frac{2 \times (h^l/Y) \times T_{rf}^l}{1/\Delta f} \times 360^\circ$ or $\pm \frac{1}{2} \times \frac{2 \times ((h^s \times \kappa)/Y) \times T_{rf}^s}{1/\Delta f} \times 360^\circ$
$C^l/C^s = \iota + \lambda$ or $frev^s/frev^l = \iota + \lambda$ close to integer (ι is integer)	$\frac{h^l}{h^{s \times (\iota + \lambda)}}$	$\frac{f_{rf}^l}{h^l/Y} \text{ or } \frac{f_{rf}^s}{(h^{s \times \iota})/Y}$	$\frac{f_{rf}^l}{h^l/Y} \text{ and } \frac{f_{rf}^s}{(h^{s \times \iota})/Y}$	$\pm \frac{1}{2} \times \frac{2 \times (h^l/Y) \times T_{rf}^l}{1/\Delta f} \times 360^\circ$ or $\pm \frac{1}{2} \times \frac{2 \times ((h^s \times \iota)/Y) \times T_{rf}^s}{1/\Delta f} \times 360^\circ$
$C^l/C^s = \iota + \lambda$ or $frev^s/frev^l = \iota + \lambda$ far away from integer (ι is expressed by $\frac{m}{n}$)	$\frac{h^l}{h^{s \times (m/n + \lambda)}}^2$	$\frac{f_{rf}^l}{(h^{l \times n})/Y} \text{ or } \frac{f_{rf}^s}{(h^{s \times m})/Y}$	$\frac{f_{rf}^l}{(h^{l \times n})/Y} \text{ and } \frac{f_{rf}^s}{(h^{s \times m})/Y}$	$\pm \frac{1}{2} \times \frac{2 \times ((h^l \times n)/Y) \times T_{rf}^l}{1/\Delta f} \times 360^\circ$ or $\pm \frac{1}{2} \times \frac{2 \times ((h^s \times m)/Y) \times T_{rf}^s}{1/\Delta f} \times 360^\circ$

The phase shift could be implemented either for the large or small synchrotron.

When the target synchrotron is empty, the phase jump is implemented for the target synchrotron.

¹Here we assume that the frequency for beating is smaller than the revolution frequency

$$2 \frac{f_{rf}^l}{f_{rf}s} = \frac{h^l f_{rev}^l}{h^s f_{rev}} = \frac{h^l C^s}{h^s C_l} = \frac{h^l}{h^s(m/n + \lambda)} = \frac{h^l \times n}{h^s \times m + h^s \times \lambda \times n}$$

Chapter 6

Realization and systematic investigation of the FAIR B2B transfer system

This chapter concentrates on the realization and systematic investigation of the B2B transfer system. In Sec. 6.1, both the phase shift and frequency beating synchronization methods are analyzed from the beam dynamic viewpoint. The WR network is investigated for the B2B transfer and the calculation of the synchronization window are presented in Sec. 6.2. The B2B transfer system for FAIR focuses first of all on SIS18 to SIS100 transfer, so the trigger possibility of the SIS18 extraction and SIS100 injection kicker is systematically investigated in Sec. 6.3. Besides, the test setup from the timing aspect is built in Sec. 6.4.

6.1 Investigation of two synchronization methods for U^{28+} B2B transfer from SIS18 to SIS100 from the beam dynamics viewpoint

This section analyzes the phase shift and frequency beating methods from the beam-dynamics viewpoint for the synchronization of SIS18 with SIS100. In this chapter, the circumference of SIS18 and SIS100 are denoted by C^{SIS18} and C^{SIS100} , the revolution frequency by $f_{h=1}^{SIS18}$ and $f_{h=1}^{SIS100}$ and the rf frequency by $f_{h=2}^{SIS18}$ and $f_{h=10}^{SIS100}$. Since SIS18 and SIS100 harmonic number are 2 and 10, the relationship between the revolution and rf frequencies are $f_{h=2}^{SIS18} = 2f_{h=1}^{SIS18}$ and $f_{h=10}^{SIS100} = 10f_{h=1}^{SIS100}$. Since C^{SIS100} is five times as long as C^{SIS18} , we could get the relation $f_{h=1}^{SIS18} = 5f_{h=1}^{SIS100}$ and $f_{h=10}^{SIS100} = f_{h=2}^{SIS18}$.

6.1.1 Phase shift method

To achieve a required phase shift, the RF frequency is modulated away from the nominal value for a period of time and modulated back [22]. Let $\Delta\phi_{shift}$ be the phase shift to be achieved and $\Delta f_{rf}(t)$ the RF frequency variation to accomplish it; then,

$$\Delta\phi_{shift} = 2\pi \int_{t_0}^{t_0+T} \Delta f_{rf}(t) dt \quad (6.1)$$

6.1. Investigation of two synchronization methods for U^{28+} B2B transfer from SIS18 to SIS100 from the beam dynamics viewpoint

where T is the period of frequency modulation and t_0 is the time at which the modulation begins. To make the frequency modulation effective, the stabilization system, beam-phase feedback loop, must be frozen before the modulation begins.

The following four examples of frequency modulation are analyzed. Case (1) trapezoid modulation, Case (2) triangular modulation, Case (3) sinusoidal modulation and Case (4) parabolic modulation. Here I assume the phase shift must be achieved within 7ms. These frequency modulations are shown in Fig. 6.1. All the four modulations give the same phase shift, $\Delta\phi_{shift} = \pi$, which is proved by substituting each form of $\Delta f_{rf}(t)$ into eq. 6.1 and performing integration.

Case (1)

$$\Delta f_{rf}(t) = \begin{cases} 50\text{Hz}/\text{ms} \times (t - t_0) & t_0 + 0 < t \leq t_0 + 2\text{ms} \\ 100\text{Hz} & t_0 + 2 < t \leq t_0 + 5\text{ms} \\ 100\text{Hz} - 50\text{Hz}/\text{ms} \times (t - t_0) & t_0 + 5\text{ms} < t \leq t_0 + 7\text{ms} \end{cases} \quad (6.2)$$

Case (2)

$$\Delta f_{rf}(t) = \begin{cases} \frac{10^3}{7 \times 3.5} \text{Hz}/\text{ms} \times (t - t_0) & t_0 + 0 < t \leq t_0 + 3.5\text{ms} \\ \frac{10^3}{7} \text{Hz} - \frac{10^3}{7 \times 3.5} \text{Hz}/\text{ms} \times (t - t_0 - 3.5\text{ms}) & t_0 + 3.5\text{ms} < t \leq t_0 + 7\text{ms} \end{cases} \quad (6.3)$$

Case (3)

$$\Delta f_{rf}(t) = \frac{10^3}{14} \text{Hz} \times \left(1 - \cos\left(\frac{2\pi}{7} \text{rad}/\text{ms} \times (t - t_0)\right)\right) \quad t_0 + 0 < t \leq t_0 + 7\text{ms} \quad (6.4)$$

Case (4)

$$\Delta f_{rf}(t) = \frac{20}{21} \times \begin{cases} 30\text{Hz}/\text{ms}^2 \times (t - t_0)^2 & t_0 + 0 < t \leq t_0 + 1\text{ms} \\ 30\text{Hz} + 60\text{Hz}/\text{ms} \times (t - t_0 - 1\text{ms}) & t_0 + 1\text{ms} < t \leq t_0 + 2.5\text{ms} \\ 30\text{Hz}/\text{ms}^2 \times [5\text{ms}^2 - (t - t_0 - 3.5\text{ms})^2] & t_0 + 2.5\text{ms} < t \leq t_0 + 4.5\text{ms} \\ 30\text{Hz} + 60\text{Hz}/\text{ms} \times [6\text{ms} - (t - t_0)] & t_0 + 4.5\text{ms} < t \leq t_0 + 6\text{ms} \\ 30\text{Hz}/\text{ms}^2 \times [7\text{ms}^2 - (t - t_0)]^2 & t_0 + 6\text{ms} < t \leq t_0 + 7\text{ms} \end{cases} \quad (6.5)$$

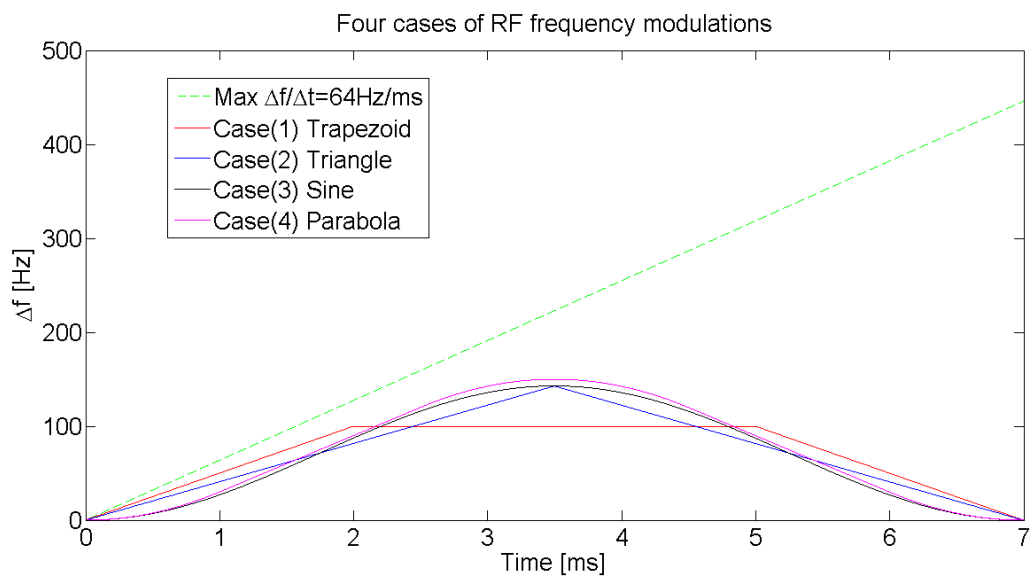


Figure 6.1: Examples of RF frequency modulation.

6.1. Investigation of two synchronization methods for U^{28+} B2B transfer from SIS18 to SIS100 from the beam dynamics viewpoint

Fig. 6.2 shows the time derivation of four rf frequency modulations, which are smaller than the maximum time derivative of rf frequency during the acceleration ramp 64Hz/ms for the adiabaticity consideration. The acceleration ramp is an adiabatical process.

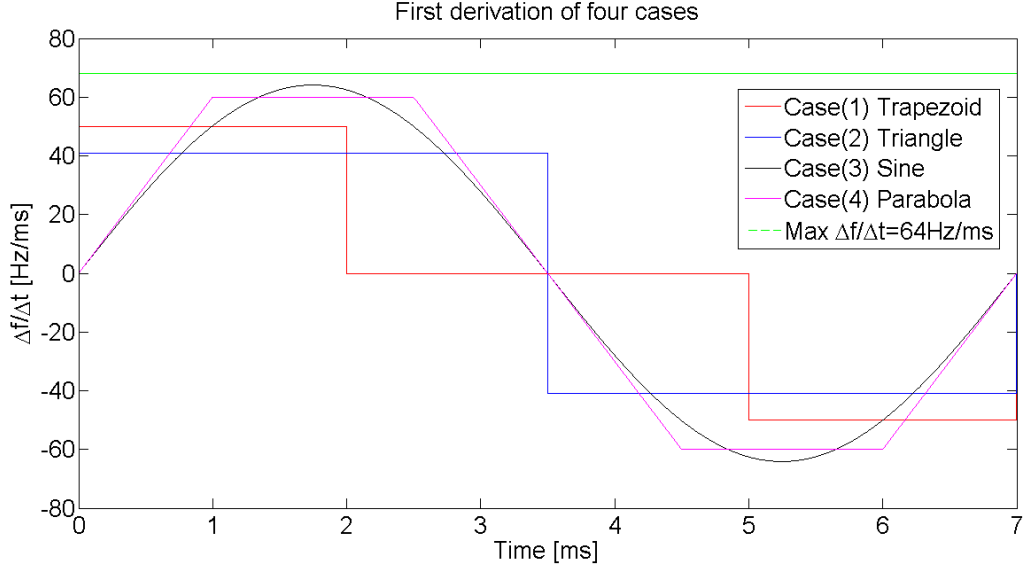


Figure 6.2: Time derivation of four modulations

Fig. 6.3 shows the corresponding phase shift modulation of four cases.

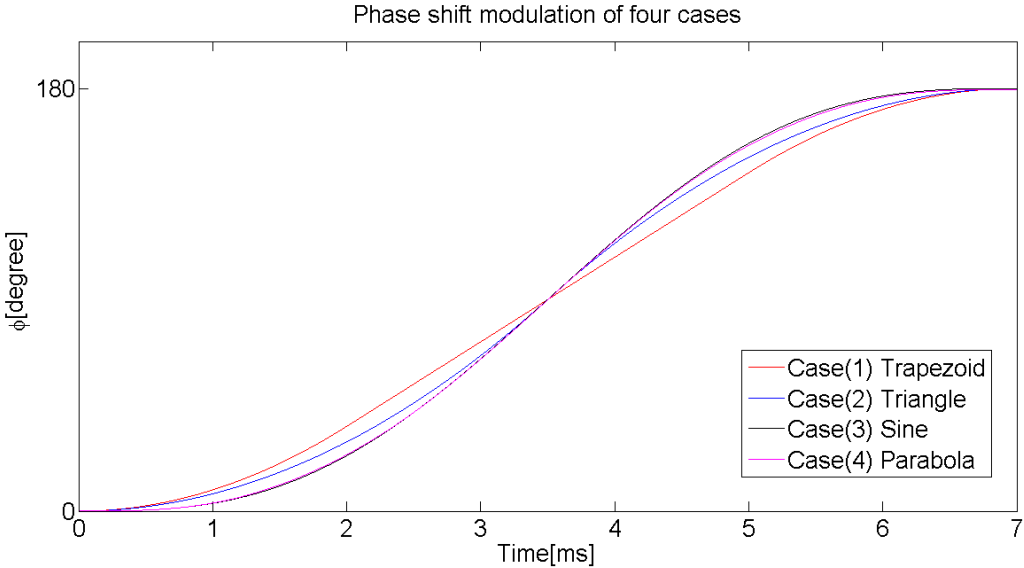


Figure 6.3: The phase shift modulation of four cases

6.1.1.1 Longitudinal dynamic analysis for the simulation

In this section, the average radial excursion, the relative momentum shift, synchronous phase, bucket size and adiabaticity of four rf frequency modulations are analyzed.

- Average radial excursion

6.1. Investigation of two synchronization methods for U^{28+} B2B transfer from SIS18 to SIS100 from the beam dynamics viewpoint

The average radial excursion is calculated for the four cases of rf frequency modulations by eq. (2.25). Fig. 6.4 shows the calculation result [50].

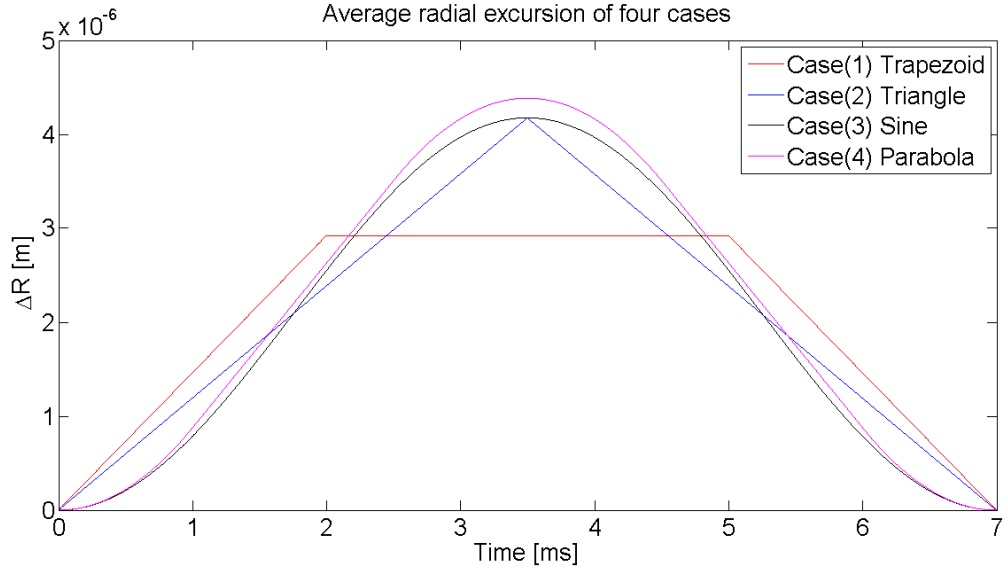


Figure 6.4: Average radial excursions of four cases.

Table 6.1: The maximum average radial excursion of four cases

	Case (1)	Case (2)	Case (3)	Case (4)
Max avg radial excursion	2.93×10^{-6}	4.17×10^{-6}	4.18×10^{-6}	4.38×10^{-6}
Time	flat	3.5 ms	3.5 ms	3.5 ms

Tab. 6.1 shows the maximum average radial excursion and the time for four cases. The maximum tolerable radial excursion of SIS18 is $\pm 2.4 \times 10^{-4}$. For all cases, the average radial excursion is within the acceptable range. Hence, all cases are applicable.

- Relative momentum shift

The relative momentum shift is calculated for the four cases of rf frequency modulations by eq. (2.26). Fig. 6.5 shows the calculation result.

6.1. Investigation of two synchronization methods for U^{28+} B2B transfer from SIS18 to SIS100 from the beam dynamics viewpoint

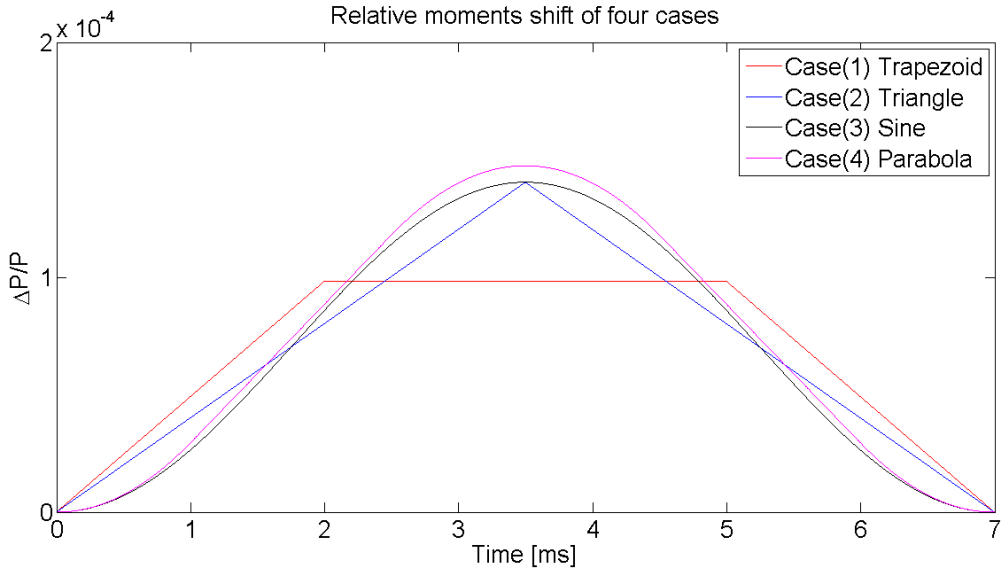


Figure 6.5: Relative momentum shift of four cases.

Table 6.2: The maximum relative momentum shift of four cases

	Case (1)	Case (2)	Case (3)	Case (4)
Max relative momentum shift	9.83×10^{-5}	1.38×10^{-4}	1.40×10^{-4}	1.48×10^{-4}
Time	flat	3.5 ms	3.5 ms	3.5 ms

Tab. 6.2 shows the maximum relative momentum shift and the time for four cases. The maximum tolerable relative momentum shift of SIS18 is ± 0.008 . For all cases, the maximum relative momentum shift is within the acceptable range. Hence, all cases are applicable.

- Synchronous phase

The rf frequency modulations make the synchronous phase deviate from the nominal value 0° . Fig. 6.6 shows the changes in the synchronous phase, $\Delta\phi_s(t)$. It is calculated by substituting values into eq. 2.33. For case (1), the phase jumps in $\Delta\phi_s(t)$ appear at the start and end of the frequency modulation, and at two points where the slope of modulation changes from upward to flat and from flat to downward. For case (2), the phase jumps in $\Delta\phi_s(t)$ appear at the start and end of the frequency modulation, and at the midpoint where the slope of modulation changes from upward to downward. For case (3) and (4), the synchronous phase $\Delta\phi_s(t)$ during the modulations are continuous. The phase jumps endanger the beam stability. Hence, only case (3) and (4) are applicable.

6.1. Investigation of two synchronization methods for U^{28+} B2B transfer from SIS18 to SIS100 from the beam dynamics viewpoint

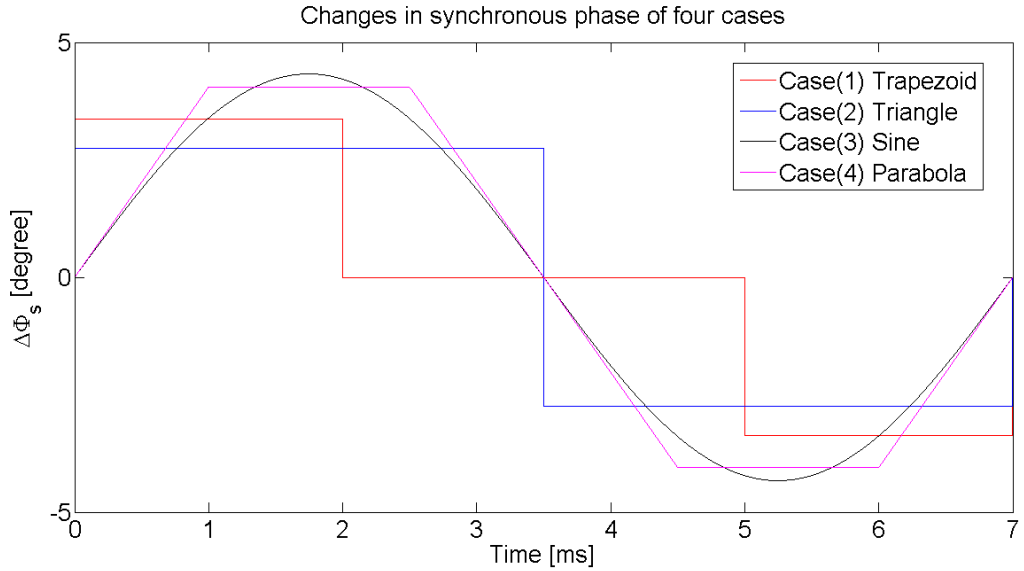


Figure 6.6: Changes in synchronous phase of four cases

- Bucket size

The bucket area factor $\alpha_b(\phi_s)$ varies during rf frequency modulations. Before the modulations, the synchronous phase $\phi_s=0^\circ$ and $\alpha_b(0^\circ)=1$. By substituting the changes in synchronous phase into eq. (6.6), we get the ratio of bucket areas of a running bucket to the stationary bucket for four cases, see Fig. (6.7).

$$\alpha_b(\phi_s) \approx \frac{1 - \sin\phi_s}{1 + \sin\phi_s} \quad (6.6)$$

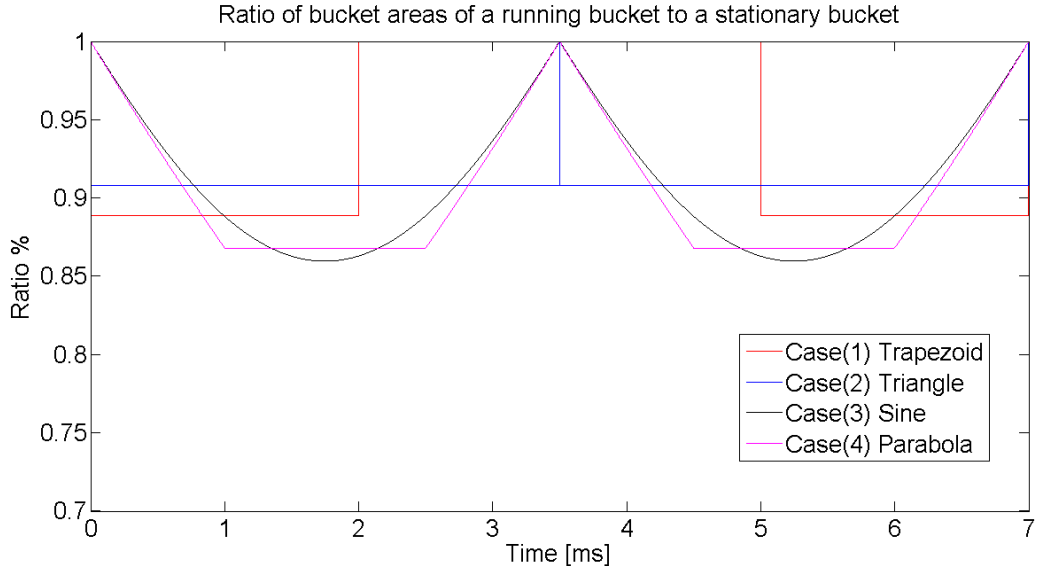


Figure 6.7: Ratio of bucket areas of a running bucket to the stationary bucket of four cases

Tab. 6.3 shows the bucket area factor for four cases. For all cases, the running bucket area factor is larger than 85%. Hence, all cases are applicable.

6.1. Investigation of two synchronization methods for U^{28+} B2B transfer from SIS18 to SIS100 from the beam dynamics viewpoint

Table 6.3: The minimum bucket area factor of four cases

	Case (1)	Case (2)	Case (3)	Case (4)
Min bucket area factor	88%	90%	86%	86%

- Adiabaticity

By substituting the values of $d\Delta\phi_s(t)/dt$ obtained from Fig. 6.6 and the other appropriate values into eq. 2.37, we can calculate the adiabaticity parameter, ε , for the case (3) and (4), see Fig. 6.8. Because $d\Delta\phi_s(t)/dt$ changes discontinuously for case (1) and (2), this abrupt change gives rise to a coherent bunch oscillation at a synchrotron frequency, resulting in emittance dilution. So the rf frequency modulations of case (1) and (2) are not applicable.

For case (4), the maximum of ε , 0.000059, occurs at 1ms, 2.5ms, 4.5ms and 6ms. From Fig. 6.6, we could see the change of the synchronous phase $d\Delta\phi_s(t)/dt$ at these time points is big but smoothly. For case (3), the maximum of ε is 0.000030. So the frequency modulation is adiabatical for case (3) and (4).

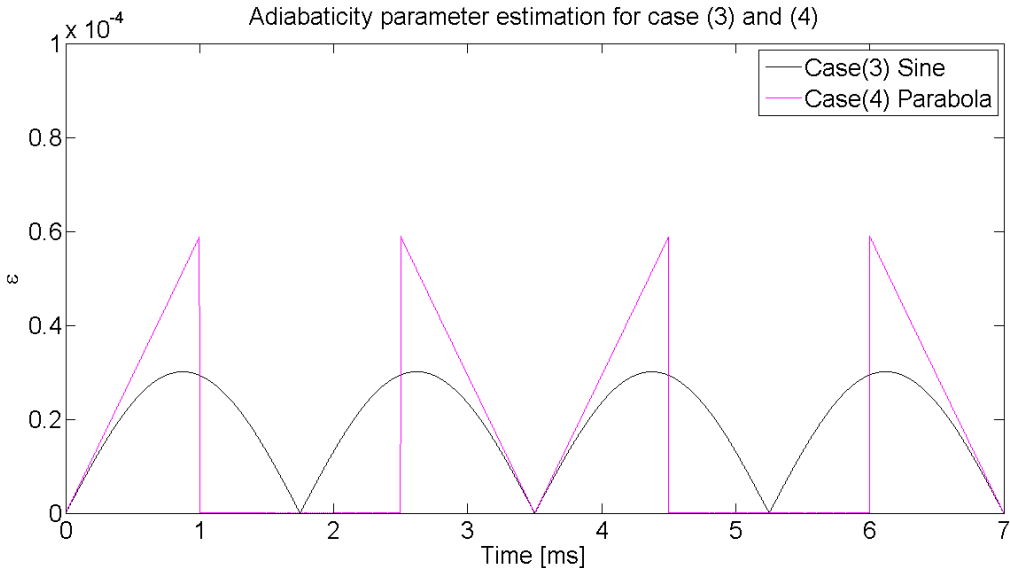


Figure 6.8: Adiabaticity parameter estimation of case (3) and (4)

6.1.1.2 Transverse dynamics analysis for the simulation

For SIS18, the chromaticity Q_x and Q_y is 4.17 and 3.4. Substituting chromaticity and maximum momentum shift (see. Tab. 6.2) into eq. 2.27. The chromatic tune shift ΔQ_x and ΔQ_y during rf modulations for four cases can be calculated.

Case (1)

$$\Delta Q_x = 4.17 \times 9.83 \times 10^{-5} = 4.10 \times 10^{-4} \quad (6.7)$$

$$\Delta Q_y = 3.4 \times 9.83 \times 10^{-5} = 3.34 \times 10^{-4} \quad (6.8)$$

6.1. Investigation of two synchronization methods for U^{28+} B2B transfer from SIS18 to SIS100 from the beam dynamics viewpoint

Case (2)

$$\Delta Q_x = 4.17 \times 1.38 \times 10^{-4} = 5.75 \times 10^{-4} \quad (6.9)$$

$$\Delta Q_y = 3.4 \times 1.38 \times 10^{-4} = 4.69 \times 10^{-4} \quad (6.10)$$

Case (3)

$$\Delta Q_x = 4.17 \times 1.40 \times 10^{-4} = 5.84 \times 10^{-4} \quad (6.11)$$

$$\Delta Q_y = 3.4 \times 1.40 \times 10^{-4} = 4.76 \times 10^{-4} \quad (6.12)$$

Case (4)

$$\Delta Q_x = 4.17 \times 1.48 \times 10^{-4} = 6.17 \times 10^{-4} \quad (6.13)$$

$$\Delta Q_y = 3.4 \times 1.48 \times 10^{-4} = 5.03 \times 10^{-4} \quad (6.14)$$

The chromatic tune shift for four cases are significantly small, which could be negligible.

6.1.2 Frequency beating method

In the case of the frequency beating method, we guarantee the extraction and injection energy always match, which means that the momentum is not affected by the frequency detune, namely $\Delta p = 0$, So the frequency beating method has no influence on the transverse dynamics.

6.1.2.1 Longitudinal dynamics analysis of the frequency beating for SIS18

For the frequency beating method, the rf frequency de-tune is done accompanying with the RF ramp. Accepting to decentre the orbit by 8mm [40] for the SIS18

$$\frac{\Delta R}{R} = \pm 2.4 \times 10^{-4} \quad (6.15)$$

From eq. 2.44 and eq. 2.49, the RF frequency and the magnetic field change at the U^{28+} extraction energy 200MeV/u ($\gamma_t = 5.8$) are

$$\frac{\Delta f}{f} = \pm 2.4 \times 10^{-4} \quad (6.16)$$

$$\frac{\Delta B}{B} = \frac{\Delta f}{f} \gamma_t^2 = \pm 8.1 \times 10^{-3} \quad (6.17)$$

where the maximum RF frequency de-tune is approximate to 370 Hz at 1.57 MHz for the U^{28+} . Fig. 6.9 shows the rf frequency derivation during the rf ramp. In the simulation, it is assumed that the rf frequency is detuned at 0.2756s with 6.08×10^6 Hz/s, see blue rectangle in Fig. 6.9. For the sake of simplicity, 200 Hz is used as the rf frequency detune. SIS18 needs approximate 33us to reach 200 Hz with 6.08×10^6 Hz/s.

From eq. 2.44 and eq. 2.49, we could get the corresponding radial excursion and the magnetic field change during the detune process. The maximum radial excursion is -1.27×10^{-4} at 33us of the rf detune process. The maximum magnetic field change is 4.3×10^{-3} at 33us of the rf detune process.

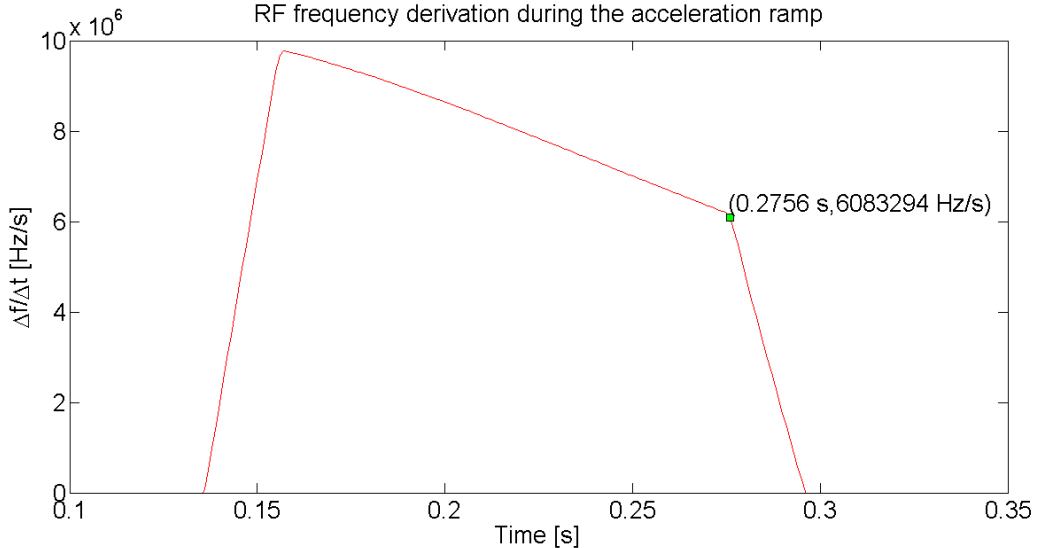


Figure 6.9: RF frequency derivation of the U^{28+} rf ramp

6.2 GMT systematic investigation for the B2B transfer system

The B2B transfer system makes use of certain aspects of the GMT system to realize the data collection, merging and redistribution. The main task of the data merging is the calculation of the synchronization window, within which the bunch could be injected into the correct bucket with the bunch to bucket center mismatch smaller than the upper bound. The data collection and redistribution make use of the WR network, so the measurement of the WR network latency is necessary.

6.2.1 Calculation of the synchronization window

According to the phase difference between two synchrotrons, the fine time for the alignment of two Reference RF Signals for both the phase shift and frequency beating methods can be calculated. This time is called “best estimate of alignment” and denoted by t_{best} , see Fig. 6.10. Because of the uncertainty [51] of the phase advance prediction and rf frequency modulation, the fine alignment lies between $t_{best} - \delta t_{best}$ and $t_{best} + \delta t_{best}$, where δt_{best} is the uncertainty of the alignment. $[t_{best} - \delta t_{best}, t_{best} + \delta t_{best}]$ is called “probable range of alignment”. In Sec. 6.2.1.1 and Sec. 6.2.1.2, the calculation of the best estimation of alignment and the probable range of alignment for the phase shift and frequency beating method will be explained. The probable range of alignment is within the synchronization window. For the correct selection of the same revolution frequency marker at different SCUs, the start of the synchronization window must be properly calculated. In Sec. 6.2.1.3, the calculation of the synchronization window will be explained.

For both the phase shift and frequency beating method, the calculation is based on the predicted phase of the rf signal locally. For example of the U^{28+} B2B transfer from SIS18 to SIS100, the PAP module extrapolates the rf phase $\psi_{h=1}^{SIS100}$ for SIS100 rf h=1 (157kHz) signal and $\psi_{h=1/5}^{SIS18}$ for SIS18 rf h=1/5 (157kHz) signal at t_ψ [44]. The more time is spent for the phase advance prediction, the better the predicted phase

6.2. GMT systematic investigation for the B2B transfer system

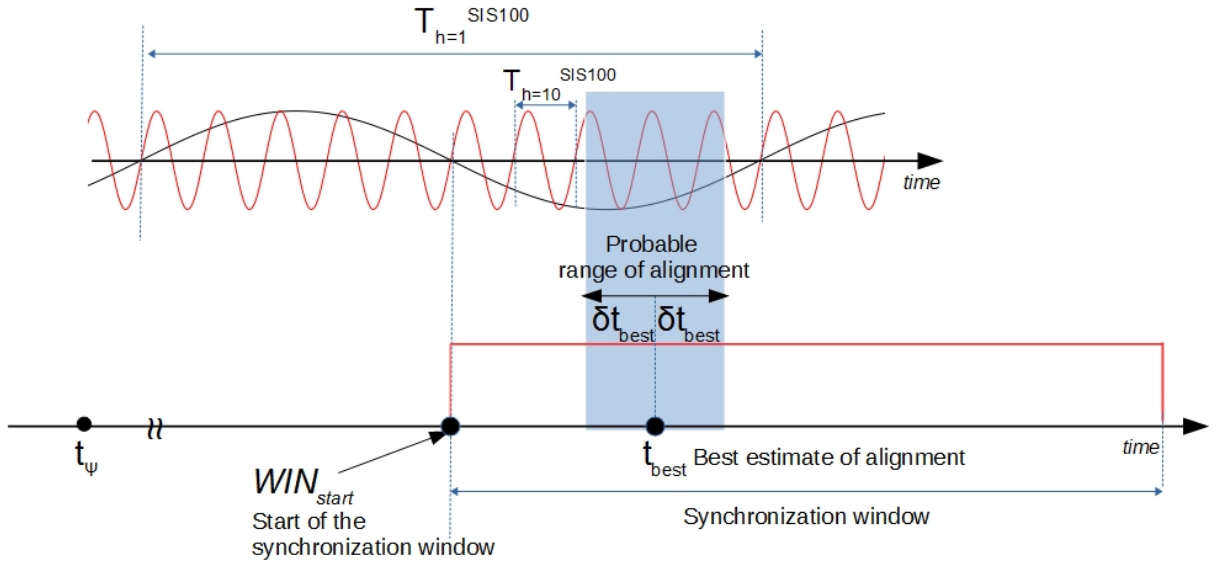


Figure 6.10: The illustration of the best estimate of alignment, the probable range of alignment and the synchronization window

will be. Fig. 6.11 illustrates some basic definition of symbols for the calculation. $\phi_{h=2}^{SIS18}$ and $\phi_{h=10}^{SIS100}$ are individual rf phase of SIS18 and SIS100 Reference RF Signals

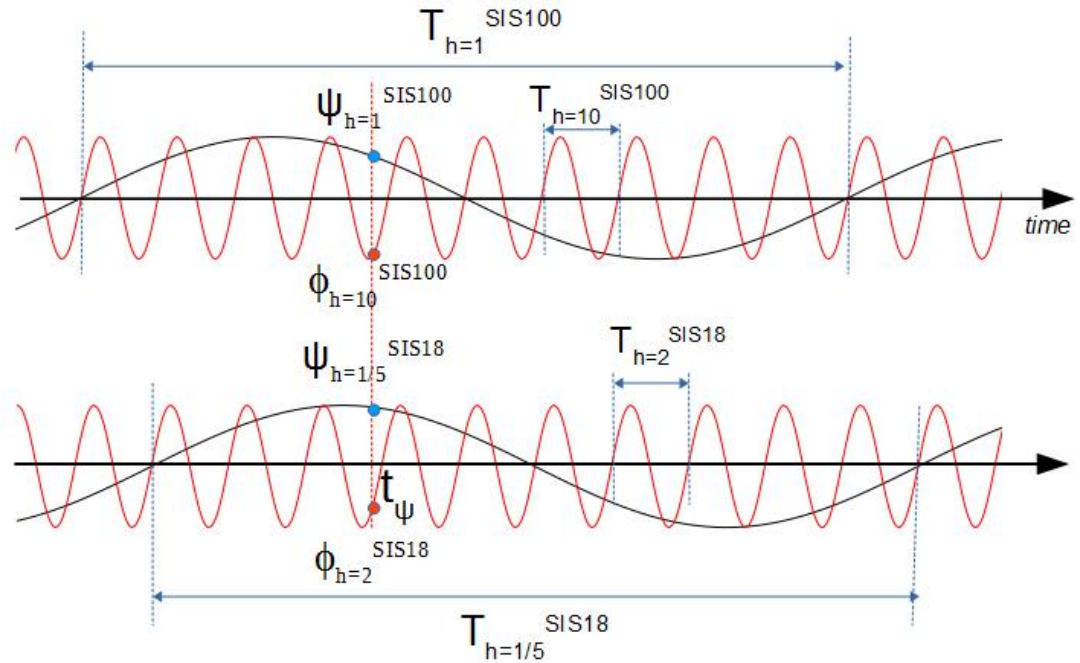


Figure 6.11: The illustration of symbols for the calculation

at t_ψ . The relationship between $\phi_{h=2}^{SIS18}$, $\phi_{h=10}^{SIS100}$ and $\psi_{h=1/5}^{SIS18}$, $\psi_{h=1}^{SIS100}$ are given by eq. 6.18 and eq. 6.19.

6.2. GMT systematic investigation for the B2B transfer system

$$\phi_{h=2}^{SIS18} = \frac{\frac{\psi_{h=1/5}^{SIS18}}{360^\circ} \times T_{h=1/5}^{SIS18} \bmod T_{h=2}^{SIS18}}{T_{h=2}^{SIS18}} \times 360^\circ \quad (6.18)$$

$$\phi_{h=10}^{SIS100} = \frac{\frac{\psi_{h=1}^{SIS100}}{360^\circ} \times T_{h=1}^{SIS100} \bmod T_{h=10}^{SIS100}}{T_{h=10}^{SIS100}} \times 360^\circ \quad (6.19)$$

substituting $T_{h=2}^{SIS18} \times 10 = T_{h=1/5}^{SIS18}$, $T_{h=10}^{SIS100} \times 10 = T_{h=1}^{SIS100}$ into eq.6.18 and eq.6.19 yields

$$\phi_{h=2}^{SIS18} = \frac{\frac{\psi_{h=1/5}^{SIS18} \times 10}{360^\circ} \times T_{h=2}^{SIS18} \bmod T_{h=2}^{SIS18}}{T_{h=2}^{SIS18}} \times 360^\circ \quad (6.20)$$

$$\phi_{h=10}^{SIS100} = \frac{\frac{\psi_{h=1}^{SIS100} \times 10}{360^\circ} \times T_{h=10}^{SIS100} \bmod T_{h=10}^{SIS100}}{T_{h=10}^{SIS100}} \times 360^\circ \quad (6.21)$$

Here we explain the inevitable uncertainty of the phase advance prediction and rf frequency modulation.

- Uncertainty of the predicted phase advance

If the phase prediction time is 500us, the uncertainty of the predicted phase advance δt_ψ is 100ps [45]. We calculate the uncertainty of the predicted phase advance, $\delta\psi_{h=1}^{SIS100}$ and $\delta\psi_{h=1/5}^{SIS18}$, from the time to phase domain.

$$\delta t_\psi = 100ps \quad (6.22)$$

$$\delta\psi_{h=1/5}^{SIS18} = \delta\psi_{h=1}^{SIS100} = \frac{100ps}{1/157kHz} \times 360^\circ \approx 0.006^\circ \quad (6.23)$$

Based on the eq. 6.23, eq. 6.20 and eq. 6.21, the uncertainty of the phase at the Reference RF Signal of SIS18 and SIS100, $\delta\phi_{h=10}^{SIS100}$ and $\delta\phi_{h=2}^{SIS18}$, is calculated.

$$\delta\phi_{h=2}^{SIS18} = \sqrt{\left(\frac{\partial\phi_{h=2}^{SIS18}}{\partial\psi_{h=2}^{SIS18}}\delta\psi_{h=2}^{SIS18}\right)^2} = \sqrt{(10 \times \delta\psi_{h=2}^{SIS18})^2} = 0.06^\circ \quad (6.24)$$

$$\delta\phi_{h=10}^{SIS100} = \sqrt{\left(\frac{\partial\phi_{h=10}^{SIS100}}{\partial\psi_{h=1}^{SIS100}}\delta\psi_{h=1}^{SIS100}\right)^2} = \sqrt{(10 \times \delta\psi_{h=1}^{SIS100})^2} = 0.06^\circ \quad (6.25)$$

- Uncertainty of the rf frequency modulation

For the rf frequency modulation, the uncertainty is 0.2° at 5.4MHz [52]. We calculate the uncertainty in time domain, see eq. 6.26.

$$\delta\Delta f_{(t)} = \frac{0.2^\circ}{360^\circ} \times \frac{1}{5.4MHz} = 100ps \quad (6.26)$$

6.2.1.1 The best estimate of alignment and the probable range of alignment for the phase shift method

Different relation between $\phi_{h=2}^{SIS18}$ and $\phi_{h=10}^{SIS100}$ requires different phase adjustment for SIS18. Fig. 6.12 illustrates all scenarios of their relation and the required phase adjustment for each scenario. We would like to introduce a phase shift of up to $\pm 180^\circ$. The blue and red line represents the phase of SIS100 and SIS18 Reference RF Signal. The clockwise arrow from the SIS18 to SIS100 rf phase represents the negative phase adjustment for SIS18 and the anticlockwise represents the positive phase adjustment. The required phase adjustment of SIS18 is denoted by $\Delta\phi_{shift}$.

- Scenario (a): $\phi_{h=10}^{SIS100} \in [0^\circ, 90^\circ]$, see Fig. 6.13 (a).
- $\phi_{h=10}^{SIS100} < \phi_{h=2}^{SIS18} < \phi_{h=10}^{SIS100} + 180^\circ$, which denotes by the yellow semicircle in Fig. 6.13 (a). The phase adjustment is

$$\Delta\phi_{shift} = -(\phi_{h=2}^{SIS18} - \phi_{h=10}^{SIS100}) \quad (6.27)$$

- $\phi_{h=2}^{SIS18} < \phi_{h=10}^{SIS100}$ or $\phi_{h=2}^{SIS18} > \phi_{h=10}^{SIS100} + 180^\circ$, which denotes by the white semicircle in Fig. 6.13 (a). The phase adjustment is

$$\Delta\phi_{shift} = 360^\circ - \phi_{h=2}^{SIS18} + \phi_{h=10}^{SIS100} \quad (6.28)$$

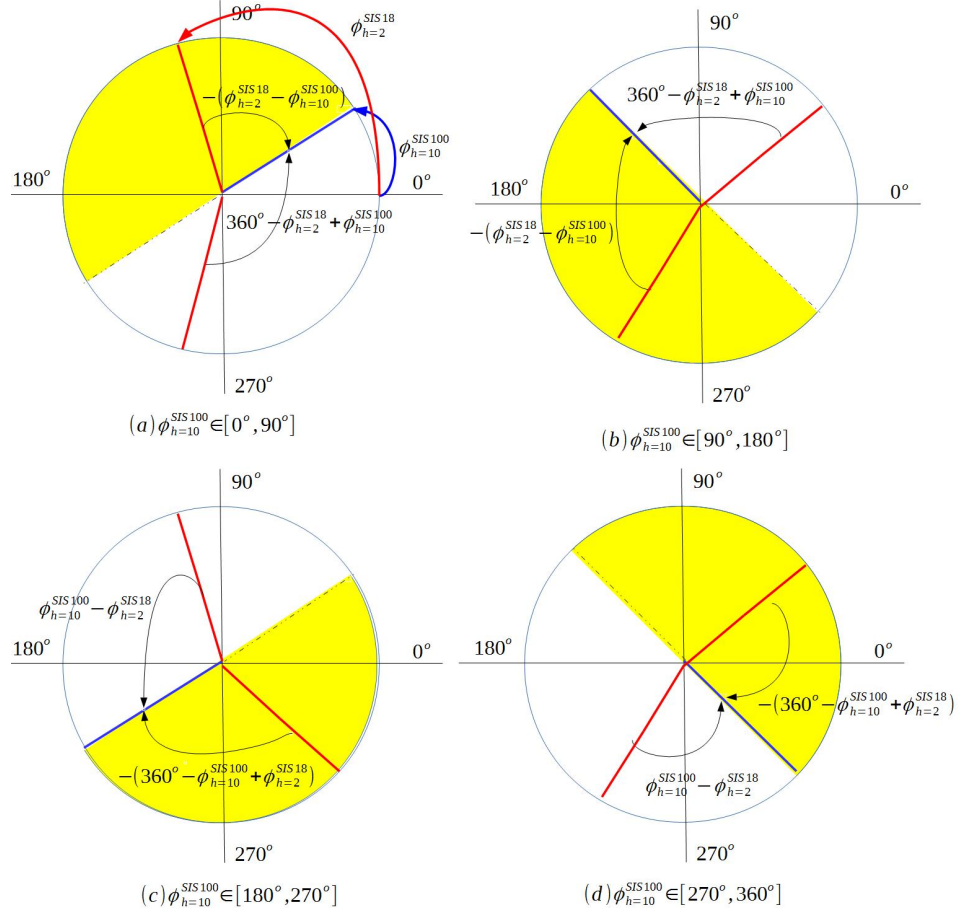


Figure 6.12: Scenarios for the phase shift method

6.2. GMT systematic investigation for the B2B transfer system

- Scenario (b): $\phi_{h=10}^{SIS100} \in [90, 180^\circ]$, see Fig. 6.13 (b).
 - $\phi_{h=10}^{SIS100} < \phi_{h=2}^{SIS18} < \phi_{h=10}^{SIS100} + 180^\circ$, which denotes by the yellow semicircle in Fig. 6.13 (b). The phase adjustment is

$$\Delta\phi_{shift} = -(\phi_{h=2}^{SIS18} - \phi_{h=10}^{SIS100}) \quad (6.29)$$

- $\phi_{h=2}^{SIS18} < \phi_{h=10}^{SIS100}$ or $\phi_{h=2}^{SIS18} > \phi_{h=10}^{SIS100} + 180^\circ$, which denotes by the white semicircle in Fig. 6.13 (b). The phase adjustment is

$$\Delta\phi_{shift} = 360^\circ - \phi_{h=2}^{SIS18} + \phi_{h=10}^{SIS100} \quad (6.30)$$

- Scenario (c): $\phi_{h=10}^{SIS100} \in [180, 270^\circ]$, see Fig. 6.13 (c). The phase adjustment is
 - $\phi_{h=2}^{SIS18} > \phi_{h=10}^{SIS100}$ or $\phi_{h=2}^{SIS18} < \phi_{h=10}^{SIS100} + 180^\circ - 360^\circ$, which denotes by the yellow semicircle in Fig. 6.13 (c). The phase adjustment is

$$\Delta\phi_{shift} = -(360^\circ - \phi_{h=10}^{SIS100} + \phi_{h=2}^{SIS18}) \quad (6.31)$$

- $\phi_{h=10}^{SIS100} - 180^\circ < \phi_{h=2}^{SIS18} < \phi_{h=10}^{SIS100}$, which denotes by the white semicircle in Fig. 6.13 (c). The phase adjustment is

$$\Delta\phi_{shift} = \phi_{h=10}^{SIS100} - \phi_{h=2}^{SIS18} \quad (6.32)$$

- Scenario (d): $\phi_{h=10}^{SIS100} \in [270, 360^\circ]$, see Fig. 6.13 (d).
 - $\phi_{h=10}^{SIS100} - 180^\circ < \phi_{h=2}^{SIS18} < \phi_{h=10}^{SIS100}$, which denotes by the yellow semicircle in Fig. 6.13 (d). The phase adjustment is

$$\Delta\phi_{shift} = \phi_{h=10}^{SIS100} - \phi_{h=2}^{SIS18} \quad (6.33)$$

- $\phi_{h=2}^{SIS18} > \phi_{h=10}^{SIS100}$ or $\phi_{h=2}^{SIS18} < \phi_{h=10}^{SIS100} + 180^\circ - 360^\circ$, which denotes by the white semicircle in Fig. 6.13 (d).

$$\Delta\phi_{shift} = -(360^\circ - \phi_{h=10}^{SIS100} + \phi_{h=2}^{SIS18}) \quad (6.34)$$

The phase adjustment is achieved by the phase shift method within the upper bound time, $T_{phase_shift}^{upper_bound}$. For the U^{28+} B2B transfer from SIS18 to SIS100, we assume that $T_{phase_shift}^{upper_bound}$ equals to 7ms, which means that the phase shift $\Delta\phi_{shift}$ is achieved within 7ms. So the best estimate of alignment is expressed by

$$t_{best} = t_\psi + T_{phase_shift}^{upper_bound} \quad (6.35)$$

The uncertainty in the phase prediction δt_ψ is 100ps, see eq. 6.22. The phase shift uncertainty $\delta\Delta\phi_{phase}$ is caused by the rf frequency modulation, whose jitter is 100ps, see eq. 6.26. The phase shift uncertainty equals to the uncertainty in the phase shift upper bound time, $\delta T_{phase_shift}^{upper_bound} = 100ps$. Both cause an uncertainty in the best estimate of alignment t_{best} .

$$\begin{aligned} \delta t_{best} &= \sqrt{\left(\frac{\partial t_{best}}{\partial t_\psi} \delta t_\psi\right)^2 + \left(\frac{\partial t_{best}}{\partial T_{phase_shift}^{upper_bound}} \delta T_{phase_shift}^{upper_bound}\right)^2} \\ &= \sqrt{(\delta t_\psi)^2 + (T_{phase_shift}^{upper_bound})^2} = \sqrt{100ps^2 + 100ps^2} \approx 140ps \end{aligned} \quad (6.36)$$

The uncertainty of the alignment for the phase shift method is about 140ps. So the proper range of alignment is $[t_{best}-140ps, t_{best}+140ps]$ for U^{28+} B2B transfer from SIS18 to SIS100.

6.2. GMT systematic investigation for the B2B transfer system

6.2.1.2 The best estimate of alignment and the probable range of alignment for the frequency beating method

Fig. 6.13 illustrates two scenarios for the frequency beating method. With the frequency beating method, SIS18 can only achieve positive phase adjustment, which is denoted by $\Delta\phi_{adjustment}$. Eq. 6.37 shows the best estimate of alignment for the phase adjustment of $\Delta\phi_{adjustment}$.

$$t_{best} = t_\psi + \frac{\Delta\phi_{adjustment}}{360^\circ \times \Delta f} \quad (6.37)$$

where Δf is the beating frequency.

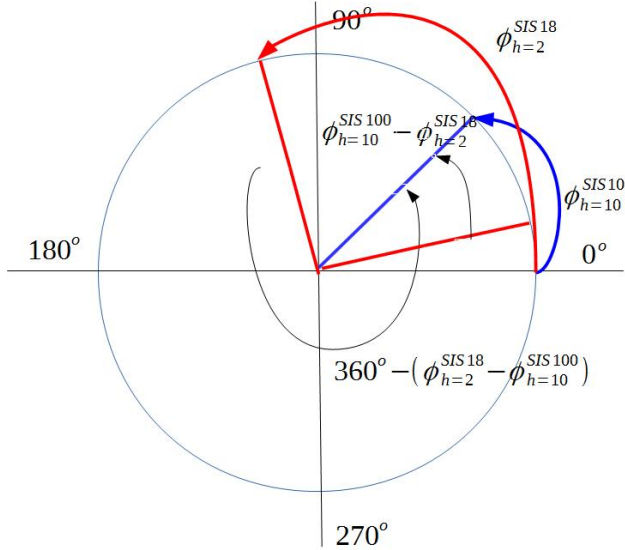


Figure 6.13: Two scenarios for the frequency beating method

According to the relation between $\phi_{h=2}^{SIS18}$ and $\phi_{h=10}^{SIS100}$, there are two scenarios, see Fig. 6.13.

- Scenario (a): $\phi_{h=2}^{SIS18} < \phi_{h=10}^{SIS100}$

$$\Delta\phi_{adjustment} = \phi_{h=10}^{SIS100} - \phi_{h=2}^{SIS18} \quad (6.38)$$

Replacing $\Delta\phi_{adjustment}$ in eq. 6.37 with eq. 6.38, we have

$$t_{best} = t_\psi + \frac{\phi_{h=10}^{SIS100} - \phi_{h=2}^{SIS18}}{360^\circ \times \Delta f} \quad (6.39)$$

- Scenario (b): $\phi_{h=2}^{SIS18} \geq \phi_{h=10}^{SIS100}$

$$\Delta\phi_{adjustment} = 360^\circ - (\phi_{h=2}^{SIS18} - \phi_{h=10}^{SIS100}) \quad (6.40)$$

Replacing $\Delta\phi_{adjustment}$ in eq. 6.37 with eq. 6.40, we have

$$t_{best} = t_\psi + \frac{360^\circ - (\phi_{h=2}^{SIS18} - \phi_{h=10}^{SIS100})}{360^\circ \times \Delta f} \quad (6.41)$$

6.2. GMT systematic investigation for the B2B transfer system

Based on these two scenarios, we could deduce the formula for the best estimate of alignment.

$$t_{best} = t_\psi + \frac{\Delta n \times 360^\circ - (\phi_{h=2}^{SIS18} - \phi_{h=10}^{SIS100})}{360^\circ \times \Delta f} \quad (6.42)$$

where Δn equals 0 when $\phi_{h=2}^{SIS18} < \phi_{h=10}^{SIS100}$ and equals 1 when $\phi_{h=2}^{SIS18} \geq \phi_{h=10}^{SIS100}$.

The uncertainty of the alignment is the result of the error propagation of uncertainties of the phase prediction and rf frequency detune, see eq. 6.43. Because the rf frequency detune has the long term stability, $\int \delta \Delta f = 0$, the uncertainty caused by rf frequency detune is 0. The uncertainty of the phase prediction $\phi_{h=2}^{SIS18}$ and $\phi_{h=10}^{SIS100}$ is 0.06° , see eq. 6.24 and eq. 6.25. Δf is 200Hz. The maximum $\Delta n \times 2\pi - (\phi_{h=2}^{SIS18} - \phi_{h=10}^{SIS100})$ is 2π .

$$\begin{aligned} \delta t_{best} &= \sqrt{\left(\frac{\partial t_{best}}{\partial \phi_{h=2}^{SIS18}} \delta \phi_{h=2}^{SIS18}\right)^2 + \left(\frac{\partial t_{best}}{\partial \phi_{h=10}^{SIS100}} \delta \phi_{h=10}^{SIS100}\right)^2 + \left(\frac{\partial t_{best}}{\partial \Delta f} \delta \Delta f\right)^2} \\ &= \sqrt{\left(\frac{-1}{2\pi \times \Delta f} \delta \phi_{h=2}^{SIS18}\right)^2 + \left(\frac{1}{2\pi \times \Delta f} \delta \phi_{h=10}^{SIS100}\right)^2 + \left(-\frac{\Delta n \times 2\pi - (\phi_{h=2}^{SIS18} - \phi_{h=10}^{SIS100})}{2\pi \times \Delta f^2} \delta \Delta f\right)^2} \\ &\leq \sqrt{\left(\frac{-1}{2\pi \times 200} 0.06^\circ\right)^2 + \left(\frac{1}{2\pi \times 200} 0.06^\circ\right)^2 + 0} \\ &\approx 1.178us \end{aligned} \quad (6.43)$$

From eq. 6.43 we could get the uncertainty of the alignment is 1.178us, so the probable range of alignment is $[t_{best} - 1.178us, t_{best} + 1.178us]$.

6.2.1.3 Calculation the synchronization window and its accuracy

In the last section, we get the probable range of alignment, within which the two Reference Rf Signals could be aligned with each other. The synchronization window is used to select the revolution frequency marker for the extraction and injection kicker firing, which is closest to the probable range of alignment, See Fig. 6.14. For the selection, the length of the synchronization window must be a least one SIS100 revolution period. The best estimate of the start of the synchronization window is exactly half revolution period before the selected revolution frequency marker. The blue and orange rectangles represent two scenarios of the probable range of alignment. In Fig. 6.14, the 2nd revolution frequency marker is the closest one to the probable range of alignment. The best estimate of the start of the synchronization window aligns with the negative zero crossing point of the revolution marker signal.

For SIS100, the rf phase of the revolution frequency is $\psi_{h=1}^{SIS100}$ at t_ψ . We could calculate the rf phase $\psi_{s.alignment}$ of the revolution frequency at the start of the probable rang of alignment, $t_{best} - \delta t_{best}$.

$$\psi_{s.alignment} = \frac{(t_{best} - \delta t_{best} - t_\psi - \frac{360^\circ - \psi_{h=1}^{SIS100}}{360^\circ} \times T_{h=1}^{SIS100}) \mod T_{h=1}^{SIS100} \times 360^\circ}{T_{h=1}^{SIS100}} \quad (6.44)$$

For the calculation of the best estimate of the start of the synchronization window, there are two scenarios. $\Delta t_{win.correct}$ is the time correction for the start of the probable range of alignment to the best estimate of the start of the synchronization window, see Fig. 6.14.

6.2. GMT systematic investigation for the B2B transfer system

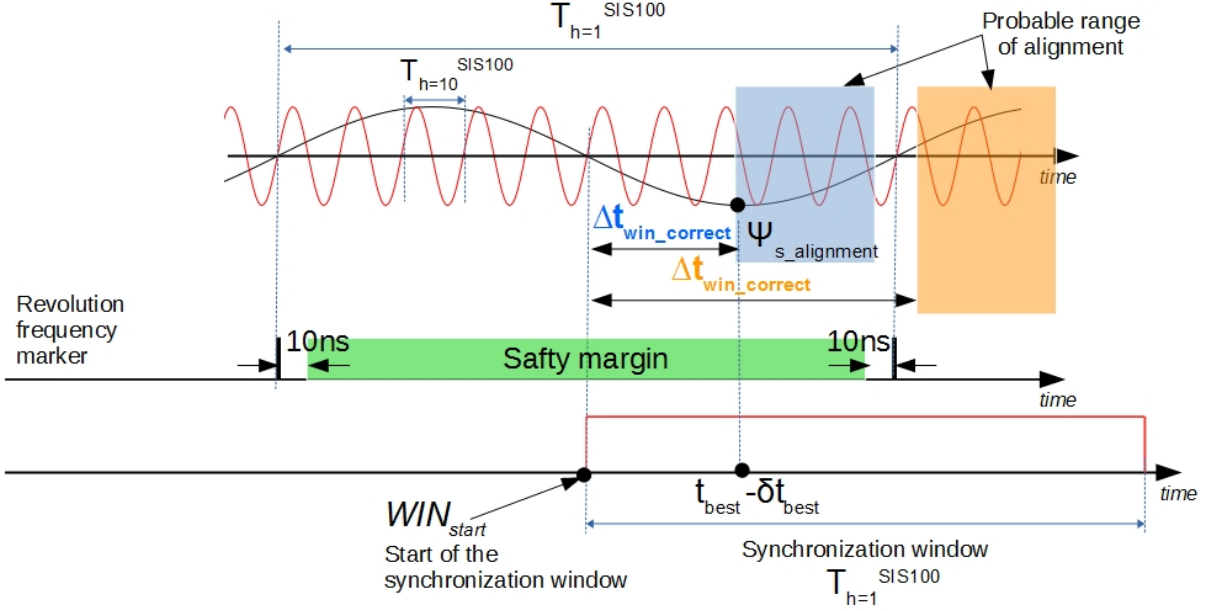


Figure 6.14: The illustration of the synchronization window and its accuracy

- $\psi_{s_alignment} \in [0^\circ, 180^\circ]$, the orange rectangle in Fig. 6.14

$$\Delta t_{win_correct} = \frac{\psi_{s_alignment}}{360^\circ} \times T_{h=1}^{SIS100} + \frac{T_{h=1}^{SIS100}}{2} \quad (6.45)$$

$$WIN_{start} = t_{best} - \delta t_{best} - \Delta t_{win_correct} \quad (6.46)$$

- $\psi_{s_alignment} \in [180^\circ, 360^\circ]$, the blue rectangle in Fig. 6.14

$$\Delta t_{win_correct} = \frac{\psi_{s_alignment} - 180^\circ}{360^\circ} \times T_{h=1}^{SIS100} \quad (6.47)$$

$$WIN_{start} = t_{best} - \delta t_{best} - \Delta t_{win_correct} \quad (6.48)$$

The actual start of the synchronization window is impossible to be exactly at the best estimate of the start of the synchronization window because of the precision and trueness [53]. The precision is defined as the closeness of agreement between the actual start of the synchronization window of different SCUs and the trueness as the closeness of agreement between the average actual start of the synchronization window of different SCUs and the best estimation start of the synchronization window. The precision comes from the random error, e.g. IO port TTL signal rising oscillation. The trueness is the systematic error, e.g. FPGA process time. The accuracy is defined as the closeness of agreement between the observed start and the best estimate of the start of the synchronization window, which is the sum of the precision and trueness. The B2B transfer system will be used for many transfers for FAIR. Therefore, we have to find the most stringent accuracy requirement. The shortest revolution period of the target machine is 433 ns, which comes from RIB transfer from CR to HESR. We keep 10ns as a forbidden range, which means that the actual start is not allowed 10 ns before and after the revolution frequency marker. The green region in Fig. 6.14 represents the safty margin for the start of

6.2. GMT systematic investigation for the B2B transfer system

the synchronization window. So the accuracy of the start of the synchronization window must meet the requirement calculated by eq. 6.49.

$$Accuracy = \pm \frac{433 - 10 \times 2}{2} \approx \pm 200 \text{ ns} \quad (6.49)$$

6.2.2 Characterization of the WR network for the B2B transfer

Within this dissertation, a network analyzed by Xena is used to characterize the properties of the WR network, which are relevant to B2B transfer. The WR network measurement is achieved by the Xena traffic generator¹, which offers a new class of professional Layer 2-3 Gigabit Ethernet test platform. It is used to measure the frame loss rate², latency³ and jitter⁴ for the WR network. For the measurement, Xena traffic generator sends the traffic streams with a unique stream ID for identifying latency, jitter and packet loss. For the measurements, the following types of traffic are considered [54].

- DM Broadcast

DM forwards broadcast timing frames⁵ with 110 bytes ethernet frame length downwards to all FECs. The average bandwidth for the DM broadcast is 100 Mbit/s. The burst⁶ speed is 12 packets per 100 µs.

- DM Unicast

DM sends 10Mbit/s unicast timing frames with 110 bytes ethernet frame length to some specified FECs at the burst speed of 3 packets per 300 µs.

- B2B Unicast

The source B2B SCU sends the timing frame with 110 bytes ethernet frame length upwards to the DM. For the B2B transfer upper bound time 10 ms of each supercycle, 2 unicast timing frames are send to the DM. The maximum repetition frequency is of the U^{28+} supercycle, 2.82 Hz. For the estimation of the upper bound bandwidth, we use 3Hz/s as the maximum repetition frequency. So the bandwidth is $3 \text{ Hz/s} \times 2 \text{ packets/supercycle} \times 110 \text{ byte} \times 8 \text{ bit} \approx 5.5 \text{ kbit/s}$.

- B2B Broadcast

¹<http://xenanetworks.com/layer-2-3-platform/>

²The ratio of the number of the lost frames to the number of the theoretic received frames of a tested port.

³The time interval between the time of Xena port receiving frame and the time of another Xena port sending frame.

⁴The absolute value of the difference between the latency of two consecutive received frames belonging to the same stream from one Xena port to another Xena port.

http://www.xenanetworks.com/wp-content/uploads/Measuring_Frame_latency_Variation.pdf

⁵<https://www-acc.gsi.de/wiki/Timing/TimingSystemEvent>

⁶A group of consecutive frames with shorter interframe gaps than frames arriving before or after the burst of frames.

6.2. GMT systematic investigation for the B2B transfer system

Maximum 10 B2B broadcast timing frames with 110 ethernet frame length are sent within 10 ms. So the bandwidth is $3 \text{ Hz/s} \times 10 \text{ packets/supercycle} \times 110 \text{ byte} \times 8 \text{ bit} \approx 26.5 \text{ kbit/s}$.

- Management Traffic

The average bandwidth for the management traffic is 10 Mbit/s. It broadcasts packets with random ethernet frame length from 64 bytes to 1518 bytes.

The requirements for the B2B Broadcast and Unicast traffic are summarized in Tab. A.1 [54].

Table 6.4: The B2B transfer requirements for the WR network

	Frame Loss Rate	Upper bound latency of WR network	Upper bound latency per WR switch layer
B2B Broadcast	10^{-12}	500 μs	30 μs
B2B Unicast	10^{-12}	500 μs	30 μs

For the WR network for FAIR, three VLANs with different priorities are applied according to the importance of the traffic.

6.2.2.1 WR network test setup

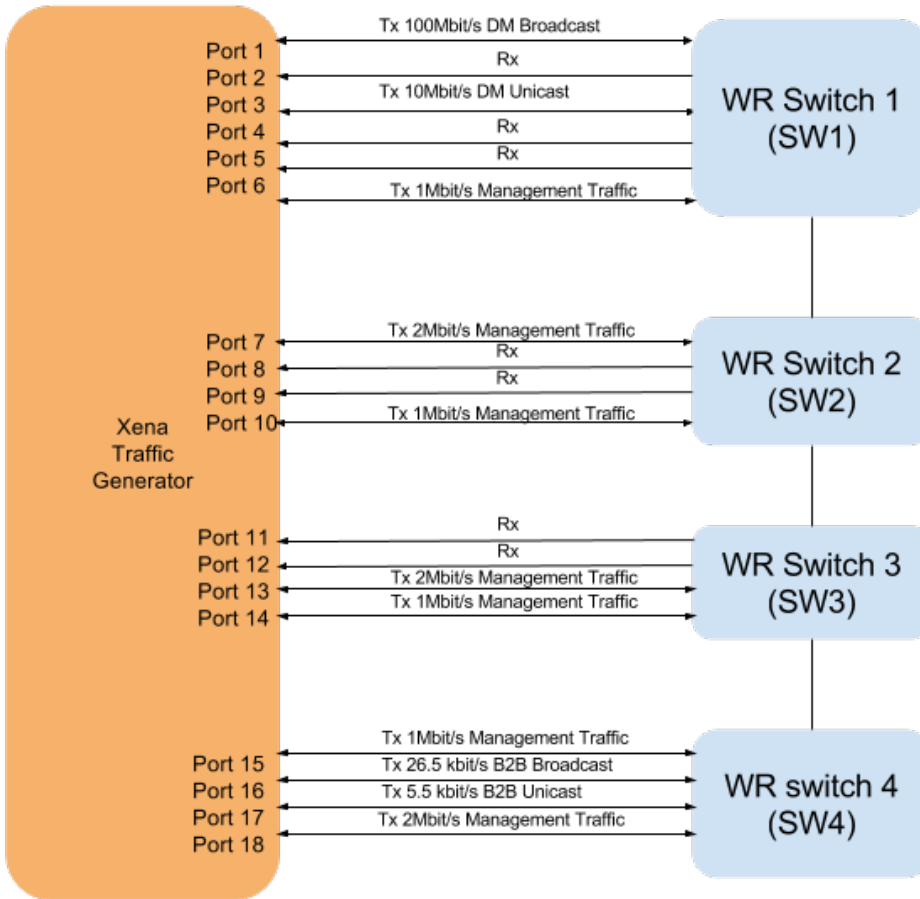


Figure 6.15: The WR network test setup

Based on the mentioned traffic, the measurement setup is built, see Fig. 6.15 [54]. Four WR switches are connected to the port 1 to 18 of the Xena traffic generator. All ports of four WR switches are assigned to three VLANs, VLAN 5, VLAN 6 and VLAN 7. Tab. 6.5 shows the bandwidth, VLAN, VLAN priority and usage of the traffic of each Xena port in details. The test is running for 14 hours.

6.2.2.2 Frame loss rate test result for B2B frames

The frame loss rate of the stream from port 17 to port 1 is measured for the B2B Unicast frames. The frame loss rate of the stream from port 16 to other ports is measured for the B2B Broadcast frame. Fig. 6.16 [54] shows the test result for both traffics. For the B2B Broadcast frames, the frame loss rate of each port is 0 %. For the B2B Unicast frames, the frame loss rate of port 1 is 0 %. So there is no B2B frame loss of the test WR network.

6.2. GMT systematic investigation for the B2B transfer system

Table 6.5: The connection between the traffic generator and WR switches

Switch	Xena Port	Traffic	VLAN	Priority	Usage
WR switch 1	Port 1	100 Mbit/s 110bytes	7	7	DM Broadcast
	Port 2	Rx traffic			
	Port 3	10 Mbit/s 110bytes	7	7	DM Unicast
	Port 4	Rx traffic			
	Port 5	Rx traffic			
	Port 6	1 Mbit/s 64 - 1518 bytes	5	5	Management Broadcast
WR switch 2	Port 7	2 Mbit/s 64 - 1518 bytes	5	5	Management Broadcast
	Port 8	Rx traffic			
	Port 9	Rx traffic			
	Port 10	1 Mbit/s 64 - 1518 bytes	5	5	Management Broadcast
WR switch 3	Port 11	Rx traffic			
	Port 12	Rx traffic			
	Port 13	2 Mbit/s 64 - 1518 bytes	5	5	Management Broadcast
	Port 14	1 Mbit/s 64 - 1518 bytes	5	5	Management Broadcast
WR switch 4	Port 15	1 Mbit/s 64 - 1518 bytes	5	5	Management Broadcast
	Port 16	26.5 kbit/s 110bytes	6	6	B2B Broadcast
	Port 17	5.5 kbit/s 110bytes	7	7	B2B Unicast
	Port 18	2 Mbit/s 64 - 1518 bytes	5	5	Management Broadcast

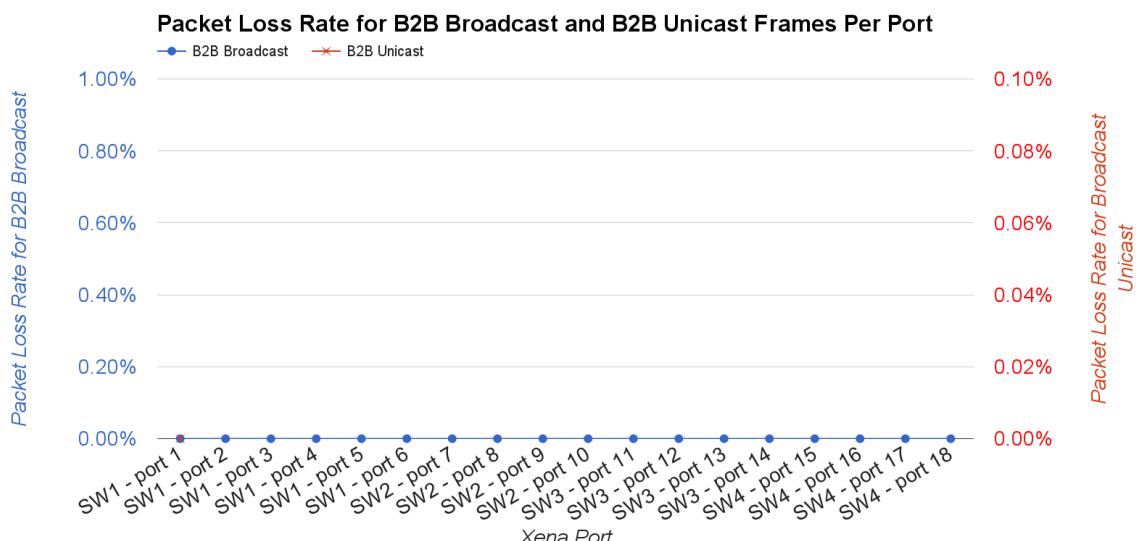


Figure 6.16: The frame loss rate for B2B Broadcast and B2B Unicast frames

6.2. GMT systematic investigation for the B2B transfer system

6.2.2.3 Latency and jitter test result for B2B frames

The latency and jitter of the stream from port 16 to other ports are measured.

- Latency and jitter for B2B Broadcast frames
 - Average Latency and jitter

Fig. 6.17 [54] shows the test result for the average latency and jitter for the B2B Broadcast frames. Tab. 6.6 shows the average latency and jitter of different WR switch layers. They meet the requirements of the B2B transfer.

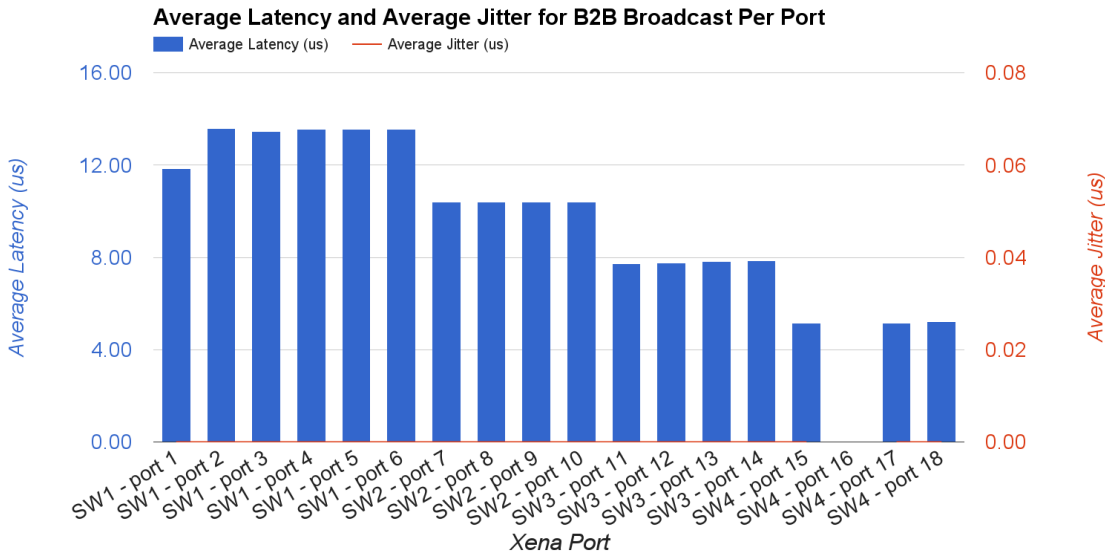


Figure 6.17: The average latency and jitter for B2B Broadcast frames

Table 6.6: The average latency and jitter of the B2B Broadcast frames

	WR switch 4	WR switch 4, 3	WR switch 4, 3, 2	WR switch 4, 3, 2, 1
Avg latency	6 μ s	8 μ s	11 μ s	14 μ s
Avg jitter	0 ns	0 ns	0 ns	0 ns

- Maximum Latency and jitter

Fig. 6.18 [54] shows the test result for the maximum latency and jitter for the B2B Broadcast frames. Tab. 6.7 shows the maximum latency and jitter of different WR switch layers. They meet the requirements of the B2B transfer.

6.2. GMT systematic investigation for the B2B transfer system

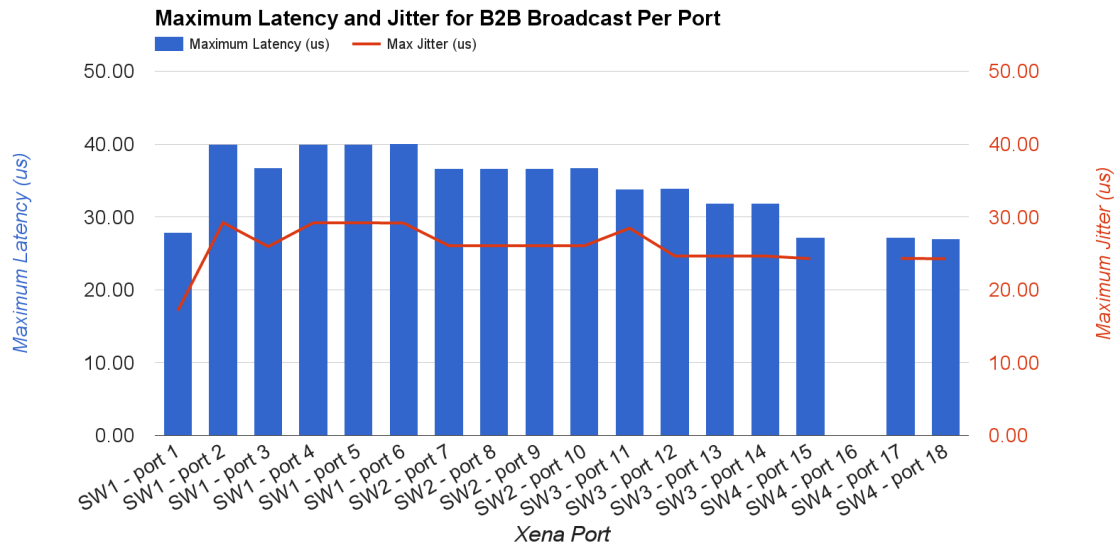


Figure 6.18: The maximum latency and jitter for B2B Broadcast frames

Table 6.7: The maximum latency and jitter of the B2B Broadcast frames

	WR switch 4	WR switch 4, 3	WR switch 4, 3, 2	WR switch 4, 3, 2, 1
Max latency	28 μ s	34 μ s	37 μ s	41 μ s
Max jitter	25 μ s	25 μ s	27 μ s	30 μ s

- Latency and jitter for B2B Unicast frames

For the B2B unicast frames, the latency and jitter of the stream from port 16 to port 1 are measured.

- Average Latency and jitter

For the B2B Unicast frames, 4 WR switch network has approximate 11 μ s average latency and 0 μ s average jitter.

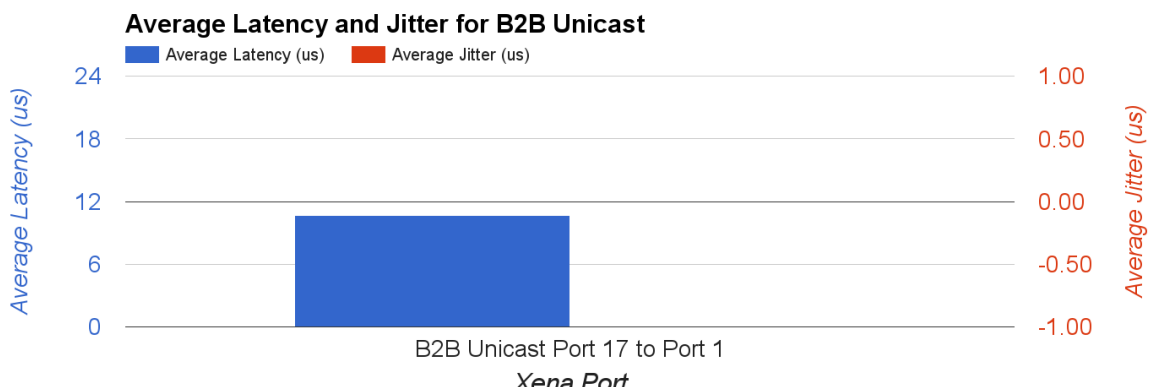


Figure 6.19: The average latency and jitter for B2B Unicast frames

6.2. GMT systematic investigation for the B2B transfer system

- Maximum Latency and jitter

For the B2B unicast frames, 4 WR switch network has approximate 23 μ s maximum latency and 13 μ s maximum jitter.

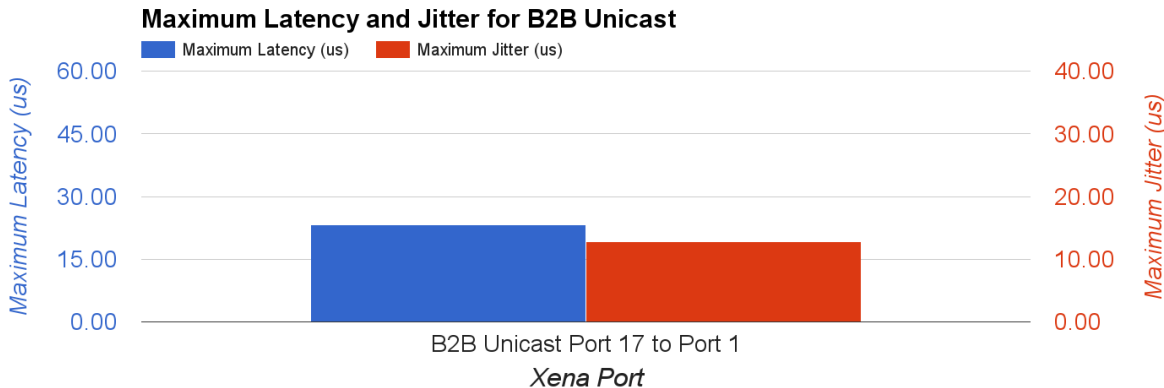


Figure 6.20: The maximum latency and jitter for B2B Unicast frames

More test configuration and results, please see “Testing the WR Network of the FAIR General Machine Timing System“.

6.2.2.4 Result and conclusion

Tab. 6.8 shows the result of the test. The frame loss rate and latency meet the requirements of the B2B Broadcast and B2B Unicast traffic.

Table 6.8: The result of the WR network test for the B2B transfer

	Frame Loss Rate	Average Latency	Maximum Latency	Average Jitter	Maximum Jitter
B2B Broadcast	0 %	6 μ s/switch	28 μ s/switch	0 μ s/switch	25 μ s/switch
B2B Unicast	0 %	11 μ s/4switch 3 μ s/switch	23 μ s/4switch 6 μ s/switch	0 μ s/4switch 0 μ s/switch	13 μ s/4switch 4 μ s/switch

For the B2B transfer system, the upper bound latency of the frames in the B2B Broadcast and B2B Unicast traffic is 500 μ s, see Tab.6.4. The latency of the WR network is decided by the layers of WR switches and the length of the optical fiber. The latency of the optical fiber is about 204 m/ μ s [55] and the longest distance in the FAIR campus is around 2 km, so the latency of a 2 km optical fiber is about 10 μ s. The layers of WR switches play a more important role in the latency.

- B2B Broadcast

Here we calculate the layer of the WR switch between the B2B source SCU and B2B target SCU, between B2B source SCU and source trigger SCU and between B2B source SCU and target trigger SCU.

$$\frac{500 \mu\text{s} - 10 \mu\text{s}}{28 \mu\text{s}/\text{switch}} \approx 17 \quad (6.50)$$

6.3. Kicker systematic investigation for the B2B transfer system

- B2B Unicast

Here we calculate the layer of the WR switch between the B2B source SCU and DM.

$$\frac{500 \mu\text{s} - 10 \mu\text{s}}{6 \mu\text{s}/\text{switch}} \approx 81 \quad (6.51)$$

6.3 Kicker systematic investigation for the B2B transfer system

The SIS18 extraction kicker consists of 9 kicker units. In the existing topology, 5 kicker units are installed in the 1st crate and the other 4 units are in the 2nd crate. The width of each kicker unit is 0.25m and the distance between two kicker units is 0.09m. The distance between two crates is 19.167m. SIS100 injection kicker consists of 6 kicker units, which are equally located. The width of each kicker unit is 0.22m and the distance between two units is 0.23m. For the B2B transfer, the rise time of SIS18 extraction kicker and SIS100 injection kicker unit are 90ns and 1/20 of the revolution period. The rise time of these kickers must fit within the bunch gap, 25% of rf reference period [26, 41]. The bunch gap is denoted by G. All the analysis in this section dose not consider the jitter of the kicker trigger signal. Here we are discussing about the following possibilities.

- For SIS18, whether the kicker units in the 2nd crate could be fired a fixed delay after the firing of the kicker units in the 1st crate for ion beams over the whole range of stable isotopes.
- For SIS100, whether the kicker units could be fired instantaneously.

6.3.1 SIS18 extraction kicker units

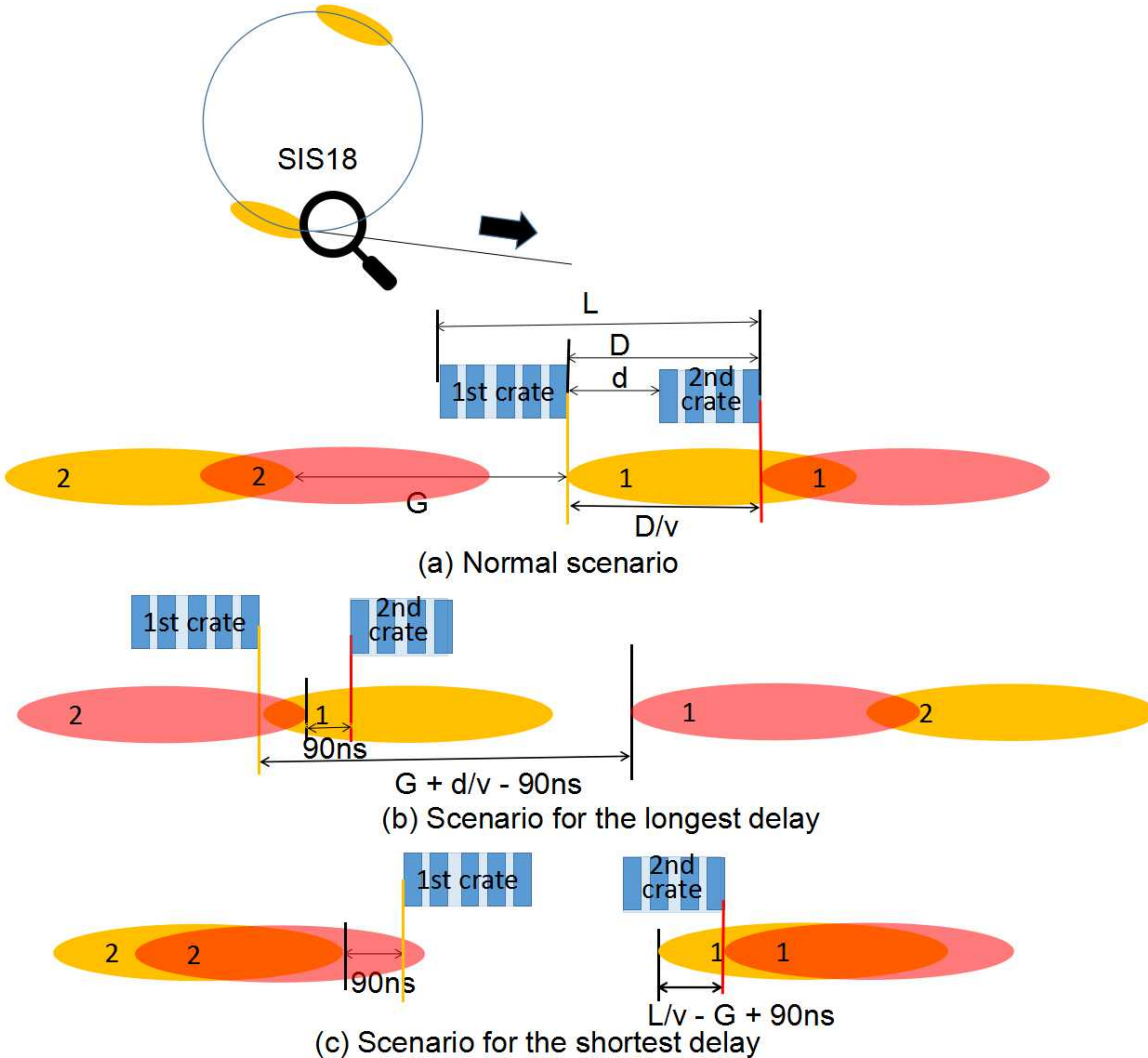


Figure 6.21: Three scenarios for the delay of SIS18 extraction kicker

Here we take three ion beams, H^+ , U^{28} and U^{73+} , to check the possibility, because the boundary ion species have the most stringent requirements. Fig. 6.21 shows three scenarios of the firing delay between two crates. Beam is firstly kicked by kicker units in the 1st crate and than kicked by the units in the 2nd crate to the transfer line. The yellow and red ellipse represents the position of the bunches, when the kicker units in the 1st and 2nd crate are fired. The number in the ellipse is used to tell different bunches. The head of the bunch is at the right side. The bunch 2 is firstly kicked. Here we assume that the kicker units in the same crate are triggered instantaneous. d denotes the distance between two crates. L denotes the distance from the leftmost to the rightmost kicker unit. D denotes the sum distance of d and the 2nd crate. d equals to 19.167 meter. L equals to 22.047m = $d + 9 \times 0.25m + 7 \times 0.09m$. D equals to 20.437m = $d + 4 \times 0.25m + 3 \times 0.09m$.

Fig. 6.21 (a) is the easiest scenario. The kicker units in the 1st crate are fired when the tail of the bunch 1 passes by the 1st crate completely. The kicker units in the 2nd crate are fired when the tail of the bunch 1 passes by the 2nd crate completely. The delay for the firing two crates in this scenario is $D/\beta c$.

6.3. Kicker systematic investigation for the B2B transfer system

Fig. 6.21 (b) shows the scenario of the maximum delay between the firing of two crates. The kicker units in the 1st crate are fired when the tail of the bunch 1 passes by the 1st crate completely. The kicker units in the 2nd crate are fired 90ns before the head of the bunch 2 passes by it. The delay equals to $G+d/\beta c-90\text{ns}$.

Fig. 6.21 (c) shows the scenario of the minimum delay. The kicker units in the 1st crate are fired 90ns before the head of the bunch 2 passes by it. The kicker units in the 2nd crate are fired when the bunch 1 passes by the 2nd crate. The delay is $L/\beta c-G+90\text{ns}$.

Tab. 6.9 shows delay for three scenarios and related parameters. The fixed delay is determined primarily by the boundary delay range from H^+ , U^{28} and U^{73+} beams, the delay range for other heavy ion species beams must be contained in these boundary range. According to the result, a fixed delay is available for firing kicker units in two crate for different beams. e.g. 80ns.

Table 6.9: The delay for firing two crates of SIS18 extraction kicker

Beam	β	time $L/\beta c$	bunch gap G	minimum delay $L/\beta c-G+90\text{ns}$	delay $D/\beta c$	maximum delay $G+d/\beta c-90\text{ns}$
H^+	0.982	75ns	184ns	0ns	69ns	163ns
U^{28+}	0.568	130ns	159ns	61ns	120ns	189ns
U^{73+}	0.872	84ns	104ns	70ns	78ns	92ns

6.3.2 SIS100 injection kicker units

Two bunches from SIS18 will be continuously injected into two RF buckets after the other in SIS100. See Fig. 6.10. The yellow ellipse represents the circulating bunch in SIS100 and the red one represents the bunch to be injected. The head of the bunch is at the left side. The preparation of the SIS100 injection kicker must be done during the bunch gap and it must be established for at least one SIS18 revolution period. For the instantaneous firing, all kicker units are fired only if the tail of the circulating bunch passes the leftmost kicker unit. The kicker pass time is the time needed for the tail of a bunch to pass from the rightmost unit to the leftmost kicker unit. The rise time of the kicker unit is 1/20 of the revolution period [26]. Therefor the preparation time is the sum of the kicker pass time and rise time. The distance from the rightmost to the leftmost kicker unit is 3.79m, $6 \times 0.22\text{m} + 5 \times 0.23\text{m}$. If the preparation time is shorter than bunch gap, all kicker units could be fired instantaneous. Tab. 6.10 shows the preparation time for H^+ , U^{28} and U^{73+} beams and their bunch gap. The preparation time is much shorter than the bunch gap. So the kicker units could be fired instantaneous.

6.4. Test setup for the data collection, merging and redistribution of the B2B transfer system

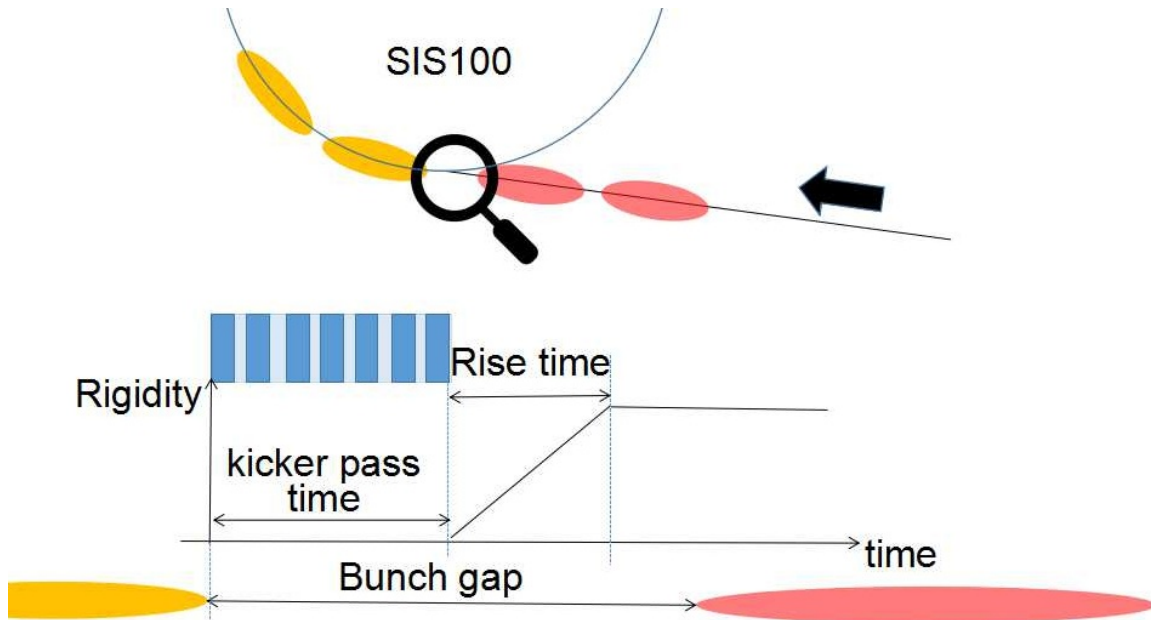


Figure 6.22: SIS100 injection kicker

Table 6.10: The delay for firing SIS00 injection kicker

Beam	β	kicker pass time $L/\beta c$	Rise time $1/20 \times T_{rev}^{SIS100}$	Preparation time $L/\beta c + 1/20 \times T_{rev}^{SIS100}$	bunch gap $2.25 \times T_{rev}^{SIS100}$
H^+	0.982	3ns	184ns	187ns	828ns
U^{28+}	0.568	22ns	318ns	333ns	1431ns
U^{73+}	0.872	15ns	207ns	222ns	932ns

6.4 Test setup for the data collection, merging and redistribution of the B2B transfer system

In this section, the test setup for the B2B transfer system is described, focusing only on the timing aspects.

6.4.1 Test functional requirement

The test setup achieves the following functional requirement.

- After receiving CMD_B2B_START, both the B2B source and target SCUs collect predicted phase equivalent data locally. The equivalence is a timestamp for the zero crossing point of the simulated Reference RF Signal of SIS18 and SIS100.
- The B2B target SCU transfers the frame containing the timestamp to the B2B source SCU.

6.4. Test setup for the data collection, merging and redistribution of the B2B transfer system

- After receiving the data, the B2B source SCU calculates the synchronization window.
- The B2B source SCU sends the frame containing the beginning of the synchronization window to the WR network.
- After receiving the frame, the trigger SCU produces TTL output indicating the start of the synchronization window.

6.4.2 Test setup

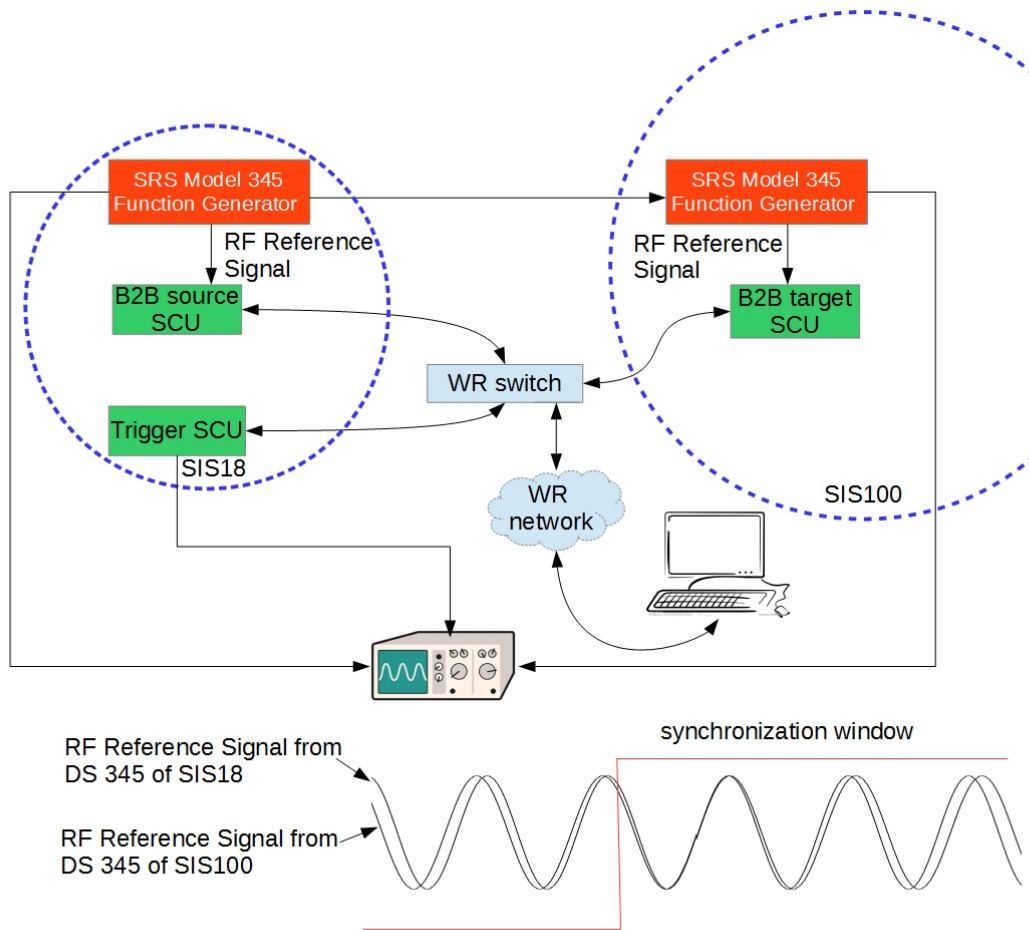


Figure 6.23: Schematic of the test setup

Fig. 6.23 shows the schematic of the test setup. In this test setup, two MODEL DS345 Synthesized Function Generators⁷ are used, which are with the frequency accuracy of ± 5 ppm of the selected frequency to simulate Reference RF Signals of SIS18 and SIS100. DS345 of SIS18 uses an internal 10 MHz clock as an external reference clock for DS345 of SIS100. The B2B source SCU, B2B target SCU and trigger SCU are connected to the same WR switch, which connects to the timing

⁷<http://www.thinksrs.com/downloads/PDFs/Manuals/DS345m.pdf>

6.4. Test setup for the data collection, merging and redistribution of the B2B transfer system

network. A PC⁸ is used as a DM to produce the B2B start timing frame. Besides, it monitors the status of the B2B transfer programs in all SCUs. The oscilloscope is used to monitor the alignment of the two simulated Reference RF Signals within the synchronization window provided by the trigger SCU.

Fig. 6.24 shows the front and back view of the test setup. DS345 of SIS18 produces the sine wave of 1.572 200 MHz frequency for the oscilloscope and DS345 of SIS100 produces the sine wave of 1.572 000 MHz for the oscilloscope, which are achieved by the LEMO cables, see green line in Fig. 6.24. DS345 produces the TTL signal for the B2B source SCU, whose rising edge is synchronized to the positive zero crossing of the sine wave of 1.572 200 MHz frequency and DS345 of SIS100 produces the TTL signal for the B2B target SCU, whose rising edge is synchronized to the sine wave of 1.572 000 MHz, which are achieved by the LEMO cables, see red line in Fig. 6.24. So the beating frequency is 200 Hz and the synchronization period is 5 ms. The B2B source, target and trigger SCUs are connected to the WR switch, which are achieved by the optical fiber, see yellow line. The WR switch is connected to the PC and the WR network. The output of the synchronization window from the B2B trigger SCU is connected to the oscilloscope, which is achieved by the LEMO cable, see green line.

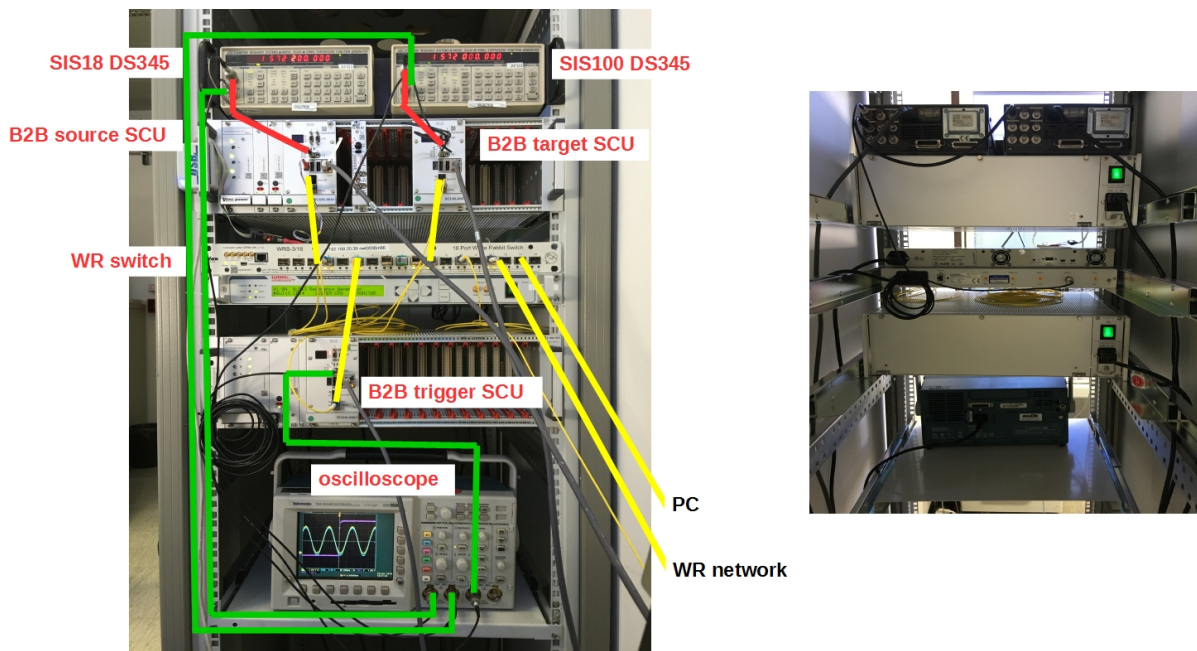


Figure 6.24: The front and back view of the test setup

Compared with the final scenario, there are some difference of the test setup.

- The SIS18 and SIS100 DS345 will be replaced by the PAP modules, which are installed in the B2B source and target SCUs as SCU slaves.
- All devices are installed in different racks. The SIS18 source SCU and B2B trigger SCU of the extraction kicker are installed in SIS18 and the SIS18 target SCU and B2B trigger SCU of the injection kicker are installed in SIS100. The connection is done via the WR network.

⁸A Linux personal computer is installed with the standard TR tools and library.
<https://www-acc.gsi.de/wiki/Timing/TimingSystemNodesCurrentRelease>

6.4. Test setup for the data collection, merging and redistribution of the B2B transfer system

- The B2B source SCU has several other SCU slaves, e.g. Phase Shift Module (PSM) for the phase shift.
- The B2B trigger SCU considers not only the synchronization window, but also the kicker delay compensation from the SM. Besides, it has several SCU slaves, which coordinate the correct B2B extraction and injection kicker with other systems, e.g. MPS.

6.4.3 The firmware of the B2B transfer system

The B2B source, B2B target and trigger SCUs have different firmware running on their soft CPU, LM32⁹. The firmware are activated by the B2B start timing frame, *CMD_START_B2B*, which indicates the source and target synchrotrons of the B2B transfer.

- Firmware for the B2B source SCU

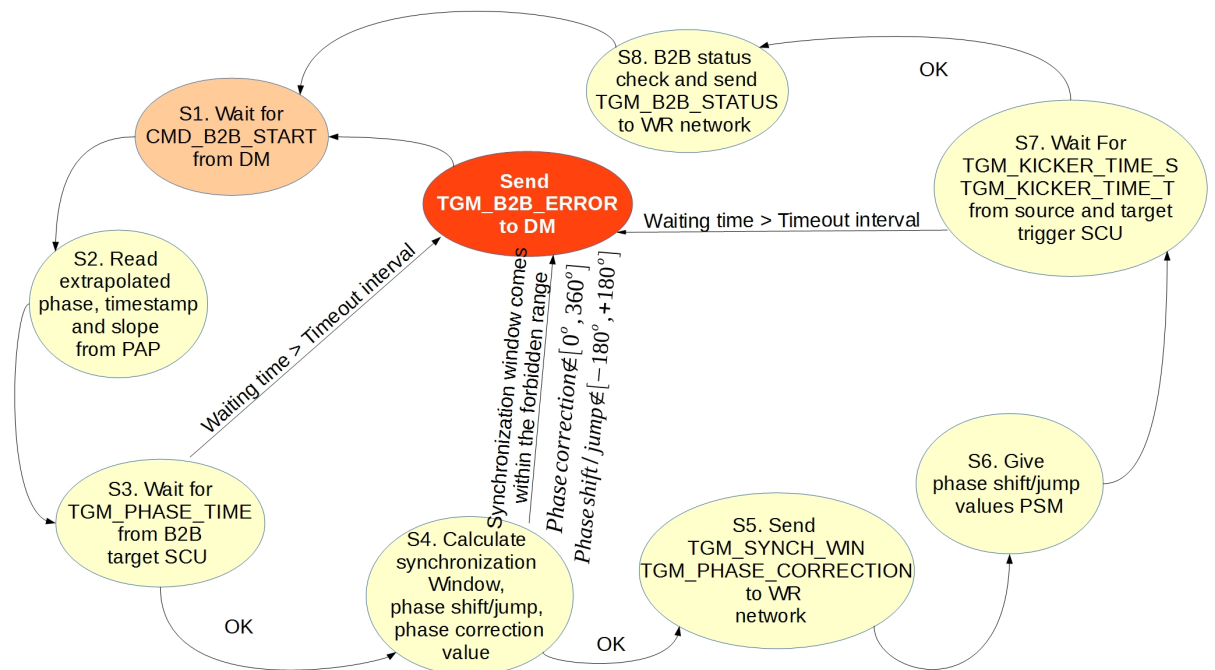


Figure 6.25: Flow chart of the firmware for B2B source SCU.
Flow chart of the firmware for B2B source SCU. “Step“ is represented as “S“ in the figure.

The firmware for the B2B source SCU is the core program of the B2B transfer system. See Fig. 6.25.

- Step 1. The program waits for the *CMD_START_B2B* timing frame.
- Step 2. When it receives the timing frame *CMD_START_B2B*, it reads the extrapolated phase, the corresponding timestamp and the phase advance slope from the PAP module.

⁹LatticeMico32 is a 32-bit microprocessor soft core from Lattice Semiconductor optimized for field-programmable gate arrays (FPGAs).

6.4. Test setup for the data collection, merging and redistribution of the B2B transfer system

- Step 3. It waits for the TGM_PHASE_TIME timing frame from the B2B target SCU, which contains the extrapolated phase, the corresponding timestamp and the slope of the phase advance.
- Step 4. When it receives the timing frame TGM_PHASE_TIME within a specified timeout interval, it calculates the synchronization window, the phase shift/jump value and the phase correction value. Or it sends a timing frame TGM_B2B_ERROR to the WR network and goes back to the step 1, which indicates the timeout error of the frame. Besides, it checks whether the phase correction is in the range of 0° to 360° , the required phase shift in the range of -180° to 180° and the start of the synchronization window not in the forbidden range. If at least one of them is not correct, it sends a timing frame TGM_B2B_ERROR to the WR network and goes back to the step 1, which indicates the calculation error.
- Step 5. It sends the timing frame TGM_SYNCH_WIN and TGM_PHASE_CORRECTION to the WR network. TGM_SYNCH_WIN indicates the start of the synchronization window and TGM_PHASE_CORRECTION is used for the trigger SCUs for the reproduction of the bucket label signal.
- Step 6. It gives the phase correction and phase shift/jump values to corresponding modules.
- Step 7. It waits for the timing frame TGM_KICKER_TIME_S from the source trigger SCU and TGM_KICKER_TIME_T from the target trigger SCU, which contains the extraction/injection kicker trigger and firing timestamp. When it does not receive the timing frames within a specified timeout interval, it sends a timing frame TGM_B2B_ERROR to the WR network and goes back to the step 1, which indicates the timeout error of the frame.
- Step 8. When it receives the timing frames mentioned in the step 7 within a specified timeout interval, it checks the B2B transfer status and sends TGM_B2B_STATUS to the WR network and goes to the step 1. The B2B transfer is successful, if all of the following checks are correct. Or the B2B transfer is failure.
 - * Trigger time < firing time of the extraction kicker of the source synchrotron
 - * Trigger time < firing time of the injection kicker of the target synchrotron
 - * Firing time of the extraction kicker < firing time of the injection kicker

- Firmware for the B2B target SCU
-

6.4. Test setup for the data collection, merging and redistribution of the B2B transfer system

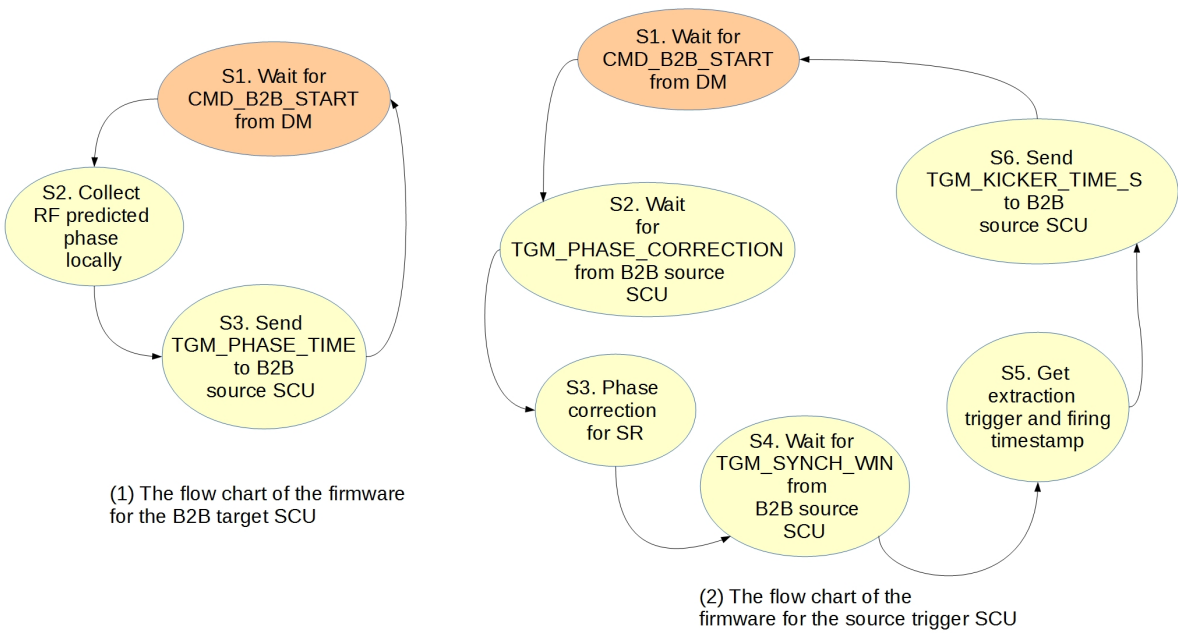


Figure 6.26: Flow chart of the firmware for B2B target SCU.
Flow chart of the firmware for B2B target SCU. “Step“ is represented as “S“ in the figure.

Fig. 6.26 (a) shows the flow chart of the program of the B2B target SCU.

- Step 1. The program waits for the CMD_START_B2B timing frame.
- Step 2. When it receives the timing frame CMD_START_B2B, it collects the predicted phase.
- Step 3. It sends the TGM_PHASE_TIME timing frame to the B2B source SCU and goes back to the step 1.

- Firmware for the trigger SCU

Fig. 6.26 (b) shows the flow chart of the program of the source trigger SCU. For the target trigger SCU, the flow chat is same only with the different name of the timing frame TGM_KICKER_TIME_T.

- Step 1. The program waits for the CMD_START_B2B timing frame.
- Step 2. The program waits for the TGM_PHASE_CORRECTION timing frame.
- Step 3. The program gives the phase correction value to the corresponding module for the bucket label signal reproduction.
- Step 4. When it receives the timing frame CMD_START_B2B, it waits for the timing frame TGM_SYNCH_WIN to indicate the synchronization window for the kicker trigger.
- Step 5. After the beam extraction, it collects the trigger and firing timestamp.
- Step 6. It sends the TGM_KICKER_TIME_S timing frame to the B2B source SCU and goes back to the step 1.

6.4. Test setup for the data collection, merging and redistribution of the B2B transfer system

6.4.4 The time constraints of the B2B transfer system

For the B2B transfer system, the time constraints are very important and strict. Fig. 6.27 shows the time constraint of the system. The *CMD_START_B2B* is executed at t_{B2B} . The RF phase prediction needs 500 μ s, so the B2B source and target SCUs collect the phase data at $t_{B2B} + 500 \mu\text{s}$ and need about 450 ns for the data collection. The B2B source SCU receives the timing frame TGM_PHASE_TIME at around $t_{B2B} + 500 \mu\text{s} + 450 \text{ ns} + 500 \mu\text{s} \approx t_{B2B} + 1 \text{ ms}$. The second 500 μ s is the upper bound latency of the WR network. After that, the B2B source SCU needs about 100 μ s for the calculation, the sending of the timing frame TGM_SYNCH_WIN and TGM_PHASE_CORRECTION and data transferring to the corresponding module. TGM_SYNCH_WIN is sent at around $t_{B2B} + 1 \text{ ms} + 100 \mu\text{s} \approx t_{B2B} + 1.1 \text{ ms}$. The trigger SCU receives TGM_PHASE_CORRECTION and TGM_SYNCH_WIN at around $t_{B2B} + 1.1 \text{ ms} + 500 \mu\text{s} \approx t_{B2B} + 1.6 \text{ ms}$. The 500 μ s is the latency of the WR network. The start of the synchronization window must be later than $t_{B2B} + 1.1 \text{ ms} + 2 \times 500 \mu\text{s} \approx t_{B2B} + 2.1 \text{ ms}$, because the TGM_SYNCH_WIN must be transferred back to the DM and the DM transfers it further to the beam instrumentation devices via WR network. The upward to DM transfer needs maximum 500 μ s and the transfer from the DM to BI needs another 500 μ s. The upper bound B2B transfer time is 10 ms, which is decided by the duration of the stable beam. There is no hard real time for the collection of the trigger and firing timestamps and timing frame TGM_KICKER_TIME_S sending, we give 1 ms for the source trigger SCU to do this task and the source trigger SCU sends TGM_KICKER_TIME_S at around $t_{B2B} + 10 \text{ ms} + 1 \text{ ms} \approx t_{B2B} + 11 \text{ ms}$. The same time constraints is also for the target trigger SCU. The B2B source SCU receives TGM_KICKER_TIME_S and TGM_KICKER_TIME_T at around $t_{B2B} + 11 \text{ ms} + 500 \mu\text{s} \approx t_{B2B} + 11.5 \text{ ms}$. The 500 μ s is the latency of the WR network. The B2B source SCU sends TGM_B2B_STATUS at around $t_{B2B} + 11.5 \text{ ms} + 100 \mu\text{s} \approx t_{B2B} + 11.6 \text{ ms}$. The BI devices receives the timing frame TGM_B2B_STATUS at around $t_{B2B} + 11.6 \text{ ms} + 2 \times 500 \mu\text{s} \approx t_{B2B} + 12.6 \text{ ms}$.

6.4. Test setup for the data collection, merging and redistribution of the B2B transfer system

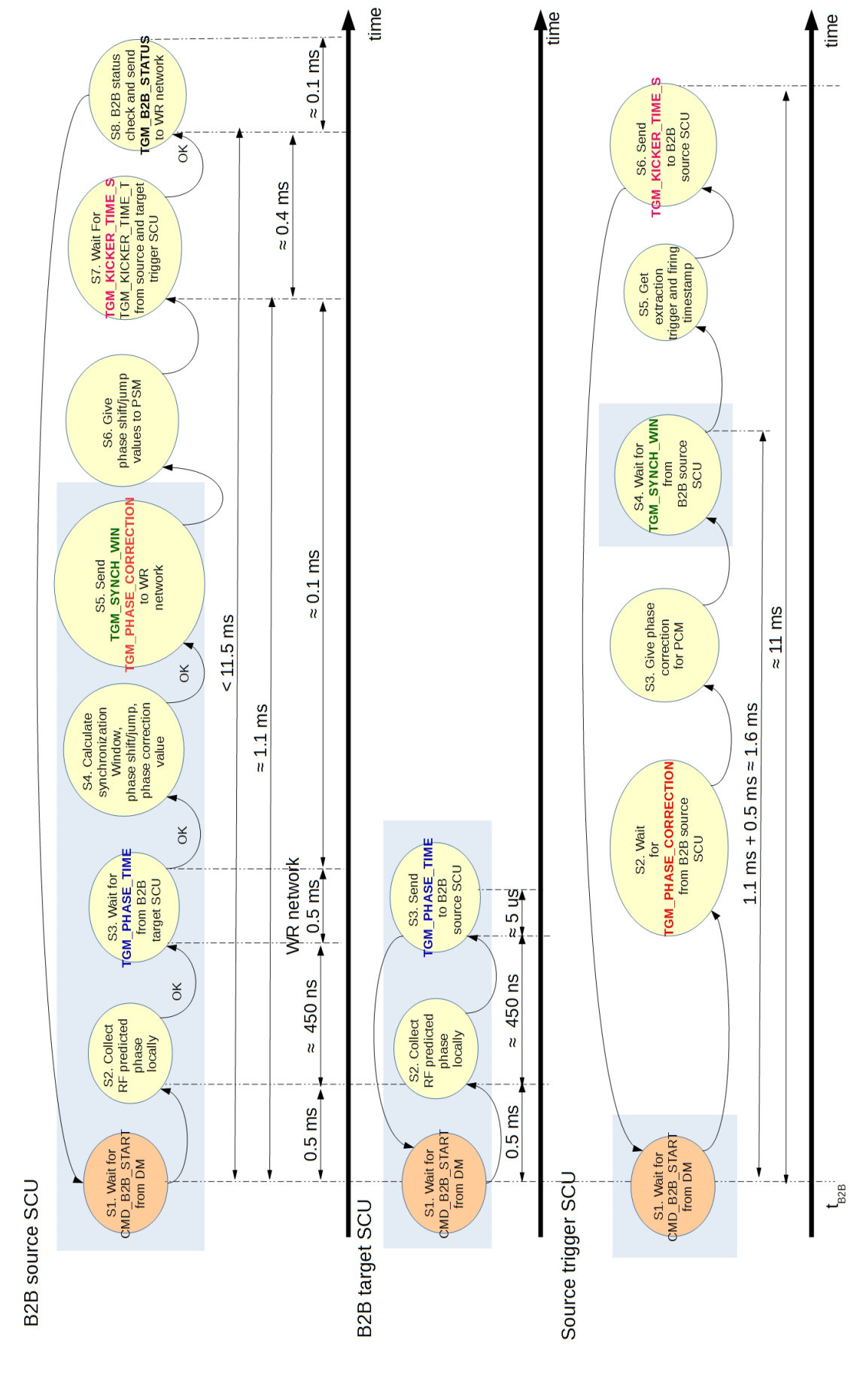


Figure 6.27: The time constraints of the B2B transfer system. The sent and received timing frame pairs have the same color. The test setup realizes the steps in the blue rectangle. (not drawn to accurate timescale)

6.4. Test setup for the data collection, merging and redistribution of the B2B transfer system

6.4.5 Test result

Because some modules of the B2B transfer system are still under the development, the test setup realizes parts of the whole function, mainly concentrated on the data collection from two simulated Reference RF signals, the calculation of the synchronization window and the distribution of the start of the synchronization window. The steps with the blue rectangle in Fig. 6.27 are realized in this test setup. The test result of the B2B programs on B2B source, B2B target and trigger SCUs are shown as follows.

```
1  
2 U28+ B2B transfer from SIS18 to SIS100 => Trigger SCU  
3 ======  
4 Waiting for timing frames ...
```

6.4. Test setup for the data collection, merging and redistribution of the B2B transfer system

5	>>>>>>>>>>>>>>>>>>>>>>	Receive TGM_SYNCH_WIN from WR network
6	Event execution timestamp: GMT 1970–01–08 21:07:27.450028674	

After both B2B source and target programs receive the *CMD_START_B2B* frame, they trigger another unit connected to the System-on-Chip¹⁰ (SoC) bus to get the timestamp of the next zero crossing point of the DS345 sine waves, which is simulated as an equivalent to the predicted phase. All timestamp are shown in the format of Greenwich Mean Time (GMT). The timestamp got by the B2B source SCU is Thu, Jan 8, 1970, 21:07:27 0.445405856 second and the timestamp got by the B2B target SCU is Thu, Jan 8, 1970, 21:07:27 0.445364560 second, see Line 10 and 14 of the test result of the B2B source SCU. The time difference between two timestamps is 41.296 µs. The frequency difference between SIS18 and SIS100 Reference RF Signals is 200Hz. It means that there are 200 more periods of the SIS18 Reference RF Signal within one second compared with the SIS100 Reference RF Signal. Every 5 ms (1/200 Hz) SIS18 Reference RF Signal has one period more than that of SIS100. The time is calculated by eq. 6.52, indicating the alignment of the zero crossing of two DS345 sine waves of SIS18 and SIS100. The time is named as “synchronization time”, denoted by Δt .

$$\frac{T_{h=2}^{SIS18}}{1/(f_{h=2}^{SIS18} - f_{h=10}^{SIS100})} = \frac{41.296\text{us}}{\Delta t} \mod T_{h=10}^{SIS100} \quad (6.52)$$

$$\Delta t = 4.622\,818\,\text{ms} \quad (6.53)$$

The number of the SIS18 Reference RF Signal periods for the synchronization is calculated as

$$\frac{\Delta t}{T_{h=2}^{SIS18}} = 7268 \quad (6.54)$$

we could get that the beating time Δt is 4.622 818 ms and the number of the SIS18 Reference RF Signal periods for the synchronization is 7268 for the test.

¹⁰A system-on-chip is an integrated circuit that integrates all components of a computer or other electronic system into a single chip.

Chapter 7

Conclusion and outlook

For many large scale accelerator facilities, it is inevitable to transfer bunched beam from one ring accelerator to another to gain higher energy or to accumulate beam for some research experiments. Without the proper transfer, the beam will be subject to various disturbances and even beam loss, e.g. dipole oscillation caused by the injection energy or phase error, quadrupole oscillation caused by the cavity voltage error. Hence, the proper bunch-to-bucket transfer between two accelerators is of great importance.

Facility for Antiproton and Ion Research (FAIR) aims at providing high-energy beam with high intensities. SIS100/300 of FAIR is under construction at GSI Helmholtz Centre for Heavy Ion Research GmbH at current stage. The B2B transfer has never been practiced between the existing machines, e.g. SIS18, ESR and CRYRING. The new developed Bunch-to-Bucket transfer system for FAIR in the dissertation is designed for all complex B2B transfer between FAIR accelerators. It is capable to transfer different species beam from one machine cycle to another. It is capable to parallel transfer beam through FAIR accelerators. It is also able to transfer the beam between two synchrotrons via FRS or Super FRS. It focuses first of all on the transfer from SIS18 to SIS100, but it will be firstly tested for the transfer from SIS18 to ESR and further to CRYRING.

The B2B transfer system for FAIR is introduced in the dissertation at hand from the functional point of view. The basic principles for B2B transfer are realized based on the existing FAIR technical basis (e.g. LLRF and FAIR control systems) and unique FAIR demands (e.g. Machine Protection System, MPS). The phase difference between two RF systems of two ring accelerators is obtained with the help of a shared reference signal at two ring accelerators. The source synchrotron works as the “B2B transfer master” for the rf phase collection, data (e.g. synchronization window, phase correction, phase shift and so on) calculation, synchronization window redistribution and B2B status check. In addition, the dissertation presents how FAIR accelerators apply the B2B transfer system and how precise the bunch-to-bucket transfer is achieved with the system. The rules for the application of the system is explained, which is determined by the relation between the circumference ratio/energy ratio and the cavity harmonic number of two synchrotron.

In addition, the beam dynamic of the U^{28+} B2B transfer from SIS18 to SIS100 is simulated for two synchronization methods, the phase shift and frequency beating method. The dissertation explains the timing constraints of the system, the calculation of the synchronization window and presents the usage of the WR network for

CHAPTER 7. CONCLUSION AND OUTLOOK

the B2B transfer system. Further, the SIS18 extraction and SIS100 injection kickers are analyzed for the different triggering possibilities.

The dissertation presents a test setup for the system, achieving the phase collection of two synchrotrons locally, phase transfer from the target to source synchrotron, synchronization window calculation at the source synchrotron, synchronization window redistribution to the WR network, synchronization window reproduced at the source/target synchrotron.

Although the B2B transfer system for FAIR is flexible and with high compatibility, there still exists several improvement.

In order to reduce the synchronization time, the synchronization process could be started during the acceleration. The phase difference between two Reference RF Signals of the source and target synchrotrons at the flattop could be predicted by comparison the phases of these two signals at any time during the acceleration. Once the phase difference at the flattop is predicted, the synchronization process can be carried out.

- Phase shift method

First, the radial loop must be turned off. At some time during the acceleration, the phases difference between the source and target synchrotrons are obtained with the help of the Synchronization Reference Signal, and the phase difference at the flattop is picked up from the look-up table. Then, a rf frequency modulation is superposed on the initial frequency pattern. The integration of the rf frequency modulation equals to the required phase difference. With this new frequency pattern, the phase difference at the flattop will be the required phase difference when the cavity rf frequency of the source and target synchrotrons reach the flattop.

- Frequency beating method

The radial loop keeps on. At some time during the acceleration, the phases difference between the source and target synchrotrons are obtained. Then, a frequency detune is superposed on the initial frequency pattern. With this new frequency pattern, the synchronization window will be calculated.

Appendix A

B2B timing frames

APPENDIX A. B2B TIMING FRAMES

Table A.1: B2B timing frames

No	Fram Name	Event ID	Priority	Source	Destination
1	CMD_START_B2B		7	DM	Source and B2B target SCU
2	TGM_PHASE_TIME		6	B2B target SCU	B2B source SCU
3	TGM_SYNCH_WIN		6	B2B source SCU	DM, source and target Trigger SCUs
4	CMD_SYNCH_WIN		7	DM	Beam Instrumentation (BI)
5	TGM_PHASE_JUMP		6	B2B source SCU	B2B target SCU
6	TGM_PHASE_CORRECTION		6	B2B source SCU	Source Trigger SCU
7	TGM_KICKER_TRIGGER_TIME_S		6	Source Trigger SCU	B2B source SCU
8	TGM_KICKER_TRIGGER_TIME_T		6	Target Trigger SCU	B2B source SCU
9	TGM_B2B_STATUS		6	B2B source SCU	DM
10	CMD_B2B_STATUS		7	DM	BI
No	Content				Description
1	64 bits timestamp				Begin of the B2B transfer process
2	16 bits phase advance and 64 bits slop				Transfer of the phase advance and the slop
3	64 bits timestamp				Indication the start of the synchronization window
4	64 bits timestamp				Indication the start of the synchronization window
5	16 bits the expected jumped phase				Indication the jumped phase for the empty target machine
6	16 bits phase correction				Target revolution frequency reproduction
7	2 × 64 bits timestamp				Timestamps of trigger and firing of extraction kicker
8	2 × 64 bits timestamp				Timestamps of trigger and firing of injection kicker
9	64 bits timestamp + 1 bit				The actual beam extraction time and the status of the B2B system
10	64 bits timestamp + 1 bit				The actual beam extraction time and the status of the B2B system

Appendix B

Timing frames transfer for the B2B transfer

APPENDIX B. TIMING FRAMES TRANSFER FOR THE B2B TRANSFER

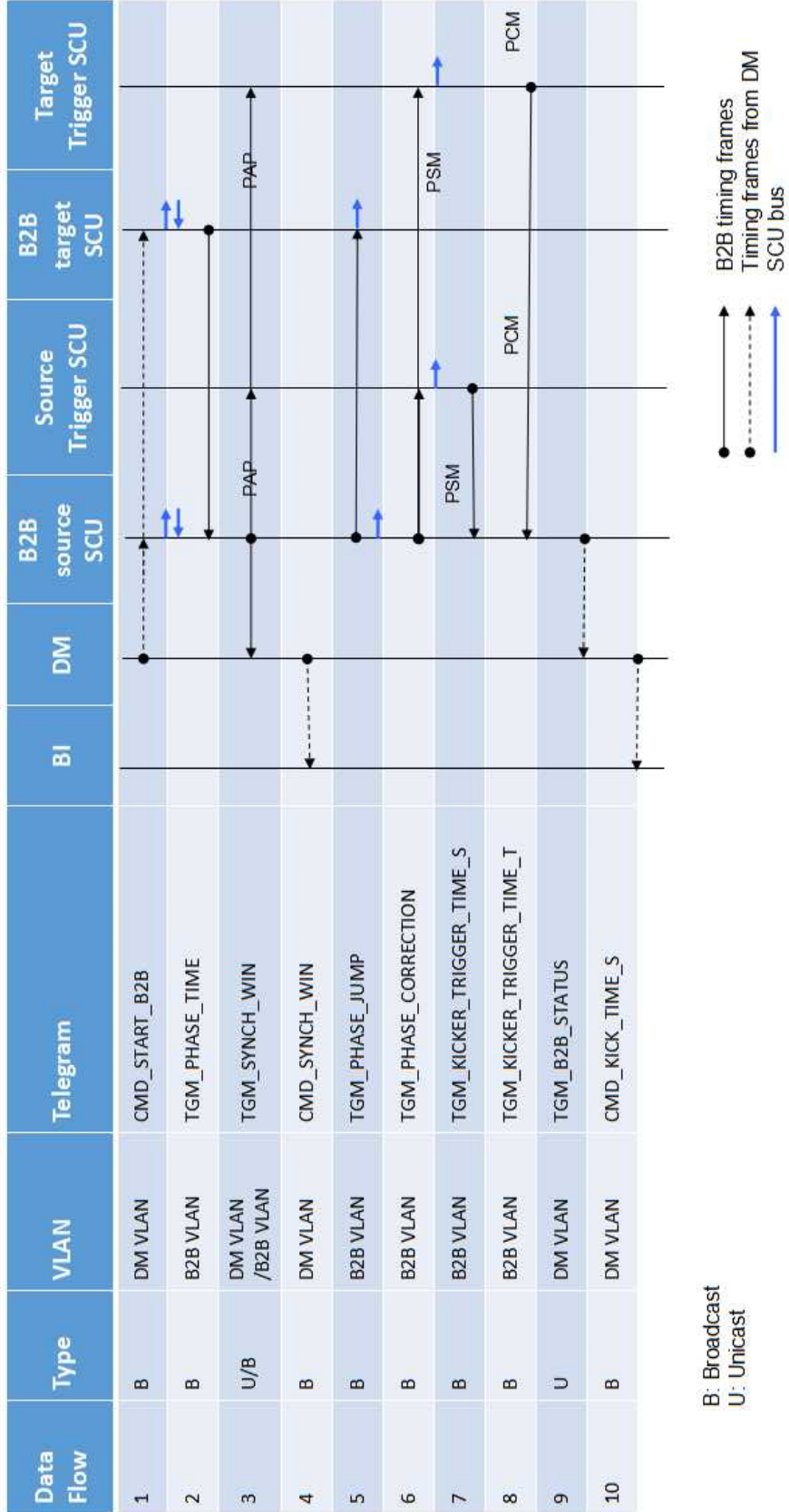


Figure B.1: Timing frames transfer for the B2B transfer

Appendix C

Parameters of B2B transfer for FAIR accelerator pairs

C.1 Parameters for the B2B transfer from SIS18 to SIS100

		Proton		Heavy Ion	
	Unit	SIS18 Ext ¹	SIS100 Inj ²	SIS18 Ext	SIS100 Inj
Design orbit	m	216.72	1083.6	216.72	1083.6
Inj orbit	m	216.72	1083.6	216.72	1083.6
$C_{SIS18} : C_{SIS100}$		5		5	
Ext kinetic energy	MeV/u	4000		200	
Inj kinetic energy	MeV/u		4000		200
Cavity h		1	10(1×4)	2	10(2×4)
f_{rf}	MHz	1.359	2.718	1.572	1.572
T_{rf}	μs	0.736	0.368	0.636	0.636
f_{rev}	MHz	1.359	0.272	0.786	0.157
T_{rev}	μs	0.736	3.678	1.272	6.359
Max $\Delta p/p$		±0.008	±0.01	±0.008	±0.01
$\Delta R/R$		$\pm 0.8 \times 10^{-4}$		$\pm 2.4 \times 10^{-4}$	
Slip factor ³		-0.026		-0.647	
Transition Energy γ_t		10		5.8	
Compaction factor α_p		0.010		0.030	
β		0.982	0.982	0.568	0.568
γ		5.294	5.294	1.215	1.215
		Injection four times		Injection four times	
		Frequency beating method			

C.1. Parameters for the B2B transfer from SIS18 to SIS100

	MHz	$f_{rf} + \Delta f =$ 1.359 + 200Hz	$f_{rf} =$ 1.359	$f_{rf} + \Delta f =$ 1.572 +200Hz	$f_{rf} =$ 1.572
Beating frequency	Hz	200 Hz		200 Hz	
Synchronization period	ms	5		5	
Synchronization window	μ s	7.356		12.718	
Mismatch	degree	$\pm 0.31^\circ$		$\pm 0.50^\circ$	
Phase shift method					

Table C.1: Parameters for the B2B transfer from SIS18 to SIS100

C.2 Parameters for the B2B transfer from SIS18 to ESR

		Proton/Heavy Ion		Heavy Ion	
	Unit	SIS18 Ext	ESR Inj	SIS18 Ext	ESR Inj
Design orbit	m	216.72	108.36	216.72	108.36
Inj orbit	m	216.72	108.36 +0.15	216.72	108.36 +0.15
$C_{SIS18} : C_{ESR}$		1.997		1.997	
Ext kinetic energy	MeV/u	550		30	
Inj kinetic energy	MeV/u		400		30
Cavity h		1	1	4	1
f_{rf}	MHz	0.989756	1.976777	1.373201	0.685651
T_{rf}	μs	1.010350	0.505874	0.728226	1.458468
f_{rev}	MHz	0.989756	1.976777	0.343300	0.685651
T_{rev}	μs	1.010350	0.505874	2.912903	1.458468
$\Delta p/p$ compared with design orbit			1%		1%
$\Delta R/R$			0.138%		0.138%
Slip factor		-0.480	-0.310	-0.909	-0.759
Transition Energy γ_t		10	2.357	5.8	2.357
Compaction factor α_p		0.010	0.18	0.030	0.18
β		0.715	0.715	0.248	0.248
γ		1.429	1.429	1.032	1.032
		Accumulation beam in injection orbit		Accumulation beam in injection orbit	
Frequency beating method					
	kHz	$f_{rf}/1 =$ 988.388 + 1368Hz	$f_{rf}/2 =$ 988.388	$f_{rf}/2 =$ 685.652 + 948Hz	$f_{rf}/1 =$ 685.65250
Beating frequency	Hz	1368 Hz		948 Hz	
Synchronization period	ms	0.731		1.055	
Synchronization window	μs	2.034		2.917	
Mismatch	degree	$\pm 0.50^\circ$		$\pm 0.51^\circ$	
Phase shift method					
$\Delta R/R$ for RF frequency match		0.2%		0.1%	

C.2. Parameters for the B2B transfer from SIS18 to ESR

For SIS18, it is impossible to change the orbit to match the RF frequency within the radius excursion range. So the phase shift method could not be implemented

Table C.2: Parameters for the B2B transfer from SIS18 to ESR

C.3 Parameters for the B2B transfer from SIS18 to ESR via FRS

		Heavy Ion Beam	Rare Isotope Beam
	Unit	SIS18 Ext	ESR Inj
Design orbit	m	216.72	108.36
Inj orbit	m	216.72	108.36 +0.15
$C_{SIS18} : C_{ESR}$		1.997	
Ext kinetic energy	MeV/u	400	
Inj kinetic energy	MeV/u		400
Cavity h		1	1
f_{rf}	MHz	1.076965	1.976777
T_{rf}	μs	0.928535	0.505874
f_{rev}	MHz	1.076965	1.976777
T_{rev}	μs	0.928535	0.505874
$\Delta p/p$ compared with design orbit			1%
$\Delta R/R$			0.138%
Slip factor		-0.366	-0.310
Transition Energy γ_t		5.8	2.357
Compaction factor α_p		0.030	0.18
β		0.778	0.715
γ		1.590	1.429
		Accumulation beam in injection orbit	
Frequency beating method			
	kHz	$f_{rf}/5 =$ 219.642 + 4249Hz	$f_{rf}/9 =$ 219.642
Beating frequency	Hz	4249 Hz	
Synchronization period	ms	0.235349	
Synchronization window	μs	9.106	
Mismatch	degree	$\pm 6.92^\circ$	
Phase shift method			
$\Delta R/R$ for RF frequency match		2%	

C.3. Parameters for the B2B transfer from SIS18 to ESR via FRS

For SIS18, it is impossible to change the orbit to match the RF frequency within the radius excursion range. So the phase shift method could not be implemented

Table C.3: Parameters for the B2B transfer from SIS18 to ESR via FRS

C.4 Parameters for the B2B transfer from ESR to CRYRING

		Proton/Antiproton		Heavy Ion					
	Unit	ESR Ext	CRYRING Inj	ESR Ext	CRYRING Inj				
Design orbit	m	108.36	54.17	108.36	54.17				
Ext orbit	m	108.36 +0.15		108.36 +0.15					
$C_{ESR} : C_{CRYRING}$		2		2					
Ext kinetic energy	MeV/u	30		4-10					
Inj kinetic energy	MeV/u		30		4-10				
Cavity h		1	1	1	1				
f_{rf}	MHz	0.686	1.372	0.254-0.401	0.508-0.802				
T_{rf}	μs	1.458	0.729	3.932-2.494	1.966-1.247				
f_{rev}	MHz	0.686	1.372	0.254-0.401	0.508-0.802				
T_{rev}	μs	1.458	0.729	3.932-2.494	1.966-1.247				
Slip factor		-0.759							
Transition Energy γ_t		2.357		2.357					
Compaction factor α_p		0.18		0.18					
β		0.248	0.248	0.092-0.145	0.092-0.145				
γ		1.032	1.032	1.004-1.011	1.004-1.011				
		One time injection		One time injection					
Phase shift method									
There is no beam in CRYRING, so the phase jump of CRYRING is preferred.									

Table C.4: Parameters for the B2B transfer from ESR to CRYRING

C.5 Parameters for the B2B transfer from CR to HESR

		Antiproton		Rare Isotope Beam	
	Unit	CR Ext	HESR Inj	CR Ext	HESR Inj
Design orbit	m	221.45	575	221.45	575
$C_{ESR} : C_{CRYRING}$		2.6		2.6	
Ext kinetic energy	GeV/u	3		0.74	
Inj kinetic energy	GeV/u		3		0.74
Cavity h		1	1	1	1
f_{rf}	MHz	1.317	0.507	1.125	0.433
T_{rf}	μs	0.759	1.972	0.889	2.309
f_{rev}	MHz	1.317	0.507	1.125	0.433
T_{rev}	μs	0.759	1.972	0.889	2.309
Max $\Delta p/p$		±3%		±1.5%	
Slip factor		-0.011		0.178	
Transition Energy γ_t		3.85		2.711	
Compaction factor α_p		0.067			
β		0.972	0.972	0.830	0.830
γ		4.221	4.221	1.794	1.794
		100 times Injection per 10 seconds		100 times Injection per 10 seconds	
Frequency beating method					
	kHz	$f_{rf}/13 =$ 101.290 + 136Hz	$f_{rf}/5 =$ 101.426	$f_{rf}/13 =$ 86.493 + 113Hz	$f_{rf}/5 =$ 86.608
Beating frequency	Hz	136 Hz		113 Hz	
Synchronization period	ms	7.353		8.850	
Synchronization window	μs	19.719		23.090	
Mismatch	degree	±0.48°		±0.47°	
Phase shift method					
$\Delta R/R$ for RF frequency match		0.2%		0.1%	
The beam in CR is stochastic cooling and electrons exist during the B2B process. The phase shift method doesn't work. The remove of electrodes is about 100 ms.					

Table C.5: Parameters for the B2B transfer from CR to HESR

C.6 Parameters for the B2B transfer from SIS100 to CR

		Proton→ Antiproton		Heavy Ion→ RIB					
	Unit	SIS100 Ext	CR Inj	SIS100 Ext	CR Inj				
Design orbit	m	1083.6	221.45	1083.6	221.45				
$C_{ESR} : C_{CRYRING}$		4.893		4.893					
Ext kinetic energy	GeV/u	28.8		1.5					
Inj kinetic energy	GeV/u		3		0.74				
Cavity h		5(1 bunch)	1	2(1 bunch)	1				
f_{rf}	MHz	1.345	1.318	0.460	1.125				
T_{rf}	μs	0.743	0.759	2.176	0.889				
f_{rev}	MHz	0.269	1.318	0.230	1.125				
T_{rev}	μs	3.716	0.759	4.352	0.889				
β		0.999	0.972	0.924	0.830				
γ		31.918	4.221	2.610	1.794				
		One time injection		One time injection					
Phase shift method									
There is no beam in CR, so the phase jump of CR is preferred.									

Table C.6: Parameters for the B2B transfer from SIS100 to CR

Bibliography

- [1] Jiaoni Bai and Thibault Ferrand. Concept of the FAIR Bunch To Bucket Transfer System, 2016.
- [2] LHC glossary definition. URL <http://www.lhcportal.com/Portal/Info/LHCGlossaryDef.pdf>.
- [3] Jürgen Eschke. International Facility for Antiproton and Ion Research (FAIR) at GSI, Darmstadt. *Journal of Physics G: Nuclear and Particle Physics*, 31(6):S967, 2005. URL <http://iopscience.iop.org/article/10.1088/0954-3899/31/6/041/meta>.
- [4] FAIR - Facility for Antiproton and Ion Research, May 2011. URL <https://www.gsi.de//forschungbeschleuniger/fair.htm>.
- [5] P. Spiller and G. Franchetti. The FAIR accelerator project at GSI. *Nuclear Instruments and Methods in Physics Research Section A*, 561(2):305–309, 2006. URL <http://www.sciencedirect.com/science/article/pii/S0168900206000507>.
- [6] M. Steck, R. Bär, U. Blell, C. Dimopoulou, A. Dolinskii, P. Forck, B. Franzke, O. Gorda, V. Gostishchev, U. Jandewerth, and others. Advanced Design of the FAIR Storage Ring Complex. In *In Proc. of EPAC*, 2008. URL <https://accelconf.web.cern.ch/AccelConf/PAC2009/papers/fr1gri03.pdf>.
- [7] Fritz Nolden, K. Beckert, P. Beller, U. Blell, C. Dimopoulou, A. Dolinskii, U. Laier, G. Moritz, C. Muehle, I. Nesmiyan, and others. The Collector Ring CR of the FAIR project. *Proc. EPAC*, 3(1):5, 2006. URL <http://accelconf.web.cern.ch/AccelConf/e06/PAPERS/MOPCH077.PDF>.
- [8] T. Abe, I. Adachi, K. Adamczyk, S. Ahn, H. Aihara, K. Akai, M. Alois, L. Andricek, K. Aoki, Y. Arai, and others. Technical design report Collector Ring. *KEK Report*, 2010. URL <http://arxiv.org/abs/1011.0352>.
- [9] R. Toelle, K. Bongardt, J. Dietrich, F. Esser, O. Felden, R. Greven, G. Hansen, F. Klehr, A. Lehrach, B. Lorentz, and others. HESR at FAIR: Status of technical planning. 2007. URL <http://epaper.kek.jp/p07/PAPERS/TUPAN024.PDF>.
- [10] M. Lestinsky, A. Bräuning-Demian, H\aaakan Danared, M. Engström, W. Enders, S. Fedotova, B. Franzke, A. Heinz, F. Herfurth, A. Källberg, and others. CRYRING@ ESR: present status and future research. *Physica Scripta*, 2015 (T166):014075, 2015. URL <http://iopscience.iop.org/article/10.1088/0031-8949/2015/T166/014075/meta>.

BIBLIOGRAPHY

- [11] M. Lestinsky and others. CRYRING@ ESR: A study group report. GSI and FAIR Report, 2012.
 - [12] Thibault Ferrand, Harald Klingbeil, and Heiko Damerau. Synchronization of Synchrotrons for bunch-to-bucket Transfers. Technical report, 2015. URL <http://cds.cern.ch/record/2053285>.
 - [13] J-PARC. URL <https://www.kek.jp/en/Facility/ACCL/J-PARC/>.
 - [14] Brookhaven National Laboratory. URL https://en.wikipedia.org/wiki/Particle_physics.
 - [15] Fermi National Accelerator Laboratory. URL <http://www.fnal.gov/pub/science/particle-accelerators/accelerator-complex.html>.
 - [16] Institute of Modern Physics of the Chinese Academy of Sciences. URL http://english.imp.cas.cn/au/bi/201312/t20131231_115141.html.
 - [17] Kaidi Man, Yizhen Guo, Guozhu Cai, Sengli Yang, and Shoujin Wang. Survey and Alignment of HIRFL-CSR at IMP. In Proc. IWAA2002, 2002. URL http://www-group.slac.stanford.edu/met/IWAA/TOC_S/PAPERS/KMan02.pdf.
 - [18] R Garoby. Timing aspect of bunch transfer between circular machines. State of the art in the PS complex, PS/RF. Technical report, Note 84-6, 17 December 84, 1984.
 - [19] Harms Barletta. Overview on Magnetic fields. URL http://uspas.fnal.gov/materials/12MSU/xverse_dynamics.pdf.
 - [20] Jochen Michael Grieser. Beam phase feedback in a heavy-ion synchrotron with dual-harmonic cavity system. PhD thesis, Technical University Darmstadt, 2015. URL <http://tuprints.ulb.tu-darmstadt.de/4634/>.
 - [21] K. Gross, U. Hartel, U. Laier, D. Lens, K. P. Ningel, S. Schäfer, B. Zipfel, and H. Klingbeil. Bunch-by-Bunch Longitudinal RF Feedback for Beam Stabilization at FAIR. In Proc. of IPAC, 2015. URL <http://accelconf.web.cern.ch/AccelConf/IPAC2015/papers/mopha021.pdf>.
 - [22] Eizi Ezura, Masahito YOSHII, Fumihiko TAMURA, and Alexander SCHNASE. Beam-Dynamics View of RF Phase Adjustment for Synchronizing J-PARC RCS with MR or MLF, 2008. URL <http://ccdb5fs.kek.jp/tiff/2008/0826/0826001.pdf>.
 - [23] Claude Bovet, Robert Gouiran, Karl Helmut Reich, and Igor Gumowski. A selection of formulae and data useful for the design of AG synchrotrons. Technical report, CERN, 1970. URL <http://cds.cern.ch/record/280305>.
 - [24] B. J. Holzer. Introduction to transverse beam dynamics. CERN Yellow Report, 2013. URL <http://arxiv.org/abs/1404.0923>.
 - [25] S Y Lee. Accelerator Physics. WORLD SCIENTIFIC, Singapore, 3 edition, November 2011. ISBN 978-981-4374-94-1 978-981-4374-95-8. URL <http://www.worldscientific.com/worldscibooks/10.1142/8335>.
-

BIBLIOGRAPHY

- [26] Blell Udo. Injection and Extraction Components of SIS 100 / 300, 2014.
- [27] Peter Forck. Lecture Notes on Beam Instrumentation and Diagnostics, 2011. URL https://scholar.google.de/scholar?q=Lecture+Notes+on+Beam+Instrumentation+and+Diagnostics&btnG=&hl=de&as_sdt=0%2C5.
- [28] T. Hoffmann. FESA—The front-End Software architecture at FAIR. PCaPAC08, 2008. URL <http://accelconf.web.cern.ch/AccelConf/pc08/papers/wep007.pdf>.
- [29] Ralf Huhmann, Ralph C. Bär, Dietrich Hans Beck, Jutta Fitzek, Günther Fröhlich, Ludwig Hechler, Udo Krause, and Matthias Thieme. The FAIR control system—System architecture and first implementations. ICALEPCS, 2013. URL <http://epaper.kek.jp/ICALEPCS2013/papers/moppc097.pdf>.
- [30] Dietrich Beck, R. Bar, Mathias Kreider, Cesar Prados, Stefan Rauch, Wesley Terpstra, and Marcus Zweig. The new White Rabbit based timing system for the FAIR facility. PCaPAC, 2012. URL <http://accelconf.web.cern.ch/Accelconf/pcapac2012/papers/fria01.pdf>.
- [31] Peter Moritz. BuTiS—Development of a Bunchphase Timing System. GSI Scientific Report, 2006. URL <http://citeseerx.ist.psu.edu/viewdoc/download?doi=10.1.1.162.1765&rep=rep1&type=pdf>.
- [32] B. Zipfel, P. Moritz, and others. Recent Progress on the Technical Realization of the Bunch Phase Timing System BuTiS. Proc. IPAC, pages 418–420, 2011. URL <http://accelconf.web.cern.ch/accelconf/ipac2011/papers/mopc145.pdf>.
- [33] Dietrich Beck, Mathias Kreider, Cesar Prados, Wesley Terpstra, Stefan Rauch, and Marcus Zweig. The General Machine Timing System for FAIR and GSI. URL https://www-acc.gsi.de/wiki/pub/Timing/TimingSystemDocuments/GMT_Description_v3-1.pdf.
- [34] Dietrich Beck. Timing Messages of GMT system for FAIR, 2015. URL <https://www-acc.gsi.de/wiki/Timing/TimingSystemEvent>.
- [35] Harald Klingbeil, Ulrich Laier, Klaus-Peter Ningel, Stefan Schäfer, Christof Thielmann, and Bernhard Zipfel. New digital low-level rf system for heavy-ion synchrotrons. Physical Review Special Topics - Accelerators and Beams, 14(10), October 2011. ISSN 1098-4402. doi: 10.1103/PhysRevSTAB.14.102802. URL <http://link.aps.org/doi/10.1103/PhysRevSTAB.14.102802>.
- [36] P. Baudrenghien. Low-level RF. 13(14):15, 2010. URL <https://cas.web.cern.ch/cas/Denmark-2010/Writeups/Baudrenghien.docx>.
- [37] Marko Mandakovic. FAIR Fast Beam Abort System. URL https://fair-wiki.gsi.de/foswiki/pub/FC2WG/FairC2WGMinutes/20151021_Fast_Beam_Abort_System_Mandakovic.pdf.
- [38] P Kainberger. PZS - SIS/ESR-Pulszentrale, 2003. URL <https://www-acc.gsi.de/data/documentation/eq-models/pzs/gm-pzs.pdf>.

BIBLIOGRAPHY

- [39] U. Krause and Volker Schaa. Re-engineering of the GSI control system. 2001. URL <http://arxiv.org/abs/physics/0111060>.
- [40] H. Liebermann and D. Ondreka. FAIR and GSI Reference Cycles for SIS18, 2013.
- [41] H. Liebermann and D. Ondreka. SIS100 Cycles, 2013.
- [42] J. Bai, T. Ferrand, D. Beck, R. Bär, O. Kester, D. Ondreka, C. Prados, and W. Terpstra. BUNCH TO BUCKET TRANSFER SYSTEM FOR FAIR. In ICALEPCS, 2015. URL <http://icalepcs.synchrotron.org.au/papers/wepgf119.pdf>.
- [43] T. Ferrand and J. Bai. System Simulation of Bunch-to-Bucket Transfer Between Synchrotrons. GSI Scientific Report, 2014. URL <http://repository.gsi.de/record/184160/files/FG-GENERAL-28.pdf>.
- [44] T. Ferrand and J. Bai. SYSTEM DESIGN FOR A DETERMINISTIC BUNCH-TO-BUCKET TRANSFER. In IPAC, 2015. URL <http://accelconf.web.cern.ch/AccelConf/IPAC2015/papers/wepma024.pdf>.
- [45] Thibault Ferrand. Development of the LLRF system for a deterministic Bunch-to-Bucket transfer for FAIR. PhD thesis, Technical University Darmstadt.
- [46] Matthias Thieme, Wolfgang Panschow, and Stefan Rauch. SCU system goes productive. GSI Scientific Report, 2013. URL <http://repository.gsi.de/record/68061/files/FG-CS-07.pdf>.
- [47] F. Herfurth, A. Brauning-Demian, W. Enders, H. Danared, and others. The low energy storage ring CRYRING@ ESR. Proc. of COOL2013 (Murren, Switzerland), 2013. URL <https://accelconf.web.cern.ch/accelconf/COOL2013/papers/thpm1ha01.pdf>.
- [48] M. Steck, C. Dimopoulou, B. Franzke, O. Gorda, T. Katayama, F. Nolden, G. Schreiber, Germany D. Möhl, Switzerland R. Stassen, H. Stockhorst FZJ, and others. Demonstration of Longitudinal Stacking in the ESR with Barrier Buckets and Stochastic Cooling. page 140, Alushta, Ukraine, 2011. URL <http://accelconf.web.cern.ch/AccelConf/COOL2011/papers/proceed.pdf#page=150>.
- [49] A. V. Smirnov, D. A. Krestnikov, I. N. Meshkov, and others. Particle accumulation with a barrier bucket RF system. In COOL, 2009.
- [50] J. Bai12, R. Bär, D. Beck, T. Ferrand13, M. Kreider, D. Ondreka, C. Prados, S. Rauch, W. Terpstra, and M. Zweig. First Idea on Bunch to Bucket Transfer for FAIR. 2014. URL http://epaper.kek.jp/PCaPAC2014/posters/fpo024_poster.pdf.
- [51] John R. Taylor. An introduction to error analysis: The study of uncertainty in physical measurements. Mill Valley, CA: Anonymous University Science Books, page 71ep, 1982.

- [52] U. Laier. Funktional-Spezifikation DDS, 2011.
- [53] Statistical and numerical tools in astrophysics I. Accuracy and precision. URL <http://www.astro.lu.se/Education/utb/ASTM11/lecture2.pdf>.
- [54] Cesar Prados and Jiaoni Bai. Testing the WR Network of the FAIR General Machine Timing System, 2016.
- [55] Calculating Optical Fiber Latency, 2012. URL <http://www.m2optics.com/blog/bid/70587/Calculating-Optical-Fiber-Latency>.

Publications

- 2015 J. Bai, T. Ferrand, D. Beck, R. Br, O. Kester, D. Ondreka, C. Prados, and W. Terpstra. BUNCH TO BUCKET TRANSFER SYSTEM FOR FAIR. *In Proc. of ICAL EPICS*, 2015
- T. Ferrand and J. Bai. SYSTEM DESIGN FOR A DETERMINISTIC BUNCH-TO-BUCKET TRANSFER. *In Proc. of IPAC*, 2015
- 2014 J. Bai, D. Beck, R. Br, D. Ondreka, T. Ferrand, M. Kreider, C. Prados, S. Rauch, W. Terpstra, and M. Zweig. FIRST IDEA ON BUNCH TO BUCKET TRANSFER FOR FAIR. *In Proc. of PCaPAC*, 2014
- M. Kreider, J. Bai, R. Br, D. Beck, A. Hahn, C. Prados, S. Rauch, W. W. Terpstra, and M. Zweig. Launching the FAIR timing system with CRYRING. *In Proc. of PCaPAC*, 2014
- T. Ferrand and J. Bai. System Simulation of Bunch-to-Bucket Transfer Between Synchrotrons. *GSI Scientific Report*, 2014
- 2013 Bai Jiao-Ni, Zeng Lei, Wang Biao, Li Peng, Li Fang, Xu Tao-Guang, and Li Zi-Gao. Modified read-out system of the beam phase measurement system for CSNS. *Chinese physics C*, 37(10):107004, 2013
- D. Beck, J. Adamczewski-Musch, J. Bai, R. Br, J. Frhauf, J. Hoffmann, M. Kreider, N. Kurz, C. Prados, S. Rauch, and others. Paving the Way for the General Machine Timing System. *GSI Scientific Report*, 2013
- Mathias Kreider, Jiaoni Bai, Dietrich Beck, Cesar Prados, Wesley Terpstra, Stefan Rauch, and Marcus Zweig. Receiver Nodes of the General Machine Timing System for FAIR and GSI
- 2012 Jiaoni Bai, Shuai Xiao, Taoguang Xu, and Lei Zeng. The Development of Timing Control System for RFQ. *In Proc. of LINAC*, 2012

Jiaoni Bai

Curriculum Vitae

"I am a slow walker, but I never stop walking." - Jiaoni Bai

Education

- 2013–Now **Doctoral Study**, *Goethe University, Frankfurt am Main, Germany*, .
- 2010–2013 **Master of Engineering Study in Computer Technology**, *Institute of High Energy Physics, Chinese Academy of Sciences, China, GPA – 8.0.*
- 2006–2010 **Bachelor of Engineering Study in Medical Informatics Engineering**, *Southern Medical University, China, GPA – 9.0.*

PhD Thesis

- Title *Development of the timing system for the Bunch-to-Bucket transfer between the FAIR accelerators at GSI Helmholtz Centre for Heavy Ion Research GmbH*
- Professor Prof. Oliver Kester
- Supervisors Dr. Dietrich Beck and Dr. David Ondreka
- Description
 - Development of the Bunch-to-Bucket transfer system
 - Programming work on FPGA
 - Measurement of the White Rabbit network performance

Master Thesis

- Title *The development of EPICS driver for customized VME hardwares*
- Supervisor Taoguang Xu
- Description
 - Development of the software interface between EPICS and VME hardware
 - Development of the operator controlling and monitoring interfaces by MEDM hardware
 - VxWorks program for Motorola VME board MVME5100

Bachelor Thesis

- Title *The CCD performance test and analysis*
- Description
 - Investigation of the influence factors for CCD
 - Test how these factors influence CCD

Awards

- 2012 Won "Scholarship of the head of the Institute of High Energy Physics, CAS" for master thesis
- 2007 Won second prize of "Mathematical Contest in Modeling in Southern Medical University"

Key skills

- Intermediate Network engineering, Bash shell script and Visual Basic programming
- Advanced VHDL program for Altera FPGAs, C, Accelerator technology and beam dynamics, VxWorks programming and EPICS

Computer literacy

- Basic Windows, Linux (Ubuntu/Debian), Microsoft Office and LaTeX applications
- Engineering Altera Quartus and Matlab applications
- Art design Photoshop and Corel VideoStudio application
- Web design Dreamweaver

Languages

- Mandarin Mothertongue Chinese
- English Good written and spoken
- German Goethe-Zertifikat B2